Nathália Santos Serrão de Castro

Msc. In Genetics and Molecular Biology

DNA-Protein interaction: a response regulatory protein associated with Mo homeostasis in *Desulfovibrio alaskensis* G20.

Dissertation for a degree in Doctor in Sustainable Chemistry

Supervisor: Isabel Maria Andrade Martins Galhardas de Moura, Prof. Dr., FCT-UNL
Co-supervisor: Marta Sofia Peixe Carepo, Dr., FCT-UNL

President: Dr.Manuel Luís Magalhães Nunes da Ponte
Examiners: Dr. Francisco Jorge Fernandes Caldeia
Dra. Sofia Rocha Pauleta
Dra. Ana Rosa Leal Lino
Dr. Manuel Aureliano Pereira Martins Alves
Dr. Stéphane Pierre Besson
Dr. Francisco Manuel Ferreia Girio
Members: Dra. Isabel Maria Andrade Martins Galhardas de Moura
Dra. Marta Sofia Peixe Carepo
Dr. César António Tonicha Laia

FACULDADE DE CIÊNCIAS E TECNOLOGIA
UNIVERSIDADE NOVA DE LISBOA

JULY/2014

DNA-Protein interaction: a response regulatory protein associated with Mo homeostasis in *Desulfovibrio alaskensis* G20

To Dr. César Laia

Acknowledgments

To prof. Isabel Moura to accept me in her scientific group and give me the entire laboratory supports to develop my PhD.

To Dr. Marta Carepo to be more than a co-supervisor and share with me all her knowledge about molecular cloning, protein expression, purification and characterization. Thanks to be my translator during my first days in Portugal and support me to solve all the bureaucracy that was necessary to stay here as a PhD student

To prof. José Moura to be more than a professor…to be a friend

To Dr. César Laia to be a friend and give me all the support during the fluorescence spectroscopy studies (from laboratory practice to results interpretation).

To Dr. Mireille Ansaldi, Laboratory de Chimie Bactérienne – Centre National de la Recherché Scientifique, to perform the DNase I footprinting experiments

To Dr. Gustavo Sousa, Centre for Immune Regulation – Faculty of Medicine University of Oslo, to perform the nano-LC-MS experiments.

To Dr. Jose Miguel Manchenõ and Yana Alvarez, Consejo Superior de Investigaciones Científicas, thank you for the care and respect that you received me in your Institution.

To Biplap Maiti to teach me how to synthetize the phosphoramidate compound and help me with the theoretical calculations.

To Nuno Cerqueira to perform the computational biochemistry analysis.

To Pablo Gonzalez e Gabriela Rivas to be a really good professionals and friends.

To Célia Silveira to be my gold key.

To my dearest Rashmi Nair to share with me her experience with proteomics and everyday moments of happiness.

To Susana Ramos to teach me to how to perform enzymatic activities studies

To Magdalena Bober and Sergy George to be more than an “Erasmus” student, to be partners.

To Fundação para Ciência e Tecnologia for financial support (SFRH/BD/47040/2008).

To Marcelo Lima to give me all his friendship before, during and after the PhD.

All my love and respect to Catarina Nunes, Jacopo Marangon and Leonardo Dall′agnol to be with me full time during this journey

RESUMO

Interacção entre DNA e proteína: uma proteína regulatória responsiva associada com a homeostasia do Mo em *Desulfovibrio alaskensis* G20

A transdução dos estímulos ambientais é fundamental para sobrevivência e adaptação bacteriana em diferentes habitats. O sistema de dois componentes é um mecanismo importante para a percepção e transdução de sinal bioquímico em bactérias. Esse sistema é composto, basicamente, por uma proteína histidina quinase e uma proteína reguladora responsiva que atuam em conjunto com a finalidade de fornecer a plasticidade bioquímica necessária para a sobrevivência e adaptação dos microorganismos.

A descoberta de um sistema envolvido na regulação da homeostasia do Mo em *Desulfovibrio alaskensis* G20 abriu novos questionamentos sobre quais seriam os mecanismos responsáveis pela regulação desse metal em bactérias sulfato-redutoras. Nesse sentido, postulou-se que um sistema composto por três proteínas (MorP, MorR e MorS) seria capaz de realizar a homeostasia do Mo. MorP ("*molybdenum response associated protein*") é uma proteína periplasmática multimérica composta por 16-18 subunidades. Estudos de EXAFS juntamente com estudos de caracterização bioquímica mostraram que a MorP possui um centro metálico do tipo Mo-2S[2Fe-2S]-2S-Mo onde cada monómero possui um átomo de Mo e um átomo de Fe. As proteínas MorS e MorR constituiriam um sistema de dois componentes, onde a MorR actuaria como um factor σ_{54} de transcrição do gene *mor*P (gene responsável pela codificação da proteína MorP).

O objectivo geral desta tese é verificar se a proteína MorR interage com a região intergénica entre *mor*P e *mor*S, e analisar como ocorre esta interacção. Adicionalmente, pretende-se verificar qual a influência de moléculas doadores de radicais fosfato na estrutura conformacional da MorR.

A presente dissertação está dividida em cinco capítulos.

O capítulo I é formado por uma introdução geral sobre as bactérias sulfato redutoras e sobre a importância do molibdato para o género *Desulfovibrio*. Esse capítulo faz uma introdução sobre o sistema de dois componentes (TCS) e seus agentes. Adicionalmente, alguns mecanismos de expressão genica, regulação e exemplos de factores de transcrição envolvidos com o TCS também são apresentados. Finalmente, a hipótese do presente estudo é apresentada.

O capítulo II é constituído pelas metodologias e agentes usados para a clonagem do gene *mor*R. As estratégias utilizadas permitiram que o gene da *mor*R fosse clonado com sucesso e permitiram a expressão da proteína MorR tanto em pequena quanto em larga escala, resultando na forma solúvel da proteína. Adicionalmente, o contexto genómico do gene *mor*R é avaliado e discutido.

O capítulo III é constituído por uma introdução sobre estudos envolvendo a fosforilação de proteínas similares a MorR. Esse capítulo também mostra os resultados da purificação e caracterização da proteína MorR. A proteína purificada é um monómero, e a proteína MorR recombinante não contem nem metal (Zn^{2+}, Mo, Cu^{2+} and Mg^{2+}) nem phosphoamino ácidos e, portanto, não é isolada no seu estado fosforilado. A região intergenica entre *mor*P e *mor*S foi amplificada e purificada, e os ensaios de mobilidade por electroforese foram realizados para mostrar se a proteína MorR ligava a esta região. Os resultados obtidos revelaram que a MorR liga a região intergenica e os experimentos de DNase I footprinting identificaram o sítio de ligação específico. O acetylphosphato e o phosphoramidato foram usados para fosforilar a MorR, e os resultados obtidos não mostraram nenhuma oligomerização após a fosforilação da proteína.

O capítulo IV é composto por uma breve introdução sobre os conceitos utilizados em espectroscopia de fluorescência e pelos resultados obtidos com o uso desta técnica. A forma prototópica de 6-FAM-67mer contendo a região intergénica alvo foi usada com a finalidade de definir qual a espécie de fluoresceína estaria presente sob as condições experimentais. Os resultados mostraram que a fluorescência de emissão da forma monoanionica predomina sob o pH 7.5 e que a fluorescência de emissão da forma dianionica começa a emergir a valores de pH acima de 8. A associação entre a MorR e duas regiões diferentes (em tamanho) foram identificadas por meio de estudos de anisotropia de fluorescência e as análises revelaram a presença de dois sítios de ligação independentes. Os resultados identificaram duas constantes de associação: 15.5 μM^{-1} para o primeiro sítio de ligação e de 0.02 μM^{-1} para o segundo sítio de ligação. A mudança conformacional induzida por fosforilação foi investigada usando acetilfosfato e fosforamidato como pequenos doadores de fosfato. Os resultados mostraram que a e fluorescência de emissão do triptofano não altera durante os ensaios experimentais. Esse resultado corrobora com a ideia de que a MorR não altera sua estrutura após esse tipo de estímulo. O estudo computacional bioquímico identificou que a fosforilação da serina é cinética e termodinamicamente mais favorável com o phosphoramidato do que com o

acetylphosphato.

O capítulo V é composto pelas conclusões do presente estudo e nós propomos um mecanismo que pretende explicar como a MorR actuaria como um regulador transcricional dos genes envolvidos na homeostase do Mo. Desse modo, nosso modelo propõe que na ausência do Mo, a MorR actuaria como um repressor da transcrição dos genes da *mor*SR (via σ_{70}) e estaria inactiva para a transcrição do gene *mor*P (via σ_{54}). Nesse contexto, MorP actuaria como um repressor da proteína MorS, sendo esta incapaz de realizar autofosforilação, e, consequentemente, todo o sistema estaria inactivo. Na presença do metal, MorP desreprimiria MorS a qual realizaria autofosforilação, e, consequentemente, fosforilaria MorR. A MorR fosforilada desligaria do promotor σ_{70} e seria capaz de activar a transcrição da *mor*P via promotor σ_{54}. Desse modo, acredita-se também que a MorR possui um mecanismo de auto-regulação.

Termos chave: Sistema de dois componentes, Molibdénio, bactéria sulfato redutora, factores de transcrição, clonagem, purificação e caracterização bioquímica de proteína, footprinting, espectroscopia de fluorescência.

ABSTRACT

DNA-Protein interaction: a response regulatory protein associated with Mo homeostasis in *Desulfovibrio alaskensis* G20

The environmental signal transduction is fundamental for bacteria survival and adaptation to different habitats. The two component system is an important mechanism for the perception and transduction of the biochemical signal in bacteria. This system is composed by a histidine kinase and a responsive regulatory protein acting together in order to provide all the biochemical plasticity for the microorganism adaptation and survival.

The discovery of a Mo responsive homeostasis system in *Desulfovibrio alaskensis* G20 opened new questions about the mechanisms involved in the regulation of this metal in sulfate reducing bacteria. In this way, it was postulated that three proteins (MorP, MorS, and MorR) could be involved in the homeostasis of Mo. The MorP ("molybdenum response associated protein") is a periplasmic multimeric protein composed by 16-18 subunits. EXAFS studies together with biochemical characterization data showed the presence of a heterometallic center, Mo-2S[2Fe-2S]-2S-Mo, shared by two subunits, where each monomer has one atom of Mo and one atom of Fe. The MorS and MorR might constitute a two component system where MorR might acts as a σ_{54} transcriptional factor for *mor*P gene (the gene responsible for the codification of MorP).

The general objective of this thesis is to verify if MorR interacts with the intergenic region between *mor*P and *mor*S, and analyze how this interaction occurs. Additionally, it does intend to verify the influence of phosphodonors molecules on MorR oligomerization.

The present thesis is divided into five chapters.

The chapter I is formed by a general introduction about sulphate reducing bacteria and the importance of molybdate for *Desulfovibrio genus*. This chapter gives an introduction of Two Component System (TCS) and its components. Additionally, some mechanisms of prokaryotic gene expression, regulation and examples of transcriptional factors involved with TCS are also presented. Finally, the hypothesis of the present work is exposed.

The chapter II is constituted by the methodologies and agents used to clone the *mor*R gene. Those strategies allowed the success of the *mor*R cloning and permitted the expression of the MorR protein both in small and in large scale, resulting in a soluble form of the protein. Additionally, the genomic context of *mor*R gene is evaluated and discussed.

The chapter III gives an introduction about some studies of phosphorylation of proteins that shares similarities with MorR. This chapter shows the results of protein purification and biochemical characterization. The purified protein is a monomer, the purification yields is 0.5mg of pure protein per liter and the recombinant MorR does not contain neither metals (Zn^{2+}, Mo, Cu^{2+} and Mg^{2+}) nor phosphoamino acids and therefore is not isolated in a phosphorylated state. The intergenic region between *mor*P and *mor*S was amplified and purified and Electrophoretic Mobility Assay was performed in order to show if MorR binds to this region. The results obtained revealed that MorR is binding to the intergenic region and the DNase I footprinting experiments identified the specific binding sites. Acetylphosphate and phosphoramidate were used to phosphorylate MorR, and the results obtained did not show any oligomerization upon phosphorylation of MorR.

The chapter IV is composed by a brief introduction about some fluorescence spectroscopy concepts and by the results obtained using this technique. The prototropic form of 6-FAM-67mer carrying the target intergenic region was determinate in order to define which fluorescein specie is present under experimental procedures. The results showed that the fluorescence emission of the monoanionic form predominates under pH 7.5 and that the fluorescence emission of the dianionic form starts to emerge above a pH of 8. The association between MorR and two different (in length) target intergenic region was assessed by fluorescence anisotropy studies and the analysis revealed the presence of two independent binding sites. The result identified two association constants: 15.5 μM^{-1} for the first binding site and 0.02μM^{-1} for the second binding site. The MorR conformational change induced by phosphorylation was investigated using acetylphosphate and phosphoramidate as small phosphodonors. The results showed that MorR phosphorylates, but the fluorescence emission of tryptophan does not shift during the experiment. This result corroborate with the idea that MorR does not alter its structure upon this stimulus. A computational biochemical study identified that phosphorylation of serine residues is kinetic and thermodynamically more favorable with phosphoramidate than acetylphosphate.

The chapter V is composed by the conclusions of the present study and we propose a mechanism that hopes to explain how MorR acts as a transcriptional regulator of genes involved with Mo homeostasis. In this way, our model propose that, in the absence of Mo, the MorR acts as a repressor of the transcription of the *mor*SR genes (via σ_{70}) and would be inactive for the transcription of the *mor*P gene (via σ_{54}). In this context, MorP would acts as a repressor of the protein MorS, which might be incapable to perform autophosphorylation, and, consequently, all the system would be inactive. In the presence of the metal, MorR would derepress MorS which would be allowed to peform autophosphorylation, and, consequently, phosphorylate MorR. The phosphorylated form of MorR would disrupt the binding to the σ_{70} promotor and would be allowed to activate the transcription of *mor*P gene. Moreover, we believe that MorR has a mechanism of autoregulation.

Keywords: Two component system, Molybdenum, sulfate reducing bacteria, transcriptional factors, cloning, purification and biochemical characterization of proteins, footprinting, fluorescence spectroscopy.

INDEX OF CONTENT

INDEX OF FIGURES

INDEX OF TABLES

ABBREVIATIONS

6-FAM	6- Carboxyfluorescein
4aHTH	Four-helix helix-turn-helix
α	Alfa
AAA+	Protein domain responsable for converting Adenosine Triphosphate hydrolysis to mechanical force
AgrA	DNA binding response regulator belonging to LytTR family
ABC	Ammonium bicarbonate
AmiR	RNA binding response regulator of amidase operon
W	Tryptophan
AraC	Response regulator of arabinose operon
ATP	Adenosine Triphosphate
β	Beta
BL21	Host cell for gene expression
nt	Nucleotide
bp	Base pair
Bprom	Prediction of Bacterial Promoters
BSA	Bovine Serum Albumin
CA	Histidine kinase catalitic domain
CAP	Catabolic Activation Protein
CheA	Chemotaxis protein A, histidine kinase
CheW	Chemotaxis protein W, purine binding
CheY	Chemotaxis protein Y, response regulator
CheZ	Chemotaxis protein Z, phosphatase
CHNS	Carbon, Hydrogen, Nitrogen and Sulfur elemental analysis
cI	Regulatory protein involved in the maintenance of lambda lysogeny
CIAP	Calf intestinal alkaline phosphatase
CpxA	Envelope stress protein, histidine kinase
*cpx*A	Gene for envelope stress protein, histidine kinase
CpxP	Envelope stress protein, periplasmic
*cpx*P	Gene for envelope stress protein that codifies the periplasmic protein
CpxR	Envelope stress protein, response regulator
*cpx*R	Gene for envelope stress protein that codifies the response regulator
*cpx*RA	Genes for envelope stress of two component system
CpxRA	Envelope stress two component system
CSIC	Consejo Superior de Investigaciones Científicas-Spain
D	Aspartic acid residue
DctD	C4-dicarboxylate transport system, response regulator
DEAE-FF	Diethylaminoethanol fast flow
DHp	Histidine kinase transmiter domain

DNA	Deoxyribonucleic acid
DrrB	Response regulator of the OmpR/PhoB subfamily
dsDNA	Duplex Deoxyribonucleic acid
DTT	Ditiotreitol
E.coli	Escherichia coli
EcoRI	Restriction enzyme obtained from Escherichia coli. R means R-factor
EDTA	Ethylenediamine tetraacetic acid
EMSA	Electrophoretic mobility shift assay
FeMoco	Molybdenum-Iron cofactor of nitrogenase
FIS	Factor of inversion
Fis-HTH	Factor of inversion helix-turn-helix
FITC	fluorescein isothiocyanate
FliM	Flagellar motor switch protein
*gln*A	Gene of glutamine synthetase
*gln*AP1	Promoter for bacterial nitrogen regulation
*gln*AP2	Promoter for bacterial nitrogen regulation required during nitrogen starvation
GlnB	PII protein involved in signalling in glutamine synthetase and regulation of NtrB activity
*gln*LP	Promoter for bacterial nitrogen regulation, autoregulation of NtrC
GlnS	Glutamine Synthetase
HK	Histidine Kinase
HTH	Helix-turn-helix
HydG	Old nomenclature of zinc resistance response regulatory protein (ZraR)
*hyd*H	Old nomenclature of gene that codifies a zinc resistance histidine kinase protein
ICP-AES	Coupled Plasma Atomic Emission Spectroscopy
IDT	Integrated DNA technologies
IHF	Integration Host Factor
IPTG	Isopropyl β-D-1-thiogalactopyranoside
IRC	Internal reaction coordinate
MES	2-(*N*-morpholino)ethanesulfonic acid
ε	Epsilon
Kav	Distribution coefficient
kDa	kilo Daltons
kq	Bimolecular quenching constant
L	Lysine
l	Lambda
lacA	Gene of bacterial transacetilase of the lactose operon
LacI	Bacterial transcriptional repressor of lactose operon
l*ac*Y	Gene of bacterial permease of the lactose operon
*lac*Z	Gene of bacterial beta-galactosidase of the lactose operon
LB	Luria Broth
LC-MS	Liquid chromatography mass spectrometry
nL	nanoliter

min	Minute
m/z	Mass-to-charge ratio
MS	Mass spectrometry
AGC	Automatic gain Control
ppm	One part per million
Da	Daltons
nr	Non-redundant GenBank coding sequencing (CDS) translations + protein data bank (PDB) + Swiss-Prot + protein information resources (PIR) + protein research foundation (PRF)
LytTR	atypical DNA binding domain
MALD TOF	matrix-assisted laser desorption ionization time of flight
mer	From Greek meros "part" denotes the oligonucleotide lenght
mg	Milligrams
mM	Micromolar
Mo	Molybdenum
Moco	Molybdenum cofactor
*mod*A	Molybdenum ABC transporter, gene of the periplasmic component
ModA	Molybdenum ABC transporter, periplasmic component
*mod*ABC	Molybdate transport genes
*mod*B	Molybdenum ABC transporter, gene of the membrane channel protein
ModB	Molybdenum ABC transporter, membrane channel protein
*mod*C	Molybdenum ABC transporter, gene of ATP binding protein
ModC	Molybdenum ABC transporter, ATP binding protein
ModE	Molybdenum ABC transporter, regulatory protein
*mor*P	Gene for molybdenum response associated protein
MorP	Molybdenum Response Associated Protein
MorR	Molybdenum response regulatory protein
morR	Gene for molybdenum response regulatory protein
morS	Gene for molybdenum sensor kinase protein
MorS	Molybdenum sensor kinase protein
MtrA	Response regulator of genes that codifies bacteria cell wall peptidases
NarL	Nitrate/nitrite response regulator
NbIR	Non-bleaching protein B
*nbl*A	A gene involved in phycobilisome degradation (bleaching)
NCBI	National Center for Biotechnology
NheI	Restriction enzyme obtained from Neisseria mucosa heidelbergensis
nm	nanometer
NMR	Nuclear Magnetic Resonance

NTP	Ribonucleoside triphosphate
NtrB	Bacterial nitrogen assimilation, histidine kinase
*ntr*B	Bacterial nitrogen assimilation, gene for histidine kinase
NtrC	Bacterial nitrogen regulatory protein
*ntr*C	Gene for nitrogen regulatory protein
NtrC 1	Nitrogen regulatory protein 1
OD	Optical Density
OmpC	Outer membrane porin, transport channel
OmpF	Outer membrane porin, transport channel
OmpR	Outer membrane porin, transcriptional regulator
PAGE	Polyacrilamide gel electrophoresis
PAS	Signal sensory domain named based on three protein that it appear (Per, Arnt, Sim)
Pb	Lead
PCR	Polymerase chain reaction
PDB	Protein Data Bank
pET	plasmid vector for cloning
PleD	Diguanylate cyclase
PMF	Peptide Mass Fingerprint
pmol	picomole
ppb	One part per billion
P_{RM}	Promoter for repression maintenance
qRT-PCR	Real time quantitative polymerase chain reaction
REC	Response regulator domain
R-finger	Arginine finger
RNA	Ribonucleic acid
RNAP	Ribonucleic acid polymerase
rpm	Revolutions per minute
RpoS	sigma 38 factor
RR	Response regulator protein
rRNA	Ribosomal ribonucleic acid
S	Sulfur
σ	sigma
SDS	Sodium dodecyl sulfate
SMART	Simple modular architecture research tool
SOC	Super Optimal Broth
SRB	Sulfate-reducing bacteria
STAGE-TIP	Stop And Go Extraction Tip
T4 DNA Ligase	Recombinant enzyme from *Escherichia coli* NM 989.
T4 PNK	T4 Polynucleotide Kinase
TAE	Buffer Tris-Acetate-EDTA
TAT	Twin Arginin Translocation
TCD	Thermal Conductivity Detector
TCS	Two Component System
TFA	Trifluoroacetic acid
TMA	Trimethyllamine
TMAO	Trimethylamine N-Oxide
TorA	Trimethylamine N-Oxide reductase I, catalytic

	subunit
TorC	Trimethylamine N-Oxide reductase I, cytochrome c-type subunit
*tor*CAD	Genes for trimethylamine N-oxide reduction system
TorD	Chaperone involved in maturation of TorA subunit of trimethylamine N-oxide reductase system
TorR	Trimethylamine N-Oxide reductase system, response regulator
*tor*RTS	genes for trimethylamine N-oxide two component system
TorS	Trimethylamine N-Oxide reductase system, histidine kinase
TorT	Trimethylamine N-Oxide reductase system, periplasmic protein
Trp	Tryptophan
UV-VIS	Ultraviolet Visible
ω	omega
w-HTH	winged helix-turn-helix
YJAI	Old nomenclature of periplasmic zinc resistance associated protein
Zn	zinc
ZraP	Periplasmic zinc resistance associated protein
*zra*P	gene for zinc resistance associated protein, the periplasmic protein
ZraR	Zinc resistance associated protein, the regulator
*zra*R	gene for zinc resistance associated protein, the regulator protein
ZraS	Zinc resistance associated protein, the histidine kinase
*zra*S	gene for zinc resistance associated protein, the histidine kinase
*zra*SR	gene for zinc resistance associated two component system

Chapter I
General Introduction

Chapter I

General Introduction

Context

The base of the present study is the bacterium Two Component System (TCS) that can be involved in Mo homeostasis. The prototypic TCS is formed by a histidine kinase (HK) sensor protein and a response regulator (RR). In the presence of an environmental stimuli, the sensor autophosphorylates and transfer the phosphoryl group to the cognate RR. The activated (*i.e.* phosphorylated) RR can participate in different metabolic circuits. Usually, RR acts as transcriptional activators that binds to DNA and interacts with RNA polymerase in order to orchestrate gene transcription. In *Desulfovibrio genu*s, some proteins are regulated by molybdenum (Mo) or contain this metal in its structure. The genome analysis of *Desulfovibrio alaskensis* G20 predicts the presence of genes involved in Mo transport, but there is no report about the Mo uptake or regulation in this bacterium. The discovery of MorP (the molybdenum response associated protein) opened new insights about the molecular mechanism of molybdenum regulation in sulphate reducing bacteria (SRB). In order to understand how Mo can influence in gene transcription in *D. alaskensis* G20, a general introduction about SRB and the importance of Mo to the bacterial proteins are presented. Moreover, the principal aspects of the TCS and gene transcription initiation are described with a special focus on transcriptional factors belonging to TCS and genetic regulation in bacteria. Finally, this introduction presents the hypothesis of the present study.

Chapter I

I.1. Sulphate reducing bacteria

Microorganisms have a broad capacity to sense and rapidly respond to oscillations in the environment. This characteristic is vital to their adaptation and survival. *Escherichia coli*, *Bacillus subtilis* and *Saccharomyces cerevisiae* have been used as model for the primary comprehension of the gene expression profile in response to environmental changes. However, the prokaryotic phylogeny is diverse and the prediction of a universal code of stress response becomes difficult to follow. A primary mechanism involved in signal transduction includes histidine kinase (HK) proteins belonging to Two Component System (TCS). A comparative analysis of 5.000 HK from 207 sequenced prokaryotic genomes showed that many signaling events were recently developed in the course of evolution and that some regulatory systems are not found in the key model microorganisms[1,2].

Sulfate-reducing bacteria (SRB) are a diverse group of anaerobic, heterotrophic and mixotrophic bacteria. These bacteria can be found widespread in anoxic habitats and have in common the ability to use sulfate as a terminal electron acceptor in the respiratory process. They are capable of tolerating a relative wide range of environmental changes, such as: temperature, pH, chloride concentration and pressure[3]. Additionally, they show high plasticity in finding alternative metabolic routes in order to survive, such as the reduction of energy metabolism through downregulation of ATPase genes[4,5]; the osmoprotection by accumulating the glycine betaine (a cellular osmoprotectant) concentration[6] and the defensive mechanisms against the reactive oxygen species (ROS). The ROS protection is an important feature of SRB since those microorganisms are anaerobes and need to control the oxidative stress and ROS production. This feature reflects in the increase diversity of proteins involved within this process, such as the rubredoxin oxidoreductase (Rbo)[7]and therubrerythrin (Rbr)[8], all of them conserved among SRB and essential to scavenge ROS without regenerating O_2. SRB are important in biotechnology and engineering, since they can be used in heavy metal bioremediation and sulfur compound removal from waste materials. On the other hand these bacteria can cause serious problems in industry because of sulfide production, which is a major cause of corrosion and degradation of metallic equipment [9].

SRB can be divided into four groups based on rRNA sequence analysis: Gram-negative mesophilic SRB, Gram-positive spore forming SRB, thermophilic bacterial SRB, and thermophilic archaeal SRB. *Desulfovibrionaceae* include a large family of Gram-negative mesophilic SRB, which comprise the genera *Desulfovibrio* and *Desulfomicrobium*[10]. Until now, 26 *Desulfovibrio* genomes of SRB are available, and the genome of *Desulfovibrio alaskensis* G20 was recently updated[11].

The *Desulfovibrio alaskensis* G20 (formerly *Desulfovibrio desulfuricans* G20) is a gram-negative mesophilic SRB that belongs to the delta subdivision of the Proteobacteria. The genome of delta subdivision is characterized by the presence of multiple copies of detoxification genes like rubrerythrin and the presence of predicted highly expressed σ_{54} activator proteins[12]. Moreover, this strain can growth syntrophically, but no conserved genome feature has been identified as the cause of this ecological ability[13]. The microbial syntrophy under methanogenic conditions requires a mutual cooperation in order to transfer H_2 or formate for electrons transferring. This type of interaction occurs between *Desulfovibrio alaskensis* G20 and *Methanospirillum hungatei* (methanogen bacteria), which is capable to induce *Desulfovibrio alaskensis* G20 growth under lactate and to produce acetate and H_2 (used by methanogen to produce CH_4). The quinine reductase complex (Qrc) and the tetrahaem periplasmic cytochrome c_3 (TpIc_3) is a family of redox complex that participate specifically in this process (of H_2 and formate metabolism) and that are required by *Desulfovibrio alaskensis* G20 to grow syntrophically with lactate[14].

I.1.1. Molybdate in *Desulfovibrio genus*

Molybdenum (Mo) is a trace element naturally occurring in the earth's crust (0.05 to 40 μg/g)[15–17]. In the group of transition metals is the most abundant in the ocean with residence time exceeding 800 thousand years[15,18]. It belongs to the fifth period of the periodic table, exists in the form of seven stable isotopes (Mo^{92}, Mo^{94}, Mo^{95}, Mo^{96}, Mo^{97}, Mo^{98} and Mo^{100}) with relative abundance of 9.2 to 24.2% and may be present in the oxidation state of -2 to +6. In rocks is mainly in the form of molybdenite (MoS_2) and in the presence of iron oxides and organic matter, even under anoxic environmental conditions, readily oxidizes to form the oxyanion molybdate (MoO_4^{-2})[15,16,18]. Molybdenum is essential

for nearly all living organisms (from bacteria to animals) and it is important for enzymatic reactions and acts as co-factor of proteins that are responsible for electron transfer in the processes of nitrogen fixation[19–22]

It is biologically available in the form of molybdate (MoO_4^{2-})[20]. In bacteria, molybdate enters the cell through specific transporters that are coded and regulated by the *mod*ABCD operon[23]. Inside the cell, molybdate is integrated into metal cofactors, such as Moco in mononuclear Mo enzymes or FeMoco in nitrogenase[24].

The *mod*ABCD operon is composed by four genes that are transcribed into a single polycistronic mRNA that codify proteins involved in Mo and W cell uptake and transport[25]. The *mod*A gene encodes a periplasmic molybdate binding protein ModA that is indispensable for high affinity of molybdate uptake by the bacteria cell [26,27]. The *mod*B gene encodes an integral membrane protein ModB which forms a twelve transmembrane helices of a membrane channel of the ModABC transporte′s. The *mod*C encodes an ATPase (ModC) subunit of the ModABC complex that energizes molybdate transport. The interface between ModC and ModB induce conformational changes that allow ATP binding and hydrolysis and subsequent transport through the channel. The *mod*D gene encodes a putative 231 amino acid residues protein of unknown function[28]. The crystallographic structure of the ModABC from *Archeoglobus fulgidus* shows a presumable pentameric $ModAB_2C_2$ quaternary structure and illustrates how the proteins are organized in order to perform the molybdate uptake[29] (figure I.1).

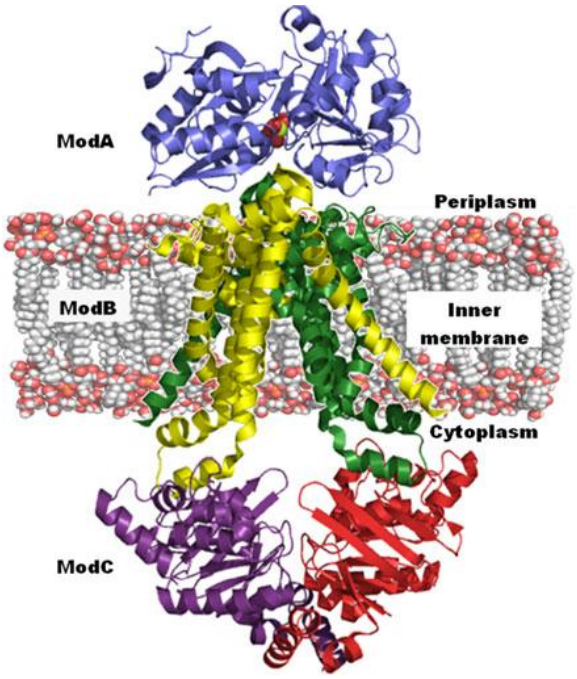

Figure I. 1.Strucuture of $ModAB_2C_2$ transporter from *Archaeoglobus fulgidus*. The ModA with Mo is represented in blue, the ModBin yellow and green and ModC in red and magenta. Taken from Aguilar-Barajas (2011) Biometals, 24, 687-707.

*mod*ABCD genes are negatively controlled by ModE protein, which binds *mod*A operator sequences. In the absence of molybdate ModE derepresses the *mod*ABCD operon allowing transcription. ModE controls its own transcriptional level through a divergent promoter (figure I.2) [30,31].

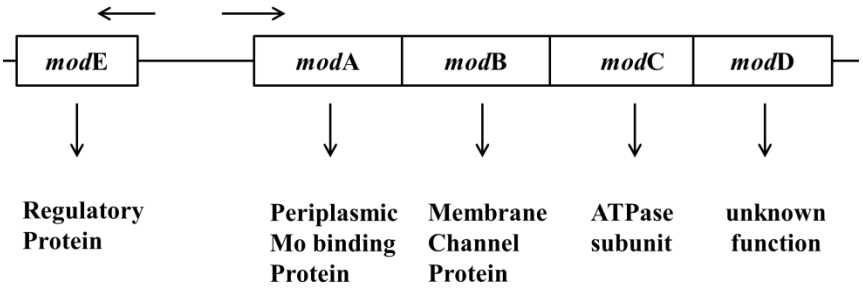

Figure I. 2.The *mod*ABCD operon from *E.coli*. The arrows above the genes represent the transcriptional orientation mediated by ModE protein.

The enzymes whose activity depends on Mo, such as sulfite oxidase, xanthine oxidase and nitrate reductase, incorporate this metal ion into a cofactor known as Moco[32]. Moco is a pyranopterin-dithiolene moiety where Mo ion is covalently bound to the dithiolate moiety. Moco is an instable molecule and it is believed that the dithiolate group

contributes to the lability. The cofactor has a tricyclic pyranopterin structure with pyrimidine , pyrazine and pyran rings forming the organic moiety of Moco (often called molybdopterin (MPT)) (figure I.3). The phosphomethyl group is also labeled in the pyran ring. The Mo and W are coordinated by two dithiolene sulfurs that are attached to the pyran ring[33].

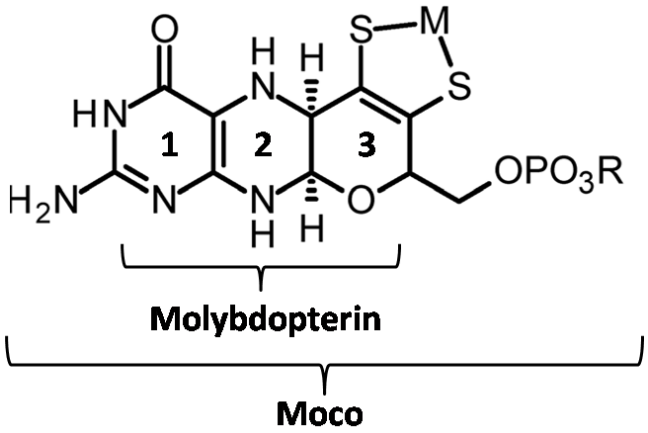

Figure I. 3. Structure of molybdenum cofactor (Moco) in the tricyclic form. 1) Pyrimidine ring. 2) Pyrazine ring. 3) Pyran ring.

Organisms from all kingdoms share a conserved pathway to synthesize Moco[34]. In bacteria, three major steps are necessary to synthesize Moco: 1- conversion of guanosine nucleotide (GTP) into cyclic pyranopterin monophosphate (cPMP); 2- Synthesis of MPT and 3- Molybdenum incorporation into MPT. The first step requires MoaA (belonging to S-adenosylmethionine-dependent radical enzyme superfamily) and MoaC that uses 5′-GTP to forms cPMP[35,36] (figure I.4). The resulted cPMP molecule is similar to MPT but lacks the dithiolene group. The second step requires the incorporation of two sulfur atoms at the C1′ and C2′ positions of cPMP. This reaction is performed by a heterotetramer MPT synthase complex that is formed by a central MoaE dimer and two MoaD subunit positioned at each MoaE side[37]. The last step is the incorporation of the metal into the MPT. This reaction requires the participation of the trimeric MogA protein which binds MPT with high affinity and mediates the ligation between MPT and Mo *in vitro*[38,39]. In humans, defects in the biosynthesis of Moco can leads to profound neurologic abnormalities in neonates[40].

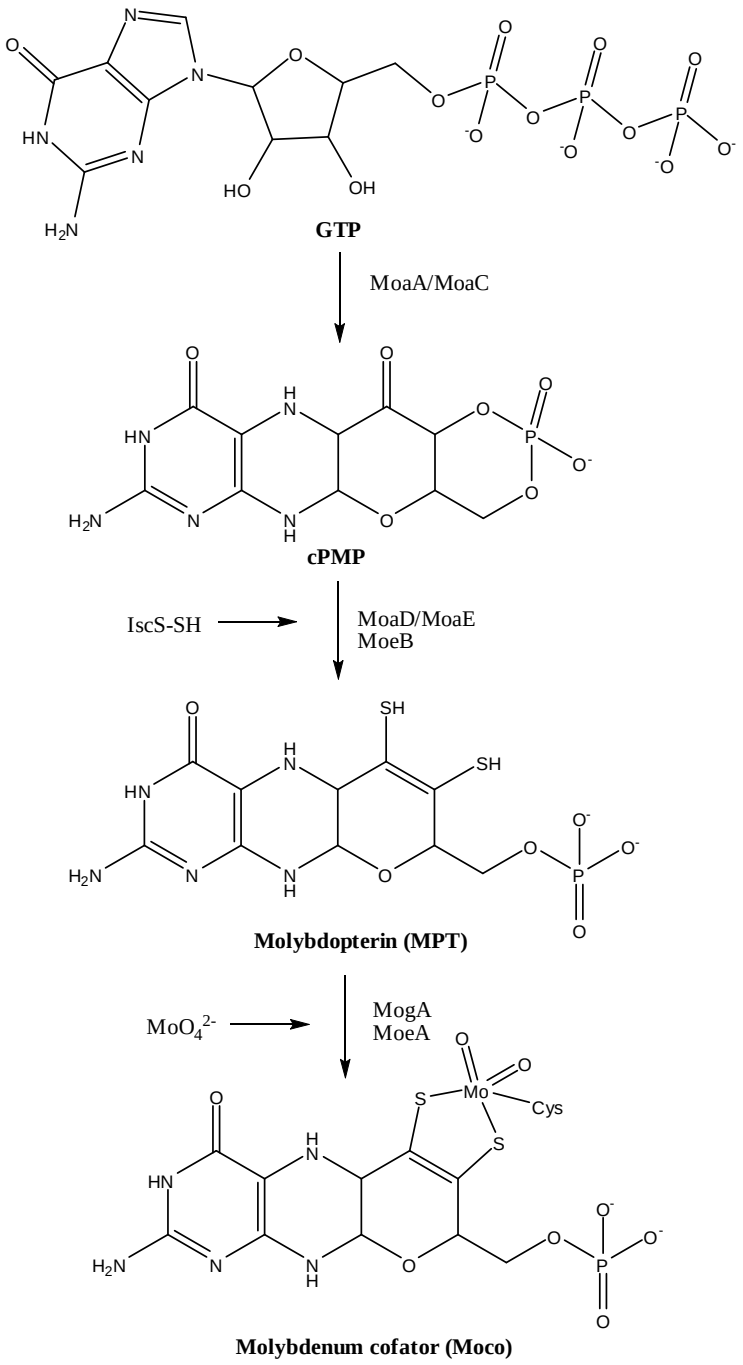

Figure I.4. The three steps of molybdenum cofactor biosynthesis

In bacteria from *Desulfovibrio genus* the role of molybdate uptake via mod operon is not elucidated yet. However, the conserved genome characteristic of *mod*ABC transporter is present in *Desulfovibrio* species genome (NCBI Gene ID 2795627) whereas there is no report about the mechanisms of molybdate transport in SRB. Conversely, it is known that some Mo proteins from *D. gigas*, *D. africanus and D.salaxigens* have been

isolated and characterized [41,42,43,44]. Such an example is the Orange Protein (ORP) that presents a Mo-Cu-S cluster. Of the utmost importance was the recent characterization of the structural instability of the ORP cofactor and the gene transcriptional regulation of *orp* from *D. vulgaris* Hildenborough. In this context, the protein locus tag (called *DVU2108*) that shares 48% of identity with ORP was identified. *DVU2108* is regulated by a σ_{54} transcriptional factor and, in conjunction with other enzymes, may play a role in cell division is SRB[45,46]. Additionally, some studies showed that Mo is an important metal in *Desulfovibrio* formate dehydrogenase (FHD) and *mod* gene expression[47,48]. In this way, Mo is capable to upregulate the *Mo/W-fdh* gene expression whereas downregulate the genes responsible for Mo transport. The *Mo/W-fdh* gene codifies a FDH that incorporate Mo or W in its structure. Moreover, isoforms of FDH, such as $FdhABC_3$, present specific behavior and the incorporation of Mo ion into the active site of FDH is selective.

The discovery of a molybdenum response associated protein (MorP) led to the hypothesis that this protein could be involved in a Mo homeostasis. MorP is a periplasmic homomultidimer (16-18 subunit) of high molecular mass (260 ± 13kDa). The authors suggested that each homodimer sharing a Mo-2S-[2Fe-2S]-2S-Mo cluster and therefore MorP can carry up to 16 Mo atoms per protein. The genomic analysis revealed a putative σ_{54} promoter, a putative sensor (*Dde*_0110), and putative regulator (*Dde*_0109), all located upstream of *mor*P. A blast search showed that MorP exhibits 40% of similarity with ZraP, which is present in *Desulfovibrio vulgaris* Hildenborough genome. qRT-PCRshowed that expression of *Dde*_0109 was up-regulated when molybdenum was present during bacterial growth. Based on these results, a mechanism of Mo homeostasis was proposed. It predicts that, in the presence of Mo, the TCS present upstream of *mor*P gene might be responsible for its transcriptional activation. In this way, the MorS (the putative sensor protein located at periplasmic membrane) senses the Mo present in the periplasmic space leading to MorS autophosphorylation. Then the phosphoryl group is transferred to MorR (the putative cognate response regulator) leading to its activation. Once MorR is activated, it is allowed to interact with σ_{54} promoter sequence in order to activate the transcription of *mor*P gene(figure I.5)[49]

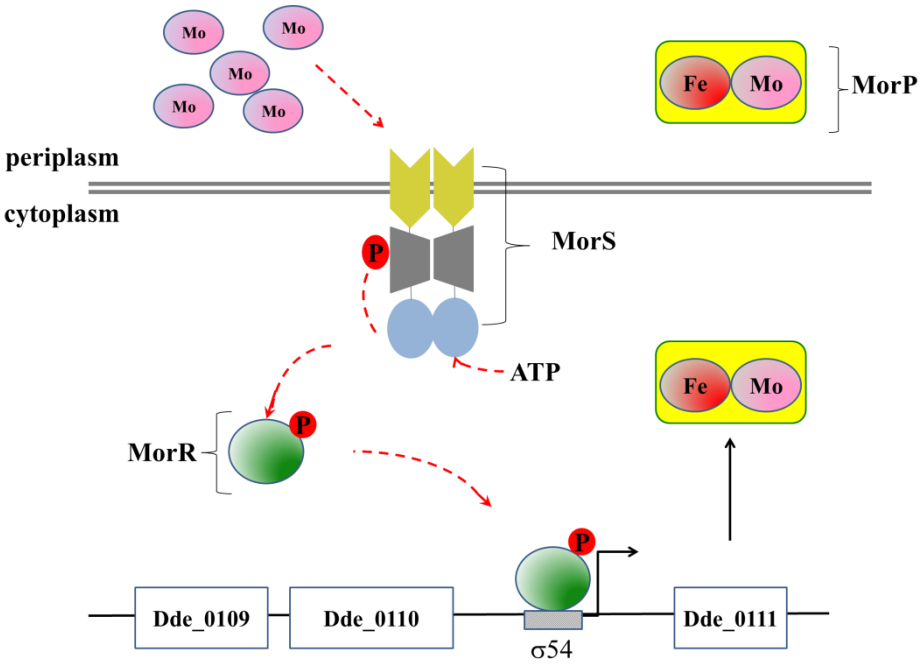

Figure I. 5.Model for transcriptional activation of *mor*P gene under control of a σ_{54} two component system.

The two component signaling proteins are among the most prevalent bacterial genes and are easily identified by sequence homology. Bacterial genomes analysis revealed that the total number of two component genes per genome is proportional to genome size and ecological niches preferences. Therefore, two component systems is one most abundant in genomes of gram-negative bacteria and cyanobacteria[50].

I.2. Introduction of TCS

Bacteria have the ability to occupy a broad range of habitats, from soil to human intestine. Changes in osmolarity, nitrogen or carbon sources are some of the common environment fluctuations that bacteria face during development, as a response to these changes in the course of bacteria evolution; a mechanism of adaptation called TCS was selected. TCS allows the bacteria to sense and respond quickly to environmental stimuli in order to survive. In this way, a signal transduction system composed by a sensor and a response regulator represents a prototypical form of TCS[51].

I.2.1. Sensor

The sensor, a component of TCS, is a dimeric histidine kinase (HK) protein responsible for sensing the environmental stimuli. A prototypical HK consists of three domains: a membrane associated sensor domain which recognizes the extracellular signals (Sensor), a cytoplasmic transmitter domain responsible for dimerization and histidine phosphotransfer (DHp), and a catalytic and ATP binding (CA) domain[52] (figure I.6). This prototype pursues the sensor domain as an extracellular loop located between two membrane-spanning segments. The DHp and CA domain forms the transmitter domain which is more conserved among bacterial response regulators and may reflect a common mechanism of output interection[53].

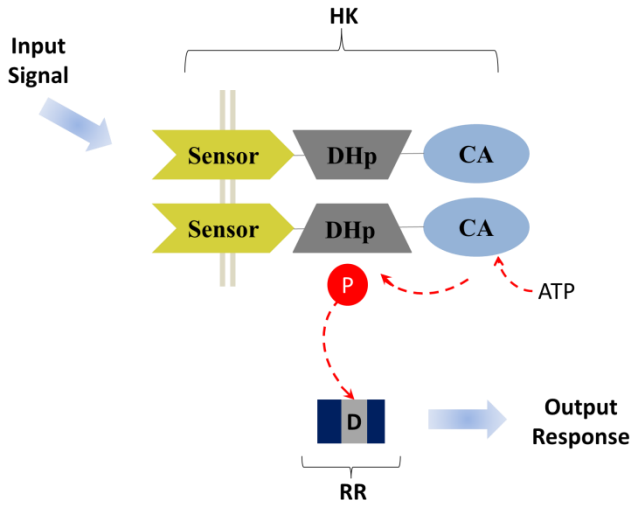

Figure I. 6.Prototypic form of two component system. The histidine kinase (HK) senses the environmental stimuli (input signal), autophosphorylates, then transfer the phosphoryl group to the cognate response regulator (RR). Adapted from Richard C. Stewart (2010) Curr. Pin. Microbiol, 13: 133-141

In spite of the architecture similarities between HK, the sensor domain shows specific structural variability which relies on its capacity to undergoes a variable input signal perception[54]. The sensor domain can deviate from the prototypical extracellular profile to membrane-embedded or intracellular type. The extracellular model has as the main representative the proteins PhoQ, DcuS and CitA which sense divalent ions such as Mg^{2+}, C_4-dicarboxylates and citrate respectively (figure I.7 a). The triad is also called PDC sensors and is characterized by a long N-terminal α-helix region with a central five-strand antiparallel β-sheet scaffold. The central β-sheet share similarities with PAS domain, but

each one preserves its own functional characteristic[55–57]. As an example of a membrane-embedded sensor, Rhodopsin II (SRII) lacks the prototypical extracellular domain and the transmembrane segment is involved in signal perception (figure I.7b). SRII is a retinylidene protein that forms a complex with the transducer HtrII (halobacterial transducer of rhodopsin II) in order to regulated cell flagelar motor response through binding and modulating the activity of the CheA (a chemotaxis HK)[58–60]. In this way, CheA controls the phosphorylation status of CheY, a cytoplasmic flagellar mortor switch regulator. The combination between SRII-HtrII complex and CheY-CheA avoid photo-oxidative damage under sunlight exposure in the presence of oxygen[61]. Some sensor proteins can be entirely cytoplasmic, such as NtrB (figure I.7c). Others are cytoplasmic but membrane anchored: the cytoplasmic sensor domain can be found at N-terminal before the first transmembrane domain or after the second transmembrane domain (figure I.7d)[52]. In spite of the cytoplasmic sensor domain localization, all of them adopt a PAS fold. PAS is a family of signaling proteins that exhibit five stranded anti-parallel β-sheet core flanked by α-helices. The intracellular sensor can be exemplified by FixL that exhibit a heme-binding-PAS domain that senses O_2 in *Rhizobium meliloti* and participates in nitrogen fixation[62].

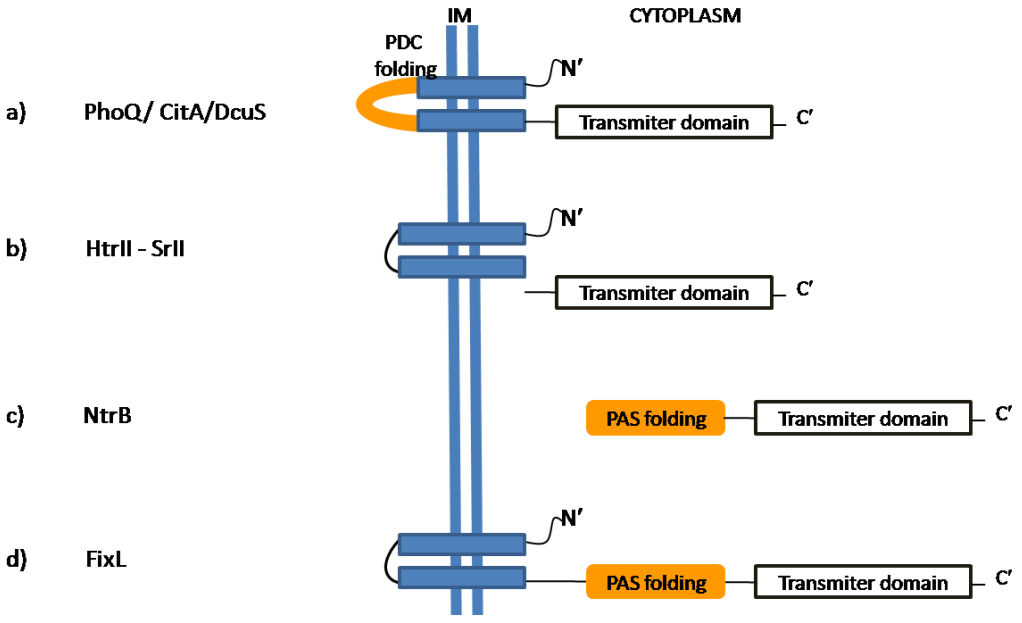

Figure I.7. The diversity of HK sensor proteins. a) PDC sensors where the extracellular domain senses the stimuli, b) HtrII-SrII where the sensor domain is membrane embedded, c) NtrB is a free cytoplasmic sensor domain, d) FixL is a membrane anchored that exhibit a cytoplasmic sensor domain with a PAS folding.

In bacteria, serine, tyrosine, threonine, histidine and aspartic acid residues are the preferable sites for phosphorylation[63–65]. However, the TCS pursue its own specificity for phosphorylation of the histidine residue in the sensor HK and for the acid aspartic residue in the RR. Upon activation, the HK undergoes phosphorylation of a conserved histidine residue at its DHp domain. This autokinase activity is a conserved characteristic of sensor proteins. After phosphorylation, the phosphoryl group is selectively transferred to an acid aspartic residue (D) localized in the cognate response regulator (RR). In this way, this system works in conjunction via specific protein-protein interaction between the HK and RR using three different strategies: the molecular recognition (the inborn capacity of the HK to recognize the cognate RR), the phosphatase activity (the HK dephosphorylate the cognate RR) and the substrate competition (the cognate RR competes for phosphorylated HK)[66]. Under the absence of an input stimulus, the HK is capable to drive *in vitro* dephosphorylation of its cognate RR, resetting or limiting the cross-talk[67].

I.2.2. Response regulator (RR)

Once the sensor protein of the TCS is phosphorylated, the phosphoryl group is transferred to a conserved D residue, located at the receiver domain of cognate RR. The phosphorylation of the RR drives a conformational change that induces its output response. However, the N-terminal receiver domain is not an inert partner in phosphotransfer. In fact, it has enzymatic activity catalyzing the phospho transfer from phospho His of HK to its own D residue. The phosphotransfer mediated by HK is not mandatory, and small molecules containing high energy phosphoryl groups can serve as phosphodonors (e.g. acetyl phosphate, carbamoyl phosphate and phosphoramidate) in *in vitro* reactions. Moreover, the RR has autophosphatase activity and regulates its own dephosphorylation. The modulation of the C-terminal effector domain is so far the most important activity known of the N-terminal regulatory domain[68,69]

All the RR proteins share a fundamentally similar strategy. They couple phosphorylation to regulation. Still, the mechanisms of regulation themselves are varied, and the diversity of effectors domains create a variety of output signals. 17% of prokaryotic RR exists as a single receiver regulator (REC) domain, as exemplified by CheY family. Members of the CheY family contain a conserved aspartic acid residue, corresponding to

D57 in CheY, and a conserved lysine residue, corresponding to L109[70]. Beyond the phosphorylation coupled to signal transduction, CheY lysine acetylation have been reported *in vitro* and *in vivo* and this post-translation modification inhibit the binding between CheY to CheA (the HK), CheZ (phosphatase) and FliM (flagellar motor switch protein)[71,72]. The majority of RR (63%) binds to DNA (e.g. OmpR, NarL, AgrA and NtrC) and the output response is associated with transcriptional activation or repression. The remaining RR are diverse and can associated with several functions, such as protein/ligand binding (CheW), enzymatic activity (PleD), RNA binding (AmiR)[73].

I.2.2.1.TCS RR and DNA binding

The majority of RRs contain a C-terminal tri-helical helix-turn-helix (HTH) DNA binding domain or a variation (e.g. winged helix-turn-helix (wHTH), four-helix helix-turn-helix (4αHTH), factor of inversion helix-turn-helix (Fis-HTH) and an atypical form called LytTR domain) (figure I.8)[74,75,76,77].

Figure I. 8.Diversity of the C-terminal domain between the DNA binding regions of examples of response regulators. In red: the REC is the common N-terminal receiver domain. In blue: the NtrC central AAA+ ATPase domain. In green: the C-terminal DNA binding domain.

The tri-helical domain is a simple structure that is complementary to the structure of B-DNA. It has a conserved recognition region where the 2nd and 3rd helices form the HTH (figure I.9). The HTH was the first DNA-recognition motif discovered, and includes a great number of DNA binding proteins, such as: Catabolic Activation Protein (CAP), LacI, 434 repressor, Trp repressor and Fis protein[78,79].

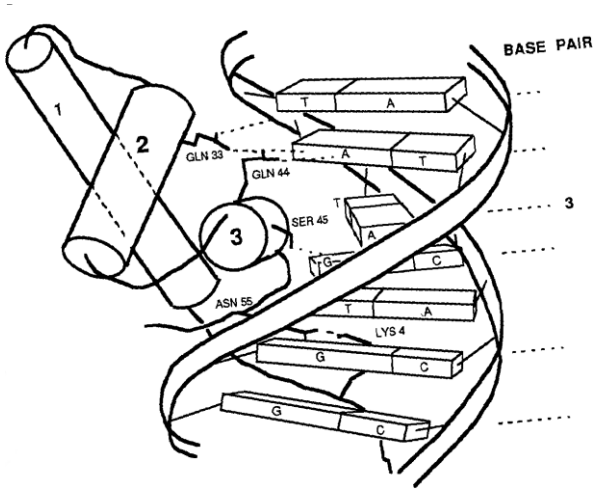

Figure I. 9.HTH motif and DNA interaction.Taken from Carl O. Pabo (1992) *Annu. Rev. Biochem*, 61, 1053-1095.

I.3. Prokaryotic gene expression and regulation

In order to comprehend how RR protein acts, it's important to understand some basic concepts of gene regulation in bacteria. Gene transcription begins with the copying of a segment of DNA into RNA, and in bacteria gene expression is frequently regulated at this level. The RNA polymerase (RNAP) is the enzyme responsible for gene transcription. The *E.coli* RNAP core is constituted by a complex ($\alpha_2\beta\beta'\omega$) that forms a stable complex in the presence or absence of DNA[80]. Bacteria contain just one form of RNAP. The structure of bacterial *E.coli* and *Thermus aquaticus* RNAP showed conserved features and both resembles as a "crab claw" where β and β′ subunits forms the two pincers, the α subunit forms a dimer and the ω constitutes the smallest subunit that is associated primary with the β′ subunits (figure I.10). Moreover, RNAP requires Mg^{2+} for catalytic activity [81,82]. RNAP is incapable of initiate transcription, but the α subunit can recognize promoter elements and participates in the initial steps of RNAP assembly[83,84]. Additionally, the α subunit consist of two independent domains: an N-terminal domain (α-NTD) and a C-terminal domain (α-CTD) that are connected by a flexible linker where the α-CTD is capable of dimerization and DNA binding[85,86].

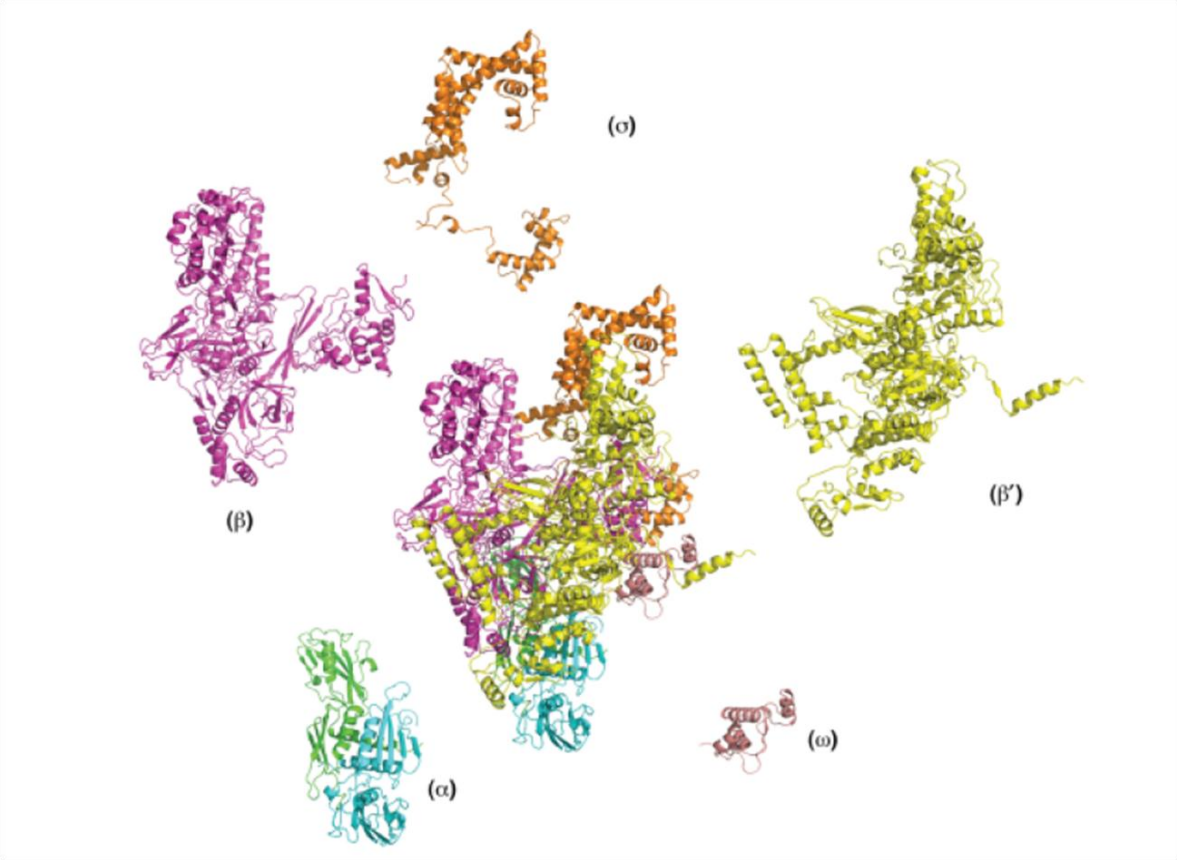

Figure I. 10 Structural organization of each subunit of bacterial core RNAP and the holoenzyme: β (magenta), β′ (yellow), α NTD (green/cyan), ω (pink) and σ (orange).Taken from Tamaswati Ghosh *et al.*, (2010) *FEBS Microbiol Rev*, 34, 611-627.

The specificity of RNAP is determined by a small key element called sigma (σ) which carries the major determinant for promoter recognition[87]. The σ_{70} and σ_{54} are the main subunits used by RNAP for transcription initiation. The σ_{70} is a large family of σ factors phylogenetically formed by fours groups[88,89]. The σ_{70} in *E.coli* belongs to group 1 (the housekeeping σ) and in conjunction with RNAP binds at promoter DNA sequences[90]. The σ70 is formed by fours structural domains (σ1.1, σ2, σ3 and σ4) where σ1.1 controls the DNA binding and σ2, σ3 and σ4 recognize the -10 and -35 conserved boxes[82,91,92].

The term holoenzyme is used to identify the complex formed by the core RNAP and the σ factor. Both holoenzymes form a stable closed complex, and the difference between them is that RNAPσ_{70} enables immediate transcription initiation, while the RNAPσ_{54} requires mechano-transcriptional activator proteins. The latter holoenzyme uses

ATP hydrolysis to drive a DNA conformational change essential for transcription initiation[93].

Transcription is divided into three steps: initiation, elongation and termination. The general aspects of transcription initiation involve the binding of the holoenzyme to a promoter sequence. This initial structure, named closed complex, is converted to an open complex in which a localized separation of the two DNA strands occurs. This exposes the bases of the coding strand, enabling the base pairing of the ribonucleoside triphosphates (NTP) for synthesis of the RNA. The first phosphodiester bound is formed and the σ factor dissociates from the complex. From this point forward, the core enzyme alone is required for extension of the RNA strand until reaching a termination signal when the mRNA and the RNAP are released[93].

I.3.1.Housekeeping σ_{70} and transcriptional factors

The interaction between the housekeeping RNAPσ_{70} and transcriptional factors is the base for the discernment between transcription activation and repression. Transcriptional factors can be classified as activators or repressors according to their interaction with RNAP and promoters. In the next section, some examples illustrate the main factors involved in transcriptional regulation by activators and repressors proteins.

I.3.1.1. Transcription activation

A particular activator molecule binding at a bacterial target promoter constitutes the simplest state for RNAPσ_{70} transcription initiation. This mechanism acts by stabilizing the RNAPσ_{70}-promoter complex or by accelerating the open complex formation[94].

The stability of RNAPσ_{70}-promoter complex can be exemplified by the MerR protein that belongs to mercury-resistence transposon Tn501. The Tn501 contains the *mer* operon which is divergently transcribed and is formed by genes for Hg detection, transport, mobilization and enzymatic detoxification, such as *mer*R, *mer*D, *mer*P, *mer*T and *mer*A, respectively[95,96]. The MerR protein exhibit transcriptional plasticity once negatively controls its own synthesis and also regulates either positively (in the presence of Hg) or negatively (in the absence of Hg) the *mer* genes[97]. The nonoptimal space (19bp) between -10 and -35 promoter create a barrier for RNAPσ_{70} initialization, since the -10 element is

misplaced, hindering the interaction with the σ subunit. The MerR transcriptional regulator causes a twist in the spacer producing a conformation change that allows transcription initiation by RNAPσ_{70} (figure I.11)[98–100].

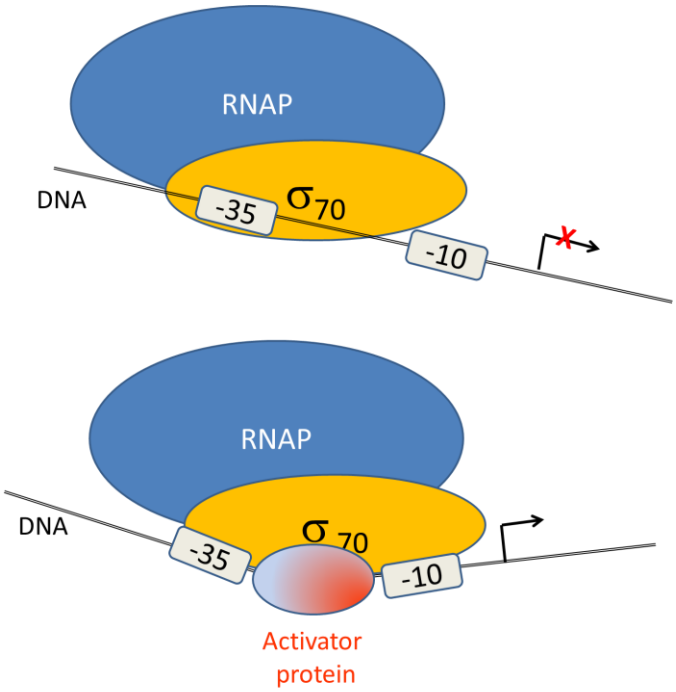

Figure I. 11.Mechanism of RNAP complex stability mediated by an activator protein.Adapted from David J. Lee (2012) *Annu. Rev. Microbiol*, 66: 125-152

The bacteriophage λ cI protein is another example of how transcriptional regulators orchestrate its function in order to make efficient transition between the lytic and lysogenic cycles. The λ cI is primary a homodimer transcriptional repressor of the lytic promoters. A cooperative binding between pair of dimers occurs through CTD contact when λ cI is bound to DNA and this feature improves a strong repression[101–103]. During lysogen, preventing transcription of lytic genes and continuous maintenance of λ cI are important. For constant λ cI production, a direct contact between the λ cI and σ4 subunit of RNAP holoenzyme may occur and this interaction induces the λ cI own transcriptional expression by the open complex formation[104–106]. The λ cI binds to a target DNA, either upstream of or overlapping the -35 element and the residues E34 and D38 interact with the σ4 subunit. The studies involving λ cI protein and RNAPσ_{70} showed that activation occurs when both partners are bound to DNA[105] (figure I.12).

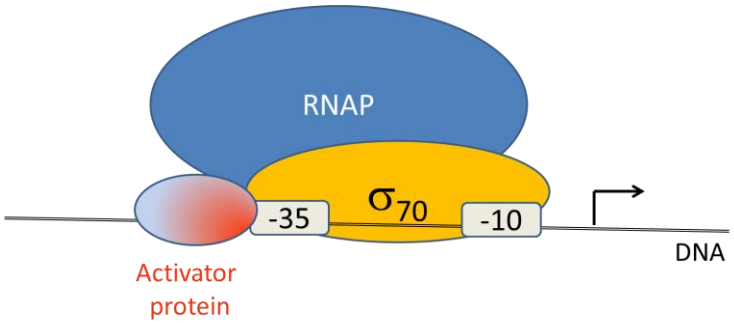

Figure I. 12. Mechanism of RNAP open complex formation mediated by an activator protein. Adapted from David J. Lee (2012) *Annu. Rev. Microbiol*, 66: 125-152

I.3.2.The σ_{54} regulation

The σ_{54} recognize promoter sequences usually located at position -24 and -12 relative to the transcriptional +1 start site. The main characteristic of RNAPσ_{54} is the inability to open the double strand DNA to form the open complex required for transcription initiation given that they depend on activator proteins, ATPases, members of the AAA^+ family. The ATP hydrolysis provide the energy needed to RNAPσ_{54} holoenzyme to isomerize from closed to open promoter complex.[107]

I.3.2.1. NtrC

The studies about NtrC (nitrogen regulatory protein C) provide a good source of information about how RNAPσ_{54} interacts with transcription factors. The well characterized promoter *glnA* of enteric bacteria is recognized by RNAPσ_{54} holoenzyme. The *glnA* gene encodes a Glutamine Synthetase (Gln*s*) and the transcription from *glnA* promoter occurs by the activated NtrC in response to nitrogen starvation[108]. The NtrC from *E. coli* is one example of a transcriptional mechano-activator protein that interacts with RNAPσ_{54} to prompt gene transcription[109]. NtrC binds to DNA located ~80 to 150 nucleotides upstream from the promoter they control (figure I.13, A) and, upon phosphorylation, it contacts RNAPσ_{54} by looping out the intermediary DNA (figure I.13, B). This process is facilitated by IHF (integration host factor) protein, which stimulates the DNA-bending[110].

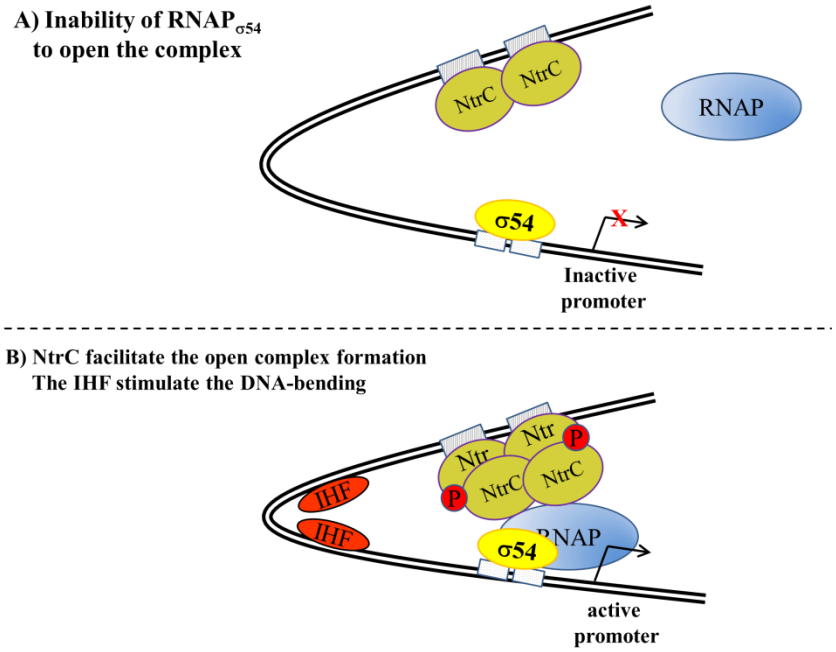

Figure I. 13.Mechanism of RNAPσ_{54} transcriptional activation mediated by NtrC protein.

The NtrC is composed by three domains: a N-terminal receiver domain, a central AAA+ ATPase domain, and a C-terminal Fis DNA binding domain. The unphosphorylated inactive form of NtrC is a dimer in solution and is able to bind DNA and ATP. NtrC has a conserved aspartate (D54) residue at the receiver domain, which is phosphorylated by NtrB (HK). Upon phosphorylation, NtrC is active as an oligomer, coupling the ATP hydrolysis to the formation of open complexes with RNAPσ_{54}[111]. The central domain of NtrC has two conserved sequences responsible for ATP binding and hydrolysis: the Walker A (GX_4GKT/S) and Walker B (h_4DE). Magnesium is essential to ATP binding and its absence results in fivefold decrease of affinity of NtrC to ATP[112]. The conserved GAFTGA motif senses the conformation adopted by the transcriptional activator. It interacts with the σ_{54} in order to form the transcriptional open complex[113]. The conserved R-finger might be involved in the intersubunit catalysis and ATP sensing. The oligomerization status constitutes a modulatory manner for ATPase activity. The central AAA+ domain is fused to HTH, the last belonging to Fis family. As previous described, Fis proteins constitute the simplest architecture of DNA binding structure and are responsible for induction of DNA bending [114].

The bacterial TCS developed many strategies to maintain the abundance of proteins. RR have the ability to function as activators and/or repressors, and have the capacity to control their own transcriptional level. The self-control of transcription is well characterized among RR that participate in TCS circuit[115,116].

As stated above, the NtrC controls the *glnA* promoter in response to low levels of nitrogen in bacteria. The *glnA* codifies the Glutamine synthetase (GlnS) which is important during bacteria growth because it is capable to converting glutamate to glutamine in medium containing low concentration of ammonia[117,118]. The *ntr*B/*ntr*C constitutes the TCS circuit for nitrogen assimilation in bacteria[119,120]. Those genes are organized as operon as shown in figure I.14. The operon is formed by *glnA*, *ntrB* and *ntrC* loci and contains three promoters: *glnAp1*, *glnAp2* and *glnLP*. The last is responsible for the unique autoregulation of TCS by NtrC. NtrC shows an ability to control the expression of the operon by interaction with $RNAP_{\sigma 70}$ and $RNAP_{\sigma 54}$. This interaction is not randomly organized and occurs according to nitrogen environmental oscillation. The *glnAp1* and *glnLP* are weak promoters used by the $RNAP_{\sigma 70}$ for transcription initiation[108]. This mechanism is capable to maintain a basal level of transcription of *glnA*, *ntrB* and *ntrC* during bacteria growth in nitrogen favorable conditions. On the other hand, the *glnAP2* promoter is required in response to nitrogen deprivation. This promoter is recognized by $RNAP_{\sigma 54}$ which is considered an alternative way for transcription[121]. In the absence of nitrogen source, the activated (phosphorylated) form of NtrC binds to *glnAP2* which is allowed to initiate transcription by $RNAP_{\sigma 54}$ to enhance *gnlA*, *ntrB* and *ntrC* transcription level[122]. The NtrB (the sensor) is responsible for NtrC activation. NtrB activity (phosphatase and kinase) is modulated by GlnB. GlnB is a protein regulated by small molecules that senses the nitrogen status. In the absence of nitrogen source, GlnB disinhibit the NtrB which is capable to autophosphorylate and transfer the phosphoryl group to NtrC. Then, the phosphorylated NtrC activates the transcription at *glnAP2* promoter. The inactive state of NtrC binds to *glnAP1* and *glnLP* and acts as a repressor deactivating the operon and returning to basal level of transcription[123].

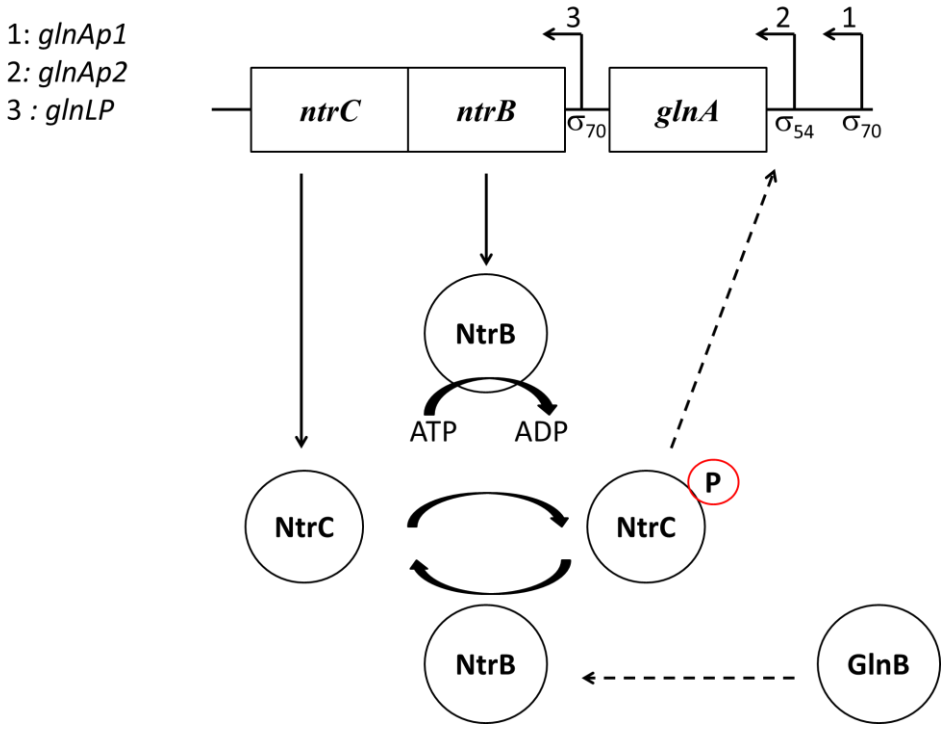

Figure I.14. *ntr*C/*ntr*B TCS regulating *glnA* transcription for nitrogen fixation in bacteria.

I.3.2.2. CpxRA

The CpxRA in *E.coli* constitute a typical TCS that display a variety of physiological roles (pilus biogenesis[124,125], induction of expression of heat shock protein [126,127], iron transport[128], virulence[129] and biofilm formation[130]). Screening tests for identification of CpxR (the RR) action indicate that this protein regulates diverse physiological activities in bacteria, such as motility, pathogenesis, envelope protein folding and copper stress response[131,132].However, the bacterial envelope stress response is the main function attributed to CpxRA[133,134]. The *cpxRA* operon is formed by *cpxA* and *cpxR*, consisting of a sensor histidine kinase (CpxA) and a cytoplasmic response regulator (CpxR). The CpxA autophosphorylate in response to envelope stress and transfer the phosphoryl group to CpxR[135]. Adjacent to *cpxRA* operon, the *cpxP* gene is divergently transcribed and is controlled by the activated (phosphorylated) form of CpxR[136].This activated CpxR binds to the intergenic region between *cpxP* and *cpxA* (consensus sequence 5′GTAAN$_{(6\text{-}7)}$GTAA) and, in conjunction with RpoS (a σ_{38}), controls its own promoter transcriptional level [137]. Moreover, the genetic circuit adopted by *cpxRA* operon can be repressed by overproduction of CpxP leading to down regulation of the Cpx pathway. This

repression is mediated by the CpxA sensor domain which is inhibited by CpxP in the absence of stress conditions[138,139]. CpxP is a periplasmic protein formed by 147 amino acids residues. The CpxP is involved in a variety of cell stress response, such as spheroplast formation, and might be involved in monitoring the periplasmic protein folding, acting as a chaperone[140–142]. Recently, the crystal structure of CpxP was solved and the protein presents as a positively charged α-helical dimer. CpxP contain a conserved LTXXQ motif which may be important for the protein function given that mutations at this site can cause structure perturbation and disrupt the Cpx inhibitory pathway[143]. A general mechanism of Cpx pathway is presented in figure I.15.

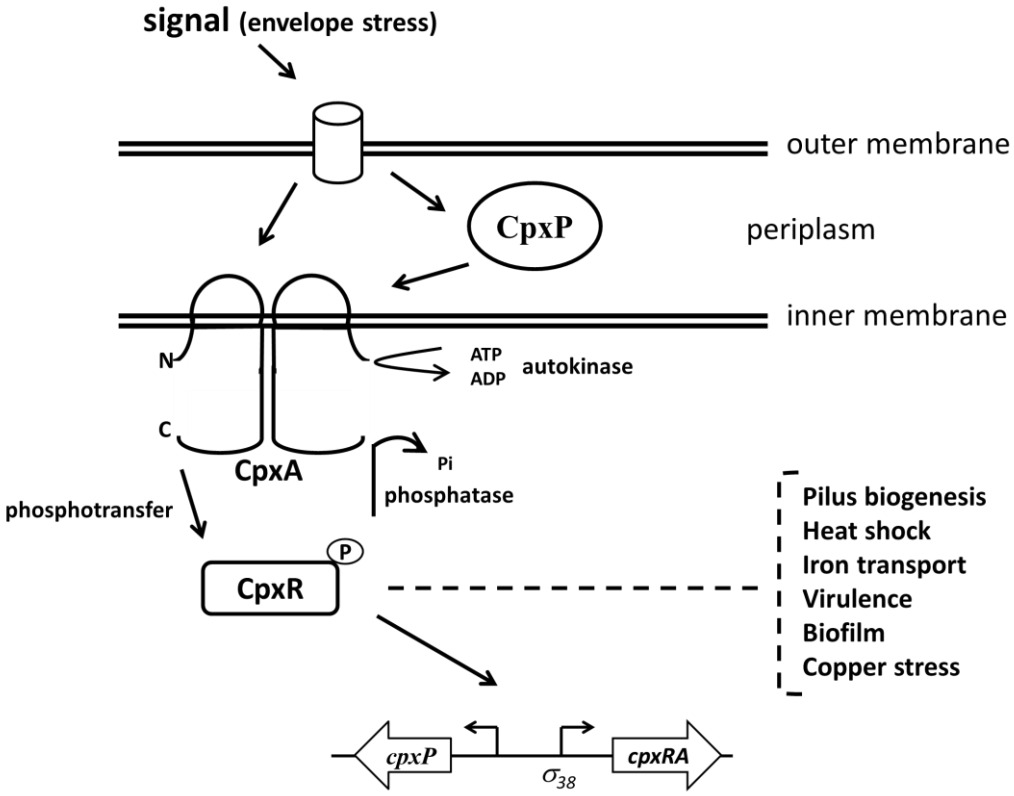

Figure I.15. Mechanism of *cpx* regulation during envelope stress response.

I.3.2.3. ZraSR

The ZraSR is another prototypical bacterial TCS formed by a sensor histidine kinase (ZraS) and a response regulator (ZraR) which activates the transcription of *zraP* gene in response to high concentration of Zn^{2+} and Pb^{2+}.This system was previous related with the genes responsible for hydrogenase 3 formation, given that its location was

positioned upstream of *hydL* gene[144]. The genes *zraSR* and *zraP* are divergently transcribed (figure I.16). The ZraR is the transcriptional regulator that binds to the intergenic region between *zraS* and *zraP*. Their gene expression requires the presence of σ_{54} *in vivo* and two possible σ_{54} binding sites were identified for *zraSR* and *zraP* promoters regions. In the absence of metal, a basal level of transcription was verified for *zraS* gene suggesting the presence of a constitutive σ_{70} promoter[145]. The *zraSR* TCS is not well comprehended but have been associated with *Salmonella* infection and its intrinsic Zn^{2+}/ Pb^{2+} tolerance have been used to design cell based biosensors sensible to these metals[146,147]. The ZraP, also known as YJAI, is a predicted monomer with a molecular mass of 13.5kDa with affinity to zinc, cobalt and cadmium. However, ZraP exhibit more affinity to $Zn^{2+}$and its transcriptional level is highly activated in the presence of this metal, characterizing ZraP as an essential protein involved in the bacterial zinc tolerance[148,149].ZraP is a periplasmic protein that forms higher-order structure (15 ZraP monomers) in the presence of $ZnCl_2$ and acts as a chaperone that suppresses the thermal aggregation of proteins in the presence of zinc. Moreover, ZraP is a member of bacterial Cpx family and acts as a repressor of ZraSR activity[150].

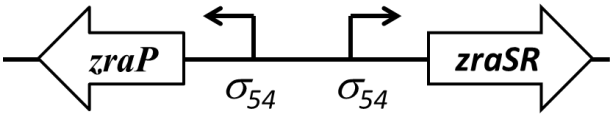

Figure I.16. *zraP* and *zraRS* genes involved in Zn^{2+} and Pb^{2+}tolerance in bacteria.

The ZraR follows the same domain architecture of NtrC: a REC, a central and a DNA binding domain. Until now, the full length structure of ZraR wasn't solved. Nevertheless, the structure of the central and CTD was determinate by crystallography. The central domain of ZraR presented as a hexameric ring typical of AAA^+ proteins and the DNA binding domain presented as a dimer (figure I.17). The hexameric structure was observed in the presence of different nucleotides implying that nucleotides play an important role for ZraR oligomerization. The GAFTGA motif was observed at the tip of the L1 loop, near to the hexameric pore and biochemical evidences showed that mutations at this motif usually abolish the interaction between the transcriptional factors and σ_{54}[151].

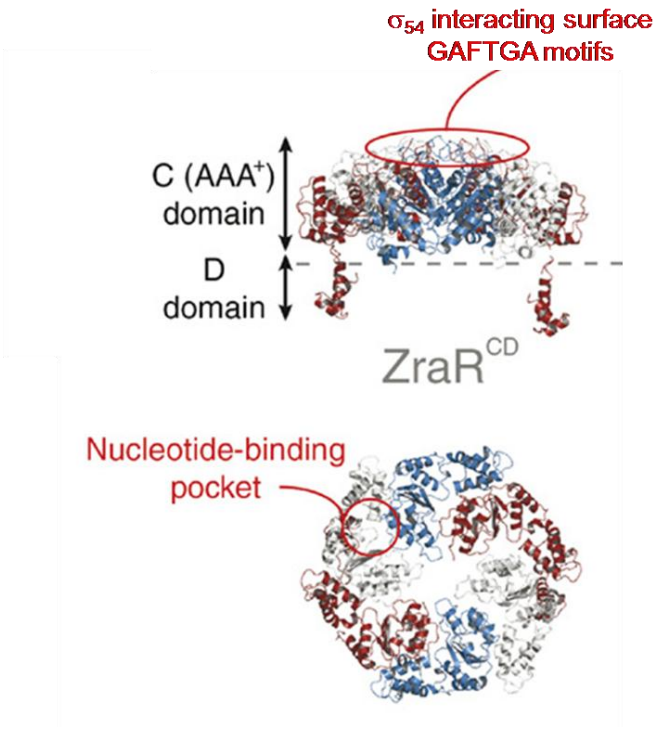

Figure I.17. The crystal strucuture of ZraR. The central (C) and DNA binding domain (D) are highlighted. Adapted from Matheus Rappas *et al.*, (2007) *Curr. Opin. Struct*. Biol., 17: 110-116

I.3.2.4. torRTS system

Negative autoregulation seems to be less common among TCS but can be represented by the *torRTS* system involved in the *E.coli* trimethylamine *N*-oxide (TMAO) respiratory circuit. *E.coli* is a facultative anaerobe microorganism that can use TMAO (an organic compound widespread in nature) as an alternative electron acceptor for bacterial anaerobic respiration[152].The *tor* system is formed by two divergent operons: the *torRTS* and *torCAD* (figure I.18). The *torRTS* codifies a response regulator (TorR), a periplasmic protein (TorT) and a sensor histidine kinase (TorS) forming a phosphorelay cascade responsible for TMAO regulation [153,154]. The *torCAD* codifies a c-type cytochrome (TorC), a TMAO-terminal reductase (TorA) and a TorA chaperone (TorD)[155]. The *torCAD* operon is under the control of the presence TMAO. TMAO binds to the TorT which induces its conformational change leading to TorT interaction with TorS. This action is accompanied by the TorS activation[156]. The TorS is formed by a N-terminal detector region anchored toward the periplasm, a transmitter cytoplasmic domain with three phosphorylation sites and by an alternative transmitter domain involved in phosphotransfer to the response

regulator TorR[157]. The TorR (active and inactive forms) binds to *torR-torC* intergenic region at four direct repeats called *tor* boxes dictating the action of the RR: as a negative autoregulator if TorR binds to box 1 and 2 and as a *torCAD* activator if binds to box 3 and 4. The negative autoregulation occurs because TorR overlaps the -10 transcription start site thus inhibiting the access by the RNAP[158]. The active form of TorR enhances the transcriptional level of *torCAD* operon. Therefore, in the presence of TMAO the *torCAD* is codified. The pentahaemic *c*-type cytochrome TorC is involved in electron transfer to TorA. TorA is a periplasmic molybdopterin responsible for performing the reduction of TMAO in trimethyllamine (TMA), a volatile compound. The incorporation of molybdenum cofactor into TorA occurs at cytoplasm and is important to the translocation of TorA to the periplasm[159]. This maturation process involve the chaperone activity of TorD and the TorA translocation requires the Twin Arginin Translocation (TAT) system[160,161].

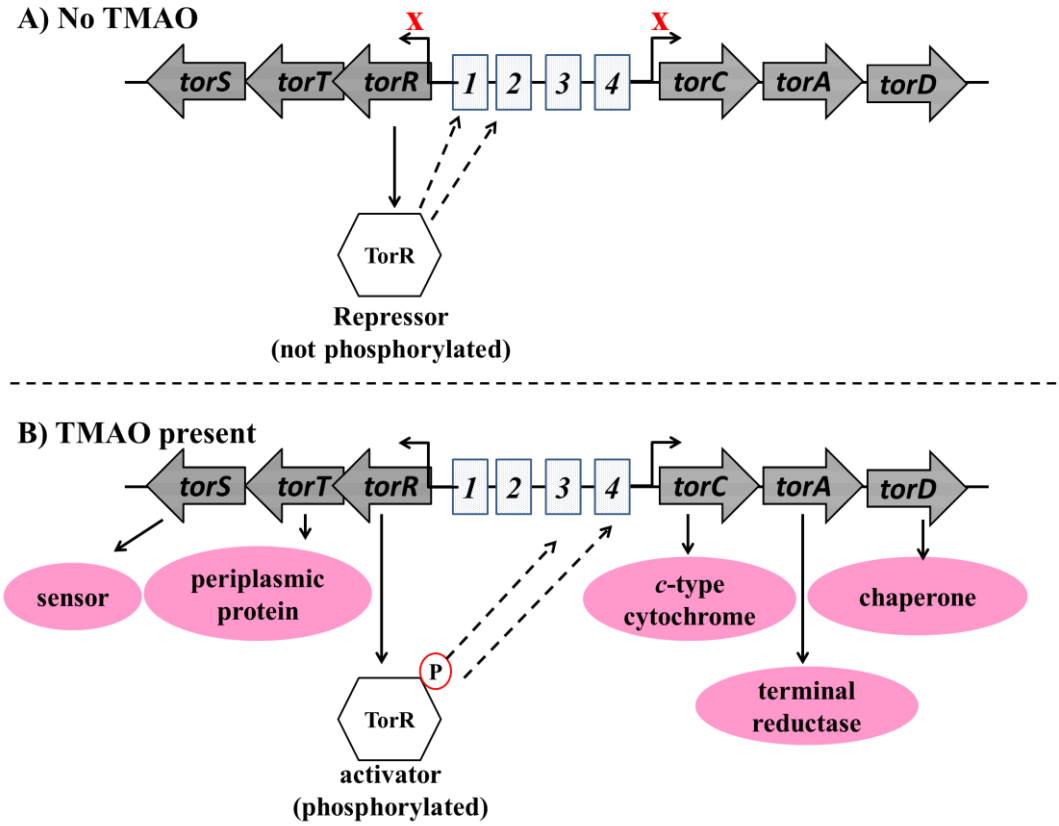

Figure I.18. The *torRTS* and *torCAD* system.

I.4. Hypothesis of the present study

MorP is a protein that may be involved with molybdenum homeostasis in *Desulfovibrio alaskensis* G20[49]. In order to understand how *mor*PRS genes are regulate, our study aims to elucidate if the putative regulator codified by *Dde*_0109 (*mor*R) binds to the intergenic region between *Dde*_0110 (*mor*S) and *Dde*_0111 (*mor*P). This study comprises an application of some DNA-protein interactions techniques associated with genetic and protein bioinformatics analysis which tried to elucidate how MorR could act as a transcriptional regulatory protein involved in Mo homeostasis in *D. alaskensis* G20. Interaction with small phosphodonors as protein phosphorylate agents were also investigated.

I.5. References

1. Zhou, J. *et al.* How sulphate-reducing microorganisms cope with stress: lessons from systems biology. *Nat. Rev. Microbiol.* **9,** 452–66 (2011).

2. Alm, E., Huang, K. & Arkin, A. The evolution of two-component systems in bacteria reveals different strategies for niche adaptation. *PLoS Comput. Biol.* **2,** e143 (2006).

3. Muyzer, G. & Stams, A. J. M. The ecology and biotechnology of sulphate-reducing bacteria. *Nat. Rev. Microbiol.* **6,** 441–54 (2008).

4. He, Q. *et al.* Energetic consequences of nitrite stress in Desulfovibrio vulgaris Hildenborough, inferred from global transcriptional analysis. *Appl. Environ. Microbiol.* **72,** 4370–81 (2006).

5. Mukhopadhyay, A. *et al.* Cell-wide responses to low-oxygen exposure in Desulfovibrio vulgaris Hildenborough. *J. Bacteriol.* **189,** 5996–6010 (2007).

6. Mukhopadhyay, A. *et al.* Salt stress in Desulfovibrio vulgaris Hildenborough: an integrated genomics approach. *J. Bacteriol.* **188,** 4068–78 (2006).

7. Coulter, E. D. & Kurtz, D. M. A role for rubredoxin in oxidative stress protection in Desulfovibrio vulgaris: catalytic electron transfer to rubrerythrin and two-iron superoxide reductase. *Arch. Biochem. Biophys.* **394,** 76–86 (2001).

8. Heather L. Lumppio, Neeta V. Shenvi, Anne O. Summers, G. V. and D. M. K. J. Rubrerythrin and rubredoxin oxidoreductase in Desulfovibrio vulgaris: a novel oxidative stress protection system. *J. Bacteriol.* **183,** 2970 (2011).

9. Javaherdashti, R. Impact of sulphate-reducing bacteria on the performance of engineering materials. *Appl. Microbiol. Biotechnol.* **91,** 1507–17 (2011).

10. Castro, H., Williams, N. & Ogram, A. Phylogeny of sulfate-reducing bacteria. *FEMS Microbiol. Ecol.* **31,** 1–9 (2000).

11. Hauser, L. J. *et al.* Complete genome sequence and updated annotation of Desulfovibrio alaskensis G20. *J. Bacteriol.* **193,** 4268–9 (2011).

12. Karlin, S., Brocchieri, L., Mrázek, J. & Kaiser, D. Distinguishing features of delta-proteobacterial genomes. *Proc. Natl. Acad. Sci. U. S. A.* **103,** 11352–7 (2006).

13. Meyer, B. *et al.* Variation among Desulfovibrio species in electron transfer systems used for syntrophic growth. *J. Bacteriol.* **195,** 990–1004 (2013).

14. Li, X., McInerney, M. J., Stahl, D. a & Krumholz, L. R. Metabolism of H2 by Desulfovibrio alaskensis G20 during syntrophic growth on lactate. *Microbiology* **157,** 2912–21 (2011).

15. Das, A. K., Chakraborty, R., Cervera, M. L. & de la Guardia, M. A review on molybdenum determination in solid geological samples. *Talanta* **71,** 987–1000 (2007).

16. Sandell, P. K. K. and E. B. Geochemistry of molybdenum. *Geochim. Cosmochim. Acta* **6,** 35–63 (1954).

17. Helz, G. R., Bura-Nakić, E., Mikac, N. & Ciglenečki, I. New model for molybdenum behavior in euxinic waters. *Chem. Geol.* **284,** 323–332 (2011).

18. Williams, R. J. P. & Fraústo da Silva, J. J. R. The involvement of molybdenum in life. *Biochem. Biophys. Res. Commun.* **292,** 293–9 (2002).

19. Mendel, R. R. Molybdenum: biological activity and metabolism. *Dalton Trans.* 3404–9 (2005).

20. Hille, R., Nishino, T. & Bittner, F. Molybdenum enzymes in higher organisms. *Coord. Chem. Rev.* **255,** 1179–1205 (2011).

21. Campo, R. J., Araujo, R. S. & Hungria, M. Molybdenum-enriched soybean seeds enhance N accumulation, seed yield, and seed protein content in Brazil. *F. Crop. Res.* **110,** 219–224 (2009).

22. Chatt, J. Molybdenum in nitrogen fixation. *J. Less Common Met.* **36,** 429–435 (1974).

23. Grunden, a M. & Shanmugam, K. T. Molybdate transport and regulation in bacteria. *Arch. Microbiol.* **168,** 345–54 (1997).

24. Schwarz, G., Mendel, R. R. & Ribbe, M. W. Molybdenum cofactors, enzymes and pathways. *Nature* **460,** 839–47 (2009).

25. Rech, S. *et al.* Regulation of the molybdate transport operon , modABCD , of Escherichia coli in response to molybdate availability. *J. Bacteriol.* **177,** 1023–1029 (1995).

26. Imperial, J., Hadi, M. & Amy, N. K. Molybdate binding by ModA, the periplasmic component of the Escherichia coli mod molybdate transport system. *Biochim. Biophys. Acta* **1370,** 337–46 (1998).

27. Rech, S., Wolin, C. & Gunsalus, R. P. Properties of the periplasmic ModA molybdate-binding protein of Escherichia coli. *J. Biol. Chem.* **271,** 2557–62 (1996).

28. Maupin-Furlow, J. A. *et al.* Genetic analysis of the modABCD (molybdate transport) operon of Escherichia coli. *J. Bacteriol.* **177,** 4851–6 (1995).

29. Hollenstein, K., Frei, D. C. & Locher, K. P. Structure of an ABC transporter in complex with its binding protein. *Nature* **446,** 213–6 (2007).

30. Grunden, a M., Ray, R. M., Rosentel, J. K., Healy, F. G. & Shanmugam, K. T. Repression of the Escherichia coli modABCD (molybdate transport) operon by ModE. *J. Bacteriol.* **178,** 735–44 (1996).

31. Anderson, L. a *et al.* Characterisation of the molybdenum-responsive ModE regulatory protein and its binding to the promoter region of the modABCD (molybdenum transport) operon of Escherichia coli. *Eur. J. Biochem.* **246,** 119–26 (1997).

32. Johnson, J. L., Hainline, B. E. & Rajagopalan, K. V. Characterization of the molybdenum cofactor of sulfite oxidase, xanthine, oxidase, and nitrate reductase. Identification of a pteridine as a structural component. *J. Biol. Chem.* **255,** 1783–6 (1980).

33. Dove, K. &. *Novel cofactors*. 474 (2001). at <Elsevier>

34. Schwarz, G. & Mendel, R. R. Molybdenum cofactor biosynthesis and molybdenum enzymes. *Annu. Rev. Plant Biol.* **57,** 623–47 (2006).

35. Hänzelmann, P. & Schindelin, H. Crystal structure of the S-adenosylmethionine-dependent enzyme MoaA and its implications for molybdenum cofactor deficiency in humans. *Proc. Natl. Acad. Sci. U. S. A.* **101,** 12870–5 (2004).

36. Wuebbens, M. M., Liu, M. T., Rajagopalan, K. & Schindelin, H. Insights into molybdenum cofactor deficiency provided by the crystal structure of the molybdenum cofactor biosynthesis protein MoaC. *Structure* **8,** 709–18 (2000).

37. Rudolph, M. J., Wuebbens, M. M., Rajagopalan, K. V & Schindelin, H. Crystal structure of molybdopterin synthase and its evolutionary relationship to ubiquitin activation. *Nat. Struct. Biol.* **8,** 42–6 (2001).

38. Liu, M. T., Wuebbens, M. M., Rajagopalan, K. V & Schindelin, H. Crystal structure of the gephyrin-related molybdenum cofactor biosynthesis protein MogA from Escherichia coli. *J. Biol. Chem.* **275,** 1814–22 (2000).

39. Nichols, J. D. & Rajagopalan, K. V. In vitro molybdenum ligation to molybdopterin using purified components. *J. Biol. Chem.* **280,** 7817–22 (2005).

40. Hospital, C. *et al.* Molybdenum cofactor deficiency. *J. Pediatr.* **123,** 93–96 (1993).

41. George, G. N. *et al.* A Novel Protein-Bound Copper−Molybdenum Cluster. *J. Am. Chem. Soc.* **122,** 8321–8322 (2000).

42. Bursakov, S. a *et al.* Antagonists Mo and Cu in a heterometallic cluster present on a novel protein (orange protein) isolated from Desulfovibrio gigas. *J. Inorg. Biochem.* **98,** 833–40 (2004).

43. Hatchikian, E. C. & Bruschi, M. Isolation and characterization of a molybdenum iron-sulfur protein from Desulfovibrio africanus. *Biochem. Biophys. Res. Commun.* **86,** 725–34 (1979).

44. Czechowski, M. *et al.* Purification and characterization of three proteins from a halophilic sulfate-reducing bacterium,Desulfovibrio salexigens. *J. Ind. Microbiol.* **1,** 139–147 (1986).

45. Fiévet, A. *et al.* The anaerobe-specific orange protein complex of Desulfovibrio vulgaris hildenborough is encoded by two divergent operons coregulated by σ54 and a cognate transcriptional regulator. *J. Bacteriol.* **193,** 3207–19 (2011).

46. Maiti, B. K. *et al.* Rearrangement of Mo-Cu-S Cluster Reflects the Structural - Instability of Orange Protein Cofactor. *Zeitschrift für Anorg. und Allg. Chemie* **639,** 1361–1364 (2013).

47. Mota, C. S. *et al.* Effects of molybdate and tungstate on expression levels and biochemical characteristics of formate dehydrogenases produced by Desulfovibrio alaskensis NCIMB 13491. *J. Bacteriol.* **193,** 2917–23 (2011).

48. Da Silva, S. M., Pimentel, C., Valente, F. M. a, Rodrigues-Pousada, C. & Pereira, I. a C. Tungsten and molybdenum regulation of formate dehydrogenase expression in Desulfovibrio vulgaris Hildenborough. *J. Bacteriol.* **193,** 2909–16 (2011).

49. Rivas, M. G. *et al.* Molybdenum induces the expression of a protein containing a new heterometallic Mo-Fe cluster in Desulfovibrio alaskensis. *Biochemistry* **48,** 873–82 (2009).

50. Capra, E. J. & Laub, M. T. Evolution of two-component signal transduction systems. *Annu. Rev. Microbiol.* **66,** 325–47 (2012).

51. Uldis N. Streips & Ronald E. Yasbin. *Modern Microbial Genetics, 1st Edition*. **0,** (Wiley-Liss, Inc., 2002).

52. Stewart, R. C. Protein histidine kinases: assembly of active sites and their regulation in signaling pathways. *Curr. Opin. Microbiol.* **13,** 133–41 (2010).

53. Nixon, T. & Ausubel, F. M. Conserved Domains in Bacterial Regulatory Proteins That Respond to Environmental Minireview Stimuli. *Cell* **49,** 579–581 (1988).

54. Krell, T. *et al.* Bacterial sensor kinases: diversity in the recognition of environmental signals. *Annu. Rev. Microbiol.* **64,** 539–59 (2010).

55. Cheung, J., Bingman, C. A., Reyngold, M., Hendrickson, W. A. & Waldburger, C. D. Crystal structure of a functional dimer of the PhoQ sensor domain. *J. Biol. Chem.* **283,** 13762–70 (2008).

56. Cheung, J. & Hendrickson, W. A. Crystal structures of C4-dicarboxylate ligand complexes with sensor domains of histidine kinases DcuS and DctB. *J. Biol. Chem.* **283,** 30256–65 (2008).

57. Sevvana, M. *et al.* A ligand-induced switch in the periplasmic domain of sensor histidine kinase CitA. *J. Mol. Biol.* **377,** 512–23 (2008).

58. Hoff, W. D., Jung, K. H. & Spudich, J. L. Molecular mechanism of photosignaling by archaeal sensory rhodopsins. *Annu. Rev. Biophys. Biomol. Struct.* **26,** 223–58 (1997).

59. Sasaki, J. & Spudich, J. L. The transducer protein HtrII modulates the lifetimes of sensory rhodopsin II photointermediates. *Biophys. J.* **75,** 2435–40 (1998).

60. Gordeliy, V. I. *et al.* Molecular basis of transmembrane signalling by sensory rhodopsin II-transducer complex. *Nature* **419,** 484–7 (2002).

61. Spudich, J. L. Variations on a molecular switch: transport and sensory signalling by archaeal rhodopsins. *Mol. Microbiol.* **28,** 1051–8 (1998).

62. Reyrat, J. M., David, M., Blonski, C., Boistard, P. & Batut, J. Oxygen-regulated in vitro transcription of Rhizobium meliloti nifA and fixK genes. *J. Bacteriol.* **175,** 6867–72 (1993).

63. Prisic, S. *et al.* Extensive phosphorylation with overlapping specificity by Mycobacterium tuberculosis serine/threonine protein kinases. *Proc. Natl. Acad. Sci. U. S. A.* **107,** 7521–6 (2010).

64. Cluzel, M.-E. *et al.* The Staphylococcus aureus autoinducer-2 synthase LuxS is regulated by Ser/Thr phosphorylation. *J. Bacteriol.* **192,** 6295–301 (2010).

65. Ge, R. *et al.* Phosphoproteome analysis of the pathogenic bacterium Helicobacter pylori reveals over-representation of tyrosine phosphorylation and multiply phosphorylated proteins. *Proteomics* **11,** 1449–61 (2011).

66. Podgornaia, A. I. & Laub, M. T. Determinants of specificity in two-component signal transduction. *Curr. Opin. Microbiol.* **16,** 156–62 (2013).

67. Kenney, L. J. How important is the phosphatase activity of sensor kinases? *Curr. Opin. Microbiol.* **13,** 168–76 (2010).

68. Lukat, G. S., McCleary, W. R., Stock, a M. & Stock, J. B. Phosphorylation of bacterial response regulator proteins by low molecular weight phospho-donors. *Proc. Natl. Acad. Sci. U. S. A.* **89,** 718–22 (1992).

69. Masayori Inouye, R. D. *Histidine kinase in signal transduction, 1st Edition*. (Elsevier Inc., 2002).

70. Lukat, G. S., Lee, B. H., Mottonen, J. M., Stock, a M. & Stock, J. B. Roles of the highly conserved aspartate and lysine residues in the response regulator of bacterial chemotaxis. *J. Biol. Chem.* **266,** 8348–54 (1991).

71. Yan, J., Barak, R., Liarzi, O., Shainskaya, A. & Eisenbach, M. In vivo acetylation of CheY, a response regulator in chemotaxis of Escherichia coli. *J. Mol. Biol.* **376,** 1260–71 (2008).

72. Liarzi, O. *et al.* Acetylation represses the binding of CheY to its target proteins. *Mol. Microbiol.* **76,** 932–43 (2010).

73. Gao, R. & Stock, A. M. Biological insights from structures of two-component proteins. *Annu. Rev. Microbiol.* **63,** 133–54 (2009).

74. Galperin, M. Y. Structural classification of bacterial response regulators: diversity of output domains and domain combinations. *J. Bacteriol.* **188,** 4169–82 (2006).

75. Sidote, D. J., Barbieri, C. M., Wu, T. & Stock, A. M. Structure of the Staphylococcus aureus AgrA LytTR domain bound to DNA reveals a beta fold with an unusual mode of binding. *Structure* **16,** 727–35 (2008).

76. Baikalov, I. *et al.* Structure of the Escherichia coli response regulator NarL. *Biochemistry* **35,** 11053–61 (1996).

77. Nikolskaya, A. N. & Galperin, M. Y. A novel type of conserved DNA-binding domain in the transcriptional regulators of the AlgR/AgrA/LytR family. *Nucleic Acids Res.* **30,** 2453–9 (2002).

78. Pabo, C. O. & Sauer, R. T. Transcription factors: structural families and principles of DNA recognition. *Annu. Rev. Biochem.* **61,** 1053–95 (1992).

79. Aravind, L., Anantharaman, V., Balaji, S., Babu, M. M. & Iyer, L. M. The many faces of the helix-turn-helix domain: transcription regulation and beyond. *FEMS Microbiol. Rev.* **29,** 231–62 (2005).

80. Kansara, S. G. & Sukhodolets, M. V. Oligomerization of the E. coli core RNA polymerase: formation of (α2ββ'ω)2-DNA complexes and regulation of the oligomerization by auxiliary subunits. *PLoS One* **6,** e18990 (2011).

81. Zhang, G. *et al.* Crystal Structure of Thermus aquaticus Core RNA Polymerase at 3.3 A° Resolution. *Cell* **98,** 811–824 (1999).

82. Murakami, K. S. X-ray crystal structure of Escherichia coli RNA polymerase σ70 holoenzyme. *J. Biol. Chem.* **288,** 9126–34 (2013).

83. Ross, W. *et al.* A third recognition element in bacterial promoters: DNA binding by the alpha subunit of RNA polymerase. *Science* **262,** 1407–13 (1993).

84. Kimura, M. & Ishihama, a. Functional map of the alpha subunit of Escherichia coli RNA polymerase: insertion analysis of the amino-terminal assembly domain. *J. Mol. Biol.* **248,** 756–67 (1995).

85. Blatter, E. E., Ross, W., Tang, H., Gourse, R. L. & Ebright, R. H. Domain organization of RNA polymerase alpha subunit: C-terminal 85 amino acids constitute a domain capable of dimerization and DNA binding. *Cell* **78,** 889–96 (1994).

86. Jeon, Y. H., Yamazaki, T., Otomo, T., Ishihama, a & Kyogoku, Y. Flexible linker in the RNA polymerase alpha subunit facilitates the independent motion of the C-terminal activator contact domain. *J. Mol. Biol.* **267,** 953–62 (1997).

87. Murakami, K. S., Masuda, S., Campbell, E. a, Muzzin, O. & Darst, S. a. Structural basis of transcription initiation: an RNA polymerase holoenzyme-DNA complex. *Science* **296,** 1285–90 (2002).

88. Lonetto, M., Gribskov, M. & Gross, C. a. The sigma 70 family: sequence conservation and evolutionary relationships. *J. Bacteriol.* **174,** 3843–9 (1992).

89. Lonetto, M. a, Brown, K. L., Rudd, K. E. & Buttner, M. J. Analysis of the Streptomyces coelicolor sigE gene reveals the existence of a subfamily of eubacterial RNA polymerase sigma factors involved in the regulation of extracytoplasmic functions. *Proc. Natl. Acad. Sci. U. S. A.* **91,** 7573–7 (1994).

90. Paget, M. S. B. & Helmann, J. D. The 70 family of sigma factors. *Genome Biol.* **4,** 1–6 (2003).

91. Murakami, K. S., Masuda, S. & Darst, S. a. Structural basis of transcription initiation: RNA polymerase holoenzyme at 4 A resolution. *Science* **296,** 1280–4 (2002).

92. Vassylyev, D. G. *et al.* Crystal structure of a bacterial RNA polymerase holoenzyme at 2.6 A resolution. *Nature* **417,** 712–9 (2002).

93. Jeremy W. Dale, S. P. *Molecular Genetics of Bacteria*. (2004).

94. Lee, D. J., Minchin, S. D. & Busby, S. J. W. Activating transcription in bacteria. *Annu. Rev. Microbiol.* **66,** 125–52 (2012).

95. Brown, N. L., Ford, S. J., Pridmore, R. D. & Fritzinger, D. C. Nucleotide sequence of a gene from the Pseudomonas transposon Tn501 encoding mercuric reductase. *Biochemistry* **22,** 4089–95 (1983).

96. Mathema, V. B., Thakuri, B. C. & Sillanpää, M. Bacterial mer operon-mediated detoxification of mercurial compounds: a short review. *Arch. Microbiol.* **193,** 837–44 (2011).

97. Lund, P. a, Ford, S. J. & Brown, N. L. Transcriptional regulation of the mercury-resistance genes of transposon Tn501. *J. Gen. Microbiol.* **132,** 465–80 (1986).

98. Lund, T. P., Brown, N. & Sciences, M. Up-promoter mutations in the positively-regulated mer promoter of Tn501. *Nucleic Acids Res.* **V,** (1989).

99. Ansari, A. Z., Chael, M. L. & O'Halloran, T. V. Allosteric underwinding of DNA is a critical step in positive control of transcription by Hg-MerR. *Nature* **355,** 87–9 (1992).

100. Brown, N. L., Stoyanov, J. V, Kidd, S. P. & Hobman, J. L. The MerR family of transcriptional regulators. *FEMS Microbiol. Rev.* **27,** 145–163 (2003).

101. Maurer, R., Meyer, B. & Ptashne, M. Gene regulation at the right operator (OR) bacteriophage lambda. I. OR3 and autogenous negative control by repressor. *J. Mol. Biol.* **139,** 147–61 (1980).

102. Jack Griffith, A. H. & M. P. DNA loops induced by cooperative binding of lambda repressor. *Nature* **322,** 750–752 (1986).

103. Bell, C. E., Frescura, P., Hochschild, a & Lewis, M. Crystal structure of the lambda repressor C-terminal domain provides a model for cooperative operator binding. *Cell* **101,** 801–11 (2000).

104. Meyer, B. J. & Ptashne, M. Gene regulation at the right operator (OR) of bacteriophage lambda. III. lambda repressor directly activates gene transcription. *J. Mol. Biol.* **139,** 195–205 (1980).

105. Li, M., Moyle, H. & Susskind, M. M. Target of the transcriptional activation function of phage lambda cI protein. *Science* **263,** 75–7 (1994).

106. Nickels, B. E., Dove, S. L., Murakami, K. S., Darst, S. a. & Hochschild, A. Protein–Protein and Protein–DNA Interactions of σ70 Region 4 Involved in Transcription Activation by λcI. *J. Mol. Biol.* **324,** 17–34 (2002).

107. Ghosh, T., Bose, D. & Zhang, X. Mechanisms for activating bacterial RNA polymerase. *FEMS Microbiol. Rev.* **34,** 611–27 (2010).

108. Hirschman, J., Wong, P. K., Sei, K., Keener, J. & Kustu, S. Products of nitrogen regulatory genes ntrA and ntrC of enteric bacteria activate glnA transcription in vitro: evidence that the ntrA product is a sigma factor. *Proc. Natl. Acad. Sci. U. S. A.* **82,** 7525–9 (1985).

109. Wedel, A. & Kustu, S. The bacterial enhancer-binding protein NTRC is a molecular machine: ATP hydrolysis is coupled to transcriptional activation. *Genes Dev.* **9,** 2042–2052 (1995).

110. Shingler, V. Signal sensory systems that impact σ^{54} -dependent transcription. *FEMS Microbiol. Rev.* **35,** 425–40 (2011).

111. Rappas, M., Bose, D. & Zhang, X. Bacterial enhancer-binding proteins: unlocking sigma54-dependent gene transcription. *Curr. Opin. Struct. Biol.* **17,** 110–6 (2007).

112. Rombel, I. *et al.* MgATP binding and hydrolysis determinants of NtrC, a bacterial enhancer-binding protein. *J. Bacteriol.* **181,** 4628–38 (1999).

113. Dago, A. E., Wigneshweraraj, S. R., Buck, M. & Morett, E. A role for the conserved GAFTGA motif of AAA+ transcription activators in sensing promoter DNA conformation. *J. Biol. Chem.* **282,** 1087–97 (2007).

114. Fu, C.-C. *et al.* Fis-protein induces rod-like DNA bending. *Chem. Phys. Lett.* **500,** 318–322 (2010).

115. Bijlsma, J. J. E. & Groisman, E. a. Making informed decisions: regulatory interactions between two-component systems. *Trends Microbiol.* **11,** 359–366 (2003).

116. Goulian, M. Two-component signaling circuit structure and properties. *Curr. Opin. Microbiol.* **13,** 184–9 (2010).

117. DAVID M. ROTHSTEIN, GREG PAHEL, BONNIE TYLER*, A. B. M. Regulation of expression from the glnA promoter of Escherichia coli in the absence of glutamine synthetase. *Proc. Natl. Acad. Sci. U. S. A.* **77,** 7372–7376 (1980).

118. Kim, M. *et al.* Need-based activation of ammonium uptake in Escherichia coli. *Mol. Syst. Biol.* **8,** 616 (2012).

119. NANCY MCFARLAND, LINDA MCCARTER, STANLEY Awrz, A. S. K. Nitrogen regulatory locus “glnR” of enteric bacteria is composed of cistrons ntrB and ntrC: Identification of their protein products. *Proc. Natl. Acad. Sci. U. S. A.* **78,** 2135–2139 (1981).

120. THOMAS P. HUNT AND BORIS MAGASANIK. Transcription of glnA by purified Escherichia coli components: Core RNA polymerase and the products of glnF, gLnG, and glnL. *Proc. Natl. Acad. Sci. U. S. A.* **82,** 8453–8457 (1985).

121. Sabine K. Vogel, A. S. and K. R. Binding affinity of Escherichia coli RNA polymerase sigma54 holoenzyme for the glnAp2, nifH and nifL promoters. *Nucleic Acids Res.* **30,** 4094–4101 (2002).

122. Ninfa, A. J. & Magasanik, B. Covalent modification of the ginG product , NRI , by the glnL product , NRII , regulates the transcription of the glnALG operon in Escherichia coli. *Proc. Natl. Acad. Sci. U. S. A.* **83,** 5909–5913 (1986).

123. L J Reitzer, B. M. Expression of glnA in Escherichia coli is regulated at tandem promoters. *Proc. Natl. Acad. Sci. U. S. A.* **82,** 1979–1983 (1985).

124. Raivio, T. L. & Silhavy, T. J. The sigmaE and Cpx regulatory pathways: overlapping but distinct envelope stress responses. *Curr. Opin. Microbiol.* **2,** 159–65 (1999).

125. Hung, D. L., Raivio, T. L., Jones, C. H., Silhavy, T. J. & Hultgren, S. J. Cpx signaling pathway monitors biogenesis and affects assembly and expression of P pili. *EMBO J.* **20,** 1508–18 (2001).

126. Hunke, S. & Betton, J.-M. Temperature effect on inclusion body formation and stress response in the periplasm of Escherichia coli. *Mol. Microbiol.* **50,** 1579–1589 (2003).

127. Danese, P. N. & Silhavy, T. J. The sigma(E) and the Cpx signal transduction systems control the synthesis of periplasmic protein-folding enzymes in Escherichia coli. *Genes Dev.* **11,** 1183–93 (1997).

128. Cao, J., Woodhall, M. R., Alvarez, J., Cartron, M. L. & Andrews, S. C. EfeUOB (YcdNOB) is a tripartite, acid-induced and CpxAR-regulated, low-pH Fe2+ transporter that is cryptic in Escherichia coli K-12 but functional in E. coli O157:H7. *Mol. Microbiol.* **65,** 857–75 (2007).

129. Jubelin, G. *et al.* CpxR/OmpR interplay regulates curli gene expression in response to osmolarity in Escherichia coli. *J. Bacteriol.* **187,** 2038–49 (2005).

130. Dorel, C., Vidal, O., Prigent-Combaret, C., Vallet, I. & Lejeune, P. Involvement of the Cpx signal transduction pathway of E. coli in biofilm formation. *FEMS Microbiol. Lett.* **178,** 169–175 (1999).

131. De Wulf, P., McGuire, A. M., Liu, X. & Lin, E. C. C. Genome-wide profiling of promoter recognition by the two-component response regulator CpxR-P in Escherichia coli. *J. Biol. Chem.* **277,** 26652–61 (2002).

132. Price, N. L. & Raivio, T. L. Characterization of the Cpx regulon in Escherichia coli strain MC4100. *J. Bacteriol.* **191,** 1798–815 (2009).

133. Pogliano, J., Lynch, A. S., Belin, D., Lin, E. C. & Beckwith, J. Regulation of Escherichia coli cell envelope proteins involved in protein folding and degradation by the Cpx two-component system. *Genes Dev.* **11,** 1169–1182 (1997).

134. Rowley, G., Spector, M., Kormanec, J. & Roberts, M. Pushing the envelope: extracytoplasmic stress responses in bacterial pathogens. *Nat. Rev. Microbiol.* **4,** 383–94 (2006).

135. Raivio, T. L. & Silhavy, T. J. Transduction of envelope stress in Escherichia coli by the Cpx two-component system. *J. Bacteriol.* **179,** 7724–33 (1997).

136. Danese, P. N. & Silhavy, T. J. CpxP, a stress-combative member of the Cpx regulon. *J. Bacteriol.* **180,** 831–9 (1998).

137. De Wulf, P., Kwon, O. & Lin, E. C. The CpxRA signal transduction system of Escherichia coli: growth-related autoactivation and control of unanticipated target operons. *J. Bacteriol.* **181,** 6772–8 (1999).

138. Raivio, T. L., Popkin, D. L. & Silhavy, T. J. The Cpx envelope stress response is controlled by amplification and feedback inhibition. *J. Bacteriol.* **181,** 5263–72 (1999).

139. Zhou, X. *et al.* Structural basis for two-component system inhibition and pilus sensing by the auxiliary CpxP protein. *J. Biol. Chem.* **286,** 9805–14 (2011).

140. Raivio, T. L., Laird, M. W., Joly, J. C. & Silhavy, T. J. Tethering of CpxP to the inner membrane prevents spheroplast induction of the cpx envelope stress response. *Mol. Microbiol.* **37,** 1186–97 (2000).

141. Digiuseppe, P. A. & Silhavy, T. J. Signal Detection and Target Gene Induction by the CpxRA Two-Component System. **185,** 2432–2440 (2003).

142. Ruiz, N. & Silhavy, T. J. Sensing external stress: watchdogs of the Escherichia coli cell envelope. *Curr. Opin. Microbiol.* **8,** 122–6 (2005).

143. Thede, G. L. *et al.* Structure of the periplasmic stress response protein CpxP. *J. Bacteriol.* **193,** 2149–57 (2011).

144. Stoker K, Reijnders WN, Oltmann LF, S. A. Initial cloning and sequencing of hydHG, an operon homologous to ntrBC and regulating the labile hydrogenase activity in Escherichia coli K-12. *J. Bacteriol.* **171,** 4448–4456 (1989).

145. Leonhartsberger, S., Huber, A., Lottspeich, F. & Bo, A. The hydH / G Genes from Escherichia coli Code for a Zinc and Lead Responsive Two-component Regulatory System. *J. Mol. Biol.* **4,** 93–105 (2001).

146. Huang, Y., Leming, C. L., Suyemoto, M. & Altier, C. Genome-wide screen of Salmonella genes expressed during infection in pigs, using in vivo expression technology. *Appl. Environ. Microbiol.* **73,** 7522–30 (2007).

147. Wang, B., Barahona, M. & Buck, M. A modular cell-based biosensor using engineered genetic logic circuits to detect and integrate multiple environmental signals. *Biosens. Bioelectron.* **40,** 368–76 (2013).

148. Noll, M. Identification of a Novel Transcription Regulator from Proteus mirabilis, PMTR, Revealed a Possible Role of YJAI Protein in Balancing Zinc in Escherichia coli. *J. Biol. Chem.* **273,** 21393–21401 (1998).

149. Ravikumar, S., Yoo, I., Lee, S. Y. & Hong, S. H. A study on the dynamics of the zraP gene expression profile and its application to the construction of zinc adsorption bacteria. *Bioprocess Biosyst. Eng.* **34,** 1119–26 (2011).

150. Appia-Ayme, C. *et al.* ZraP is a periplasmic molecular chaperone and a repressor of the zinc-responsive two-component regulator ZraSR. *Biochem. J.* **442,** 85–93 (2012).

151. Bordes, P. *et al.* The ATP hydrolyzing transcription activator phage shock protein F of Escherichia coli : Identifying a surface that binds sigma 54. *Proc. Natl. Acad. Sci. U. S. A.* **100,** 2278–83 (2003).

152. Unden G, B. J. Alternative respiratory pathways of Escherichia coli: energetics and transcriptional regulation in response to electron acceptors. *Biochim. Biophys. Acta* **1320,** 217–234 (1997).

153. Simon, G., Méjean, V., Jourlin, C., Chippaux, M. & Pascal, M. C. The torR gene of Escherichia coli encodes a response regulator protein involved in the expression of the trimethylamine N-oxide reductase genes. *J. Bacteriol.* **177,** 275 (1995).

154. Jourlin C, Simon G, Pommier J, Chippaux M, M. V. The periplasmic TorT protein is required for trimethylamine N-oxide reductase gene induction in Escherichia coli. *J. Bacteriol.* **178,** 1219–1223 (1996).

155. Méjean, V. *et al.* TMAO anaerobic respiration in Escherichia coli: involvement of the tor operon. *Mol. Microbiol.* **11,** 1169–79 (1994).

156. Baraquet, C. *et al.* TorT, a member of a new periplasmic binding protein family, triggers induction of the Tor respiratory system upon trimethylamine N-oxide electron-acceptor binding in Escherichia coli. *J. Biol. Chem.* **281,** 38189–99 (2006).

157. Jourlin, C., Ansaldi, M. & Méjean, V. Transphosphorylation of the TorR response regulator requires the three phosphorylation sites of the TorS unorthodox sensor in Escherichia coli. *J. Mol. Biol.* **267,** 770–7 (1997).

158. Ansaldi, M., Simon, G., Lepelletier, M., Méjean, V. & Simon, N. The TorR High-Affinity Binding Site Plays a Key Role in Both torR Autoregulation and torCAD Operon Expression in Escherichia coli. *J. Bacteriol.* **182,** 961 (2000).

159. Santini, C. L. *et al.* A novel sec-independent periplasmic protein translocation pathway in Escherichia coli. *EMBO J.* **17,** 101–12 (1998).

160. Pommier, J., Méjean, V., Giordano, G. & Iobbi-Nivol, C. TorD, a cytoplasmic chaperone that interacts with the unfolded trimethylamine N-oxide reductase enzyme (TorA) in Escherichia coli. *J. Biol. Chem.* **273,** 16615–20 (1998).

161. Dalbey, R. E. & Robinson, C. Protein translocation into and across the bacterial plasma membrane and the plant thylakoid membrane. *Trends Biochem. Sci.* **24,** 17–22 (1999).

Chapter II

*mor*R gene, cloning and MorR expression

*mor*R gene, cloning and MorR expression

Context

In order to obtain the putative regulator MorR for biochemical characterization, the gene *Dde*_0109 was cloned using a pET system. Then, the recombinant plasmid was isolated and the competent cells BL21 (DE3) were transformed. This method provides advantages for protein purification toward native protein expression, such as: high growth rates of *E.coli* joined with high percentage of their total protein as the expressed gene product and control of the gene transcription. Finally, the protein was expressed as soluble form which enables subsequent protein purification. Moreover, the genetic context of *mor*R gene is also present in this chapter. Therefore, the analysis revealed that this gene shares high similarities with other response regulators that belong to two component system that are present in Gram-negative bacteria. Moreover, *mor*R is located downstream of *mor*S (a putative histidine kinase sensor) and *mor*P gene (previously associated with Mo homeostasis). The bioinformatics analysis of the intergenic region between *mor*S and *mor*P revealed the presence of divergent conserved boxes that may be associated with the genetic control of the entire system via σ_{70} and σ_{54}.

II.1. Methodology

II.1.1 Molecular cloning of *mor*R

Genetic engineering techniques were applied in order to obtain a recombinant plasmid carrying the *mor*R gene from *D.alaskensis* G20. The gene was amplified, cloned on pET expression-vector and transformed into different *E.coli* competent cells used first for plasmid multiplication (Nova Blue Giga Single Competent Cells, Novagen) and after for gene transcription induction (BL21 (DE3) Competent Cells, Nzytech).

II.1.1.1 Cloning vector characteristic

The pET system is a set of cloning vectors capable of maintaining a gene under the control of a strong bacteriophage T7 promoter. The gene transcription is induced by T7 RNA polymerase. T7 RNA polymerase needs to be provided by the hosted cell, and the expression is induced by Isopropyl β-D-1-thiogalactopyranoside (IPTG)[1].

The pET-21c was chosen as cloning vector for this study, since it fulfills some principal prerequisites: it has the correct insert size and cloning sites, it is easy to handle and available in our laboratory. The map of pET-21c is presented in figure II.1.

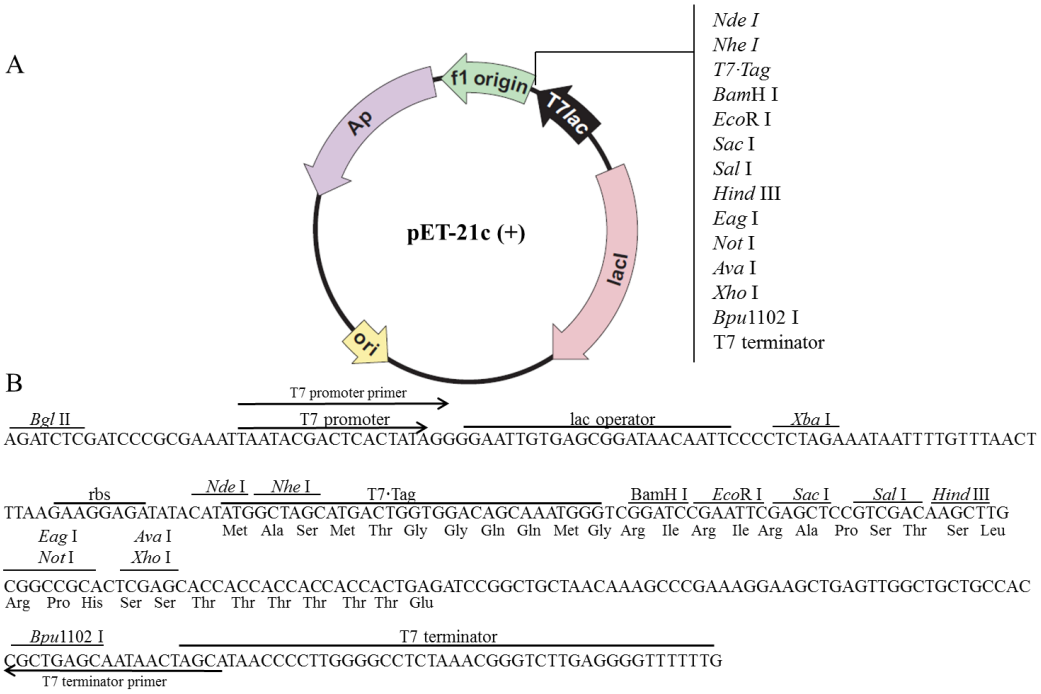

Figure II. 1. pET21C cloning vector. A: the cloning vector map. Ap: ampicillin resistance. Ori: origin of replication. lacI: lac repressor. T7 lac: 25bp lac operator sequence. f1 origin: bacteriophage origin of replication, and restriction sites are presented. B: The cloning/ expression region is evidenced. Adapted from Novagen pet-21-a-d (+) and Novagen 2002-2003 Catalog chapter 5.

II.1.1.2 DNA restriction mapping

The *mor*R gene is composed by 1401 nucleotides. A restriction map of *mor*R was created using a bioinformatic tool available at NEBcutter V.2.0 (http://tools.neb.com/NEBcutter2/). This online program compares the target DNA sequence with *E.coli* genetic code, and performs a screening for all NEB (New England Biolabs) restriction enzymes. The restriction map evaluation acts as an exclusion criterion, showing which restriction enzyme cut the target gene.

For pET-21c, the *Nde*I is the preferable restriction enzyme to start the cloning procedure given that its restriction site is located immediately downstream of the ribosome binding site (rbs) (figure II.1). However, for experimental approaches, the use of *Nde*I was banished once the restriction map (Figure II.2) showed that this enzyme can also cut the *mor*R gene sequence. For that reason, the *Nhe*I was selected as the first enzyme to start the cloning procedure. However, this experimental selection predicted the creation of three additional amino acids in the N-terminal of the MorR sequence: one methionine, one alanine and one serine. The evaluation of the possibilities of cloning using the pET21c allowed the selection of *Nhe*I and *EcoR*I as restriction enzymes for *mor*R cloning.

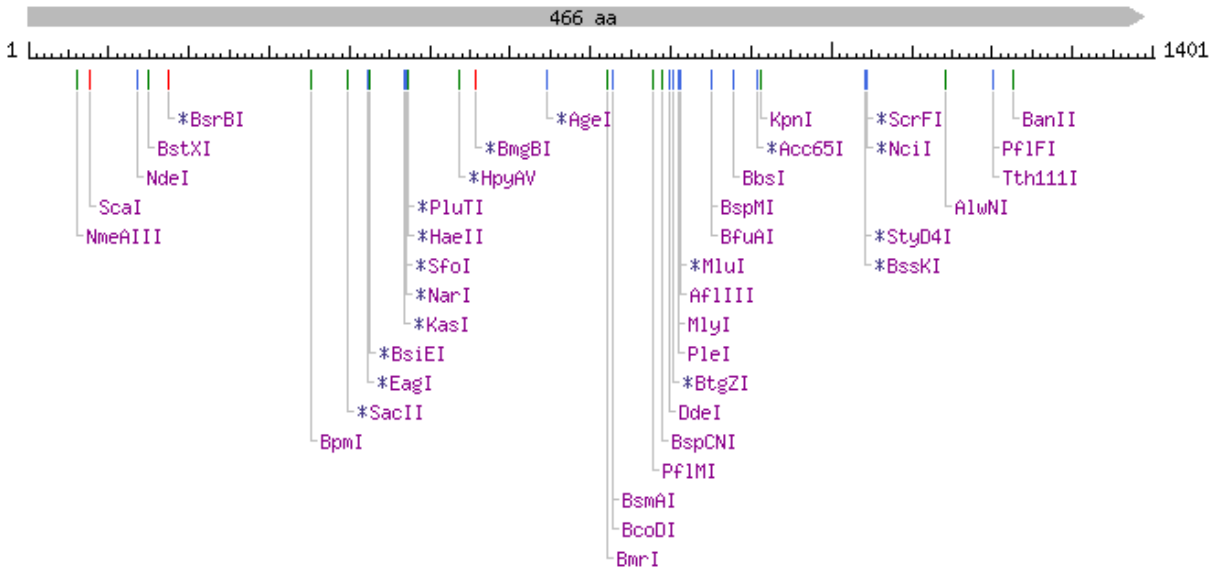

Figure II. 2. Restriction map for *mor*R gene obtained from NEBcutter. The scale bar represents the number of nucleotides (1401bp) of morR from *Desulfovibrio alaskensis* G20, and on the top the correspondent number of aminoacids residues (466 aa). The display below the scale shows the single cutter restriction enzymes sites for this gene sequence. Sites show in red have blunt ends, blue have 5` extensions and green 3` extensions. Enzymes marked with * are susceptible to DNA methylation.

II.1.1.3 DNA amplification

A pair of oligonucleotides (table II.1) was designed based on *mor*R DNA sequence. Flanking regions containing the restriction sites for *Nhe*I and *Eco*RI were added.

Table II. 1. Primers designed for PCR reaction. Primer orientation, sequence and restriction endonuclease site are shown. Restriction sites are underlined in the primer sequence.

Primer orientation	Sequence	Restriction enzyme
Forward	5' AGGAGCTAGCATGACAAACGCTCC3'	*Nhe*I
Reverse	5' GGCCGAATTCTTATTCCATGCCGT 3'	*Eco*RI

The primers were resuspended in deionized water according to manufacturer`s instruction, and the PCR reaction was carried out using a High Fidelity PCR Enzyme Mix (Fermentas) with some modification to the manufacturer`s procedure (table II.2).

Table II. 2. The PCR protocol for *mor*R gene amplification. The PCR mixture was designed for a total reaction volume of 20 µl.

Reagent	Final concentration/or volume
10X High Fidelity PCR buffer with 15mM $MgCl_2$	1x/2.5µL
DNTP mix, 1mM each	0.27mM each
Forward primer	0.27µM
Reverse primer	0.27µM
Template genomic DNA	10pg – 1µg
High Fidelity PCR Enzyme	0.5 units
Deionized water up to	20 µL

The PCR was performed using a MyCycler thermal cycling instrument (BioRad). The experimental conditions are schematically represented in figure II.3.

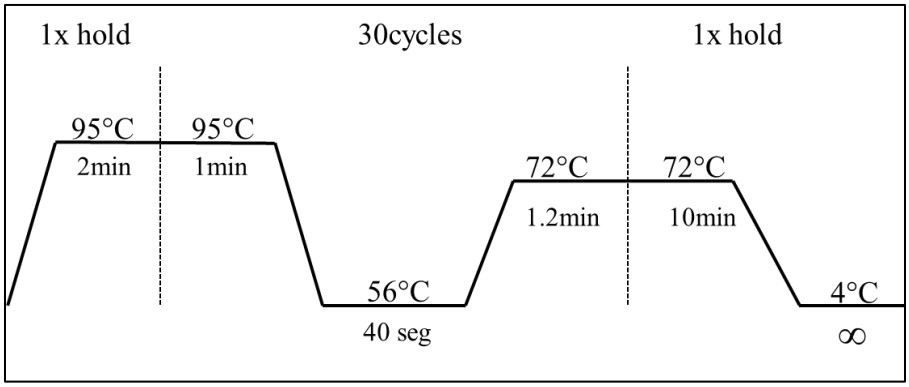

Figure II.3. Scheme of the PCR cycle conditions. PCR thermal and time cycling are schematically represented.

II.1.1.4 Vector and fragment digestion with restriction enzymes

The expression vector pET-21c and PCR fragment containing *mor*R were used as template for digestion with *Nhe*I and *Eco*RI endonuclease enzymes in order to create cohesive flanking regions. The digestion was performed in 1X Buffer Tango™ (Fermentas), and 16 units of each restriction enzyme were added sequentially. The total reaction time was 4h (2 hours for each enzyme) at 37ºC (table II.3). The product of reaction was then purified using NZY gel pure (Nzytech), and visualized in 1% agarose gel.

Table II. 3. pET-21c and *mor*R PCR fragment preparation with restriction enzymes. Amplified *mor*R PCR product and pET-21c were digested with endonuclease enzymes *Nhe*I and *Eco*RI as follows.

Reagent	pET-21c		PCR fragment
Nuclease- free water	5 µL		15 µL
10X Buffer Tango ™	4 µL		4 µL
Sample	30µL (1µg/µl)		20µL (0.5 µg/µl)
*Nhe*I	16 units		16 units
		2 hoursat 37ºC	
*Eco*RI	16 units		16 units
		2 hoursat 37ºC	

II.1.1.5 Vector and insert ligation

The vector and insert ligation was performed using Rapid DNA Ligation Kit (Roche) according to the manufacturer's instruction. The ratio of expression vector to insert was 1:3, e.g. 50 ng linearized plasmid plus 150 ng insert DNA. Vector and insert were mixed in 1X DNA Dilution Buffer, and then incubated with T4 DNA Ligation Buffer and T4 DNA Ligase for 30 minutes at room temperature.

The Nova Blue Giga Single Competent cells were immediately transformed with the recombinant plasmid. According to a standard protocol, the cells were thawed on ice, and 1µL of the plasmidial DNA was added. The mixture was incubated on ice for 5 min, heated during 30 sec in a 42ºC water bath and incubated on ice for 2 min more; and 250 µL of Super Optimal Broth (SOC) medium were then added. The cells grew for 1 h, spread in Luria Broth (LB) agarose plate supplemented with ampicillin (100 µg/ml), and grew overnight at 37ºC. Five colonies were selected. They were used as DNA template for PCR using the primers that amplify for *mor*R (table II.1). This procedure confirmed the presence of *mor*R gene in the plasmid.

The PCR positive colonies were isolated, and grown overnight in 5ml of LB medium supplemented with ampicillin (100 µg/ml). The plasmids were extracted from competent cells using a small-scale extraction kit from Nzytech. The 5ml of bacterial growth were centrifuged at 11.000 rpm, the pellet was lysed with buffer A1 (a Tris-EDTA Buffer, but the concentration is not provided by the manufacturer), centrifuged, the supernatant was then loaded into a spin column and centrifuged for 1 min at 11.000 rpm. The spin columns were washed with buffer AY (a mixture of guanidine hydrochloride with ethanol, but the concentration is not provided by the manufacturer), dried, and the plasmids were eluted with buffer AE (a solution of water). Finally, the plasmids were visualized in 1% agarose gel. An aliquot of 20µl (100ng/µl) of each plasmid was analyzed by DNA sequencing reaction in order to evaluate if the cloning had succeed. The sequencing was carried out using T7 promoter primer (5'-TAATACGACTCACTATAGGG-3') and T7 terminator primer (5'-GCTAGTTATTGCTCAGCGG-3'), using the BigDye Terminator 3 (Applied Biosystems) The reaction product was purified by gel filtration and resolved in an ABI 3730XL sequencer. The resulting sequences were analyzed in order to identify its correctness and the conserved nucleotide sequences from the vector that are important for protein expression , such as the ribosome binding site (rbs) and T7 promoter, that could result from the cloning process. The cloning and transformation steps are represented in figure II.4.

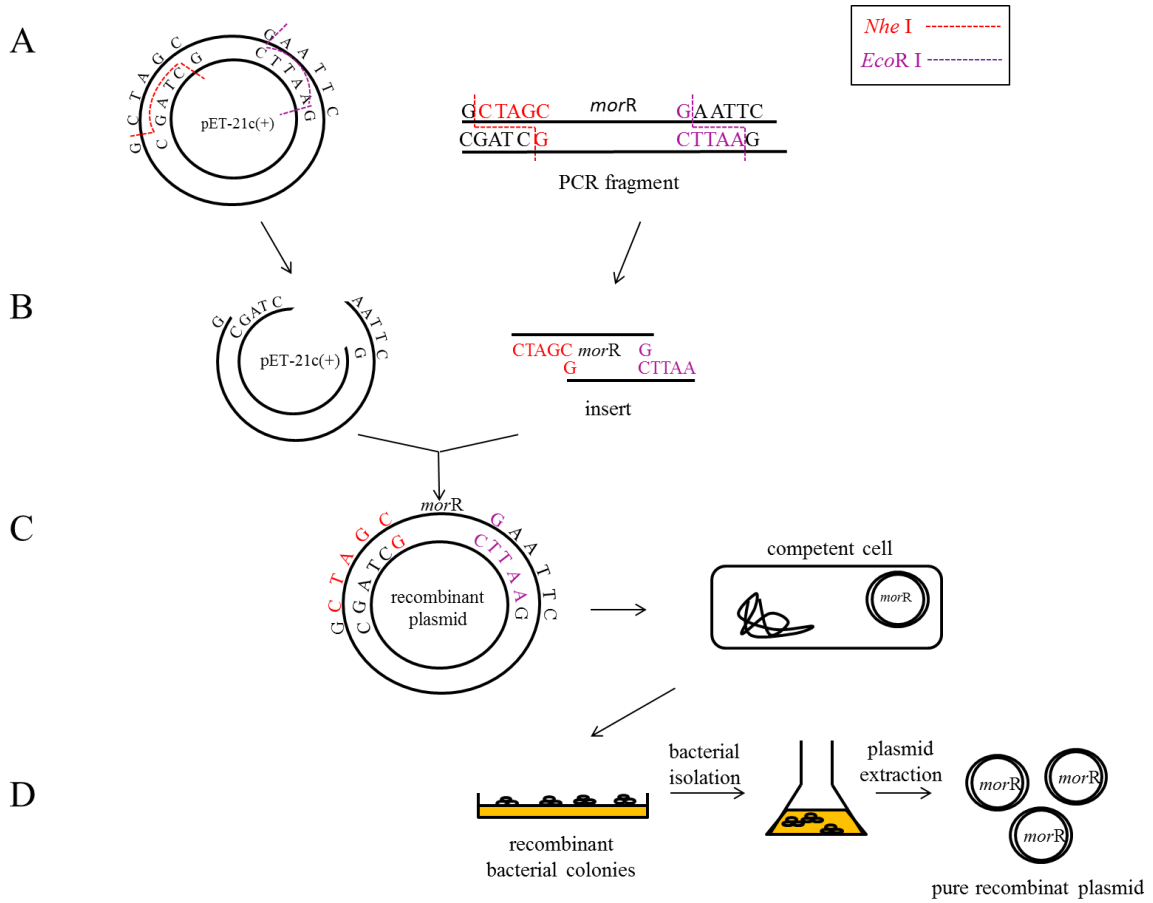

Figure II.4. Main principal steps of *mor*R gene cloning. A) pET-21c (+) and PCR fragment containing *mor*R gene with the recognition sites for *Nhe*I (in red) and *Eco*RI (in purple). B) pET-21c (+) and PCR fragment containing *mor*R gene after digestion protocol exhibiting the cohesive overhangs produced. C)recombinant plasmid carrying *mor*R gene after ligation, and subsequent plasmid transformation on Giga Blues competent cells. D)recombinant bacterial colonies in LB agar plate, isolation, and plasmid extraction and purification.

II.1.2 Protein expression

II.1.2.1 Small scale protein expression and optimization

The Bl21 (DE3) competent cells (Nzytech) was transformed with the recombinant plasmid, pETMorR, according to the manufacturer`s protocol with some modifications. 1µL of the recombinant plasmid DNA (0.2 to 50ng DNA) was added to 25 µL of competent cells, and the mixture was incubated on ice for 30 minutes. The cells were submitted to a heat shock treatment for 40 seconds at 42ºC in water bath, and subsequently incubated on ice for 2 minutes. 113µL of SOC Medium was added, and the cells grew for 1 hour, at 37ºC, on an orbital shaker at 225 rpm. After this period, 50 µl of the transformed

cells were spread on LB agar plates containing 100µg/ml ampicillin, and incubated overnight at 37ºC.

A well separated colony was selected, picked-up and submitted to growth in 25ml of LB medium supplemented with 100 µg/ml ampicillin in order to obtain a pre-inoculum. The pre-inoculum grew overnight at 37ºC, with agitation (225 rpm).

The small scale protein expression was optimized taking into account three different parameters: the optical density at 600nm (OD_{600}) (0.5 and 1.0), the IPTG concentration (0, 0.5 and 1 mM) and time of induction (zero hour, 4 hours and overnight). The log phase of bacterial cells growth is the ideal stage to induce protein expression, and OD_{600} around 0.5 to 1.5 is a good range of choice. The IPTG concentration should be also optimized, since its concentration needs to be maintained along the experiment.

The experiment was performed by inoculating 1ml of the pre-inoculum in 100 ml of LB medium (100 µg/ml ampicillin). After inoculation, the cells grew at 37ºC, in an orbital shaker at 225 rpm, until the OD_{600} reached 0.5. An aliquot of 5ml was collected immediately before induction (time zero hour). The cells were induced with 0, 0.5 and 1 mM of IPTG. For each tested conditions, an aliquot of 5ml was collected and stored at 4ºC after 4 hours and overnight period. The same procedure was performed when cells reached an OD_{600} of 1.0 (figure II.5).

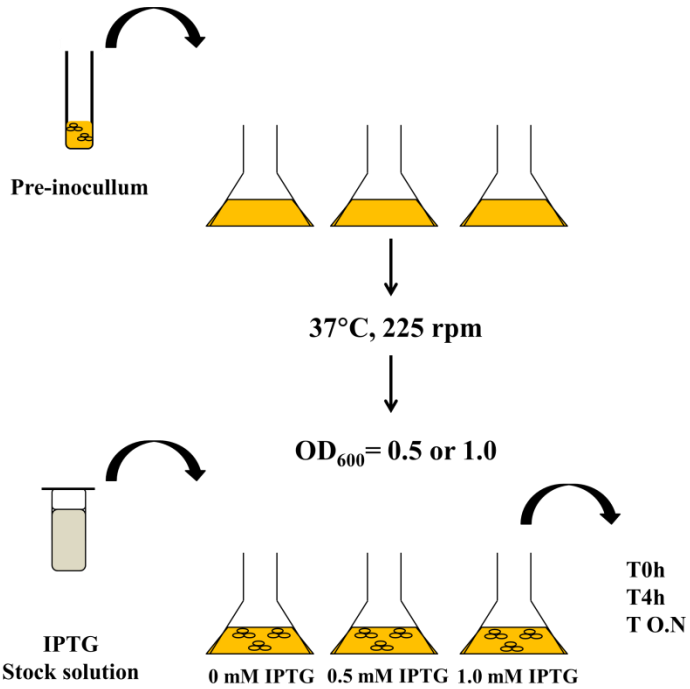

Figure II.5..Small scale MorR expression. The MorR expression was optimized according to the experimental conditions: the optical density at 600nm (OD_{600}) (0.5 and 1.0), the IPTG concentration (0, 0.5 and 1 mM) and time (T) of induction (zero hours, 4 hours and overnight).

In order to adjust the amount of bacterial cells present in each different aliquot, the values of OD_{600} were normalized for 1.2, and this procedure allowed protein expression visualization by Sodium Dodecyl Sulfate-Polyacrilamide Gel Electrophoresis (SDS-PAGE). The cells were centrifuged at 14.000 rpm for 10 minutes; the pellet was resuspended in 40µl of SDS sample buffer, and boiled for 8 min. An aliquot of 5µl was then analyzed by SDS-PAGE in 12.5% acrylamide gels.

II.1.2.2 Large scale protein expression

In order to obtain amounts of protein enabling MorR purification the cells were grown in large scale. A single colony was selected from a plate containing the transformed BL21 (DE3) cells carrying the recombinant plasmid pETMorR, and placed in 80 ml of LB medium supplemented with 100µg/ml ampicillin to obtain a pre-inoculum. The pre-inoculum grew overnight at 37ºC, in an orbital shaker at 225 rpm. A 10 ml sample of the pre-inoculum was added to each 1 L of LB medium supplemented with 100µg/ml ampicillin, until a total volume of 6 L. When cells reach an OD_{600nm} of 1.0, 1 mM of IPTG

was added to induce heterologous *mor*R transcription, and, consequently, protein expression.

After an overnight growth period, the cells were harvested by centrifugation at 8.000 rpm for 16 min at 4°C, and after resuspended in 10mM Tris-HCl, pH 7.6 (3ml/g of wet cells). The cells were thermally disrupted by rapid liquid nitrogen freezing and thawing processes, followed by mechanical lysis by French-press at 28,000 psi. Proteolytic activity was inhibited with EDTA-free Protease Inhibitor Cocktail (Roche), and DNase I from bovine pancreas (Roche) was added to remove (undesirable) single and double strand DNA. Unbroken cells and cell debris were removed by centrifugation at 8.000 rpm for 16 min at 4ºC.The soluble extract was obtained by ultracentrifugation at 44.000 rpm for 1h at 4ºC.

II.2. Results and Discussion

II.2.1 *mor*R genomic context

Genomic analysis of *D. alaskensis* G20 revealed the presence of a putative responsive regulatory protein codified by *Dde*_0109 gene, corresponding to *mor*R, which is formed by 1401 nucleotides (GI: 3758851)[2] and is annotated in the genome as *zra*R, zinc associated response regulator. A Blast search revealed that this gene shares common features with other transcriptional regulatory genes present in different gram negative bacteria (figure II.6).

The main characteristic of this type of transcriptional regulatory genes is the genomic position and orientation which reveals the presence of surrounding genes classically involved in signal transduction, and the divergent gene regulation profile. The *mor*R gene is conserved on *Desulfovibrio* genus, but also has a good similarity with other regulatory genes (*zra*R) present in some pathogenic bacteria. A megablast search revealed that *mor*R shares 76% of sequence homology with transcriptional regulator *zra*R in *Desulfovibrio vulgaris* str. Hildenborough, 72% with *fis* transcriptional regulators in *Desulfovibrio vulgaris* str.`Miyazaki F` and 60% with three others *zra*R transcriptional regulator present in *Escherichia coli* O127:H6 str. E2348/69; *Shigellaflexneri* 2a str. 301 and *Salmonella entericaserovar Typhimurium* LT2.

The similarity arises on the fact that all these bacterial species are Gram-negative (containing a periplasmic space), and the *zra*R gene is located downstream of a sensor histidine kinase (*zra*S) and by a gene that codifies a periplasmic protein (*zra*P), characterizing a type of gene rearrangement classically involved in TCS. This architecture is in agreement with the idea that genes responsible for codifying regulatory proteins are often situated near their target genes[3]. The general conservation of this type of gene rearrangement among some gram negative bacteria could indicate ecological preferences and biochemical signaling capacity under stress conditions[4]. Members of *zra*RSP TCS are divergently transcribed from *zraS*P intergenic region, and are involved, primarily, with a zinc associated response. ZraP is a periplasmic protein involved in envelope stress response, metal homeostasis and acts as a chaperone[5,6,7].

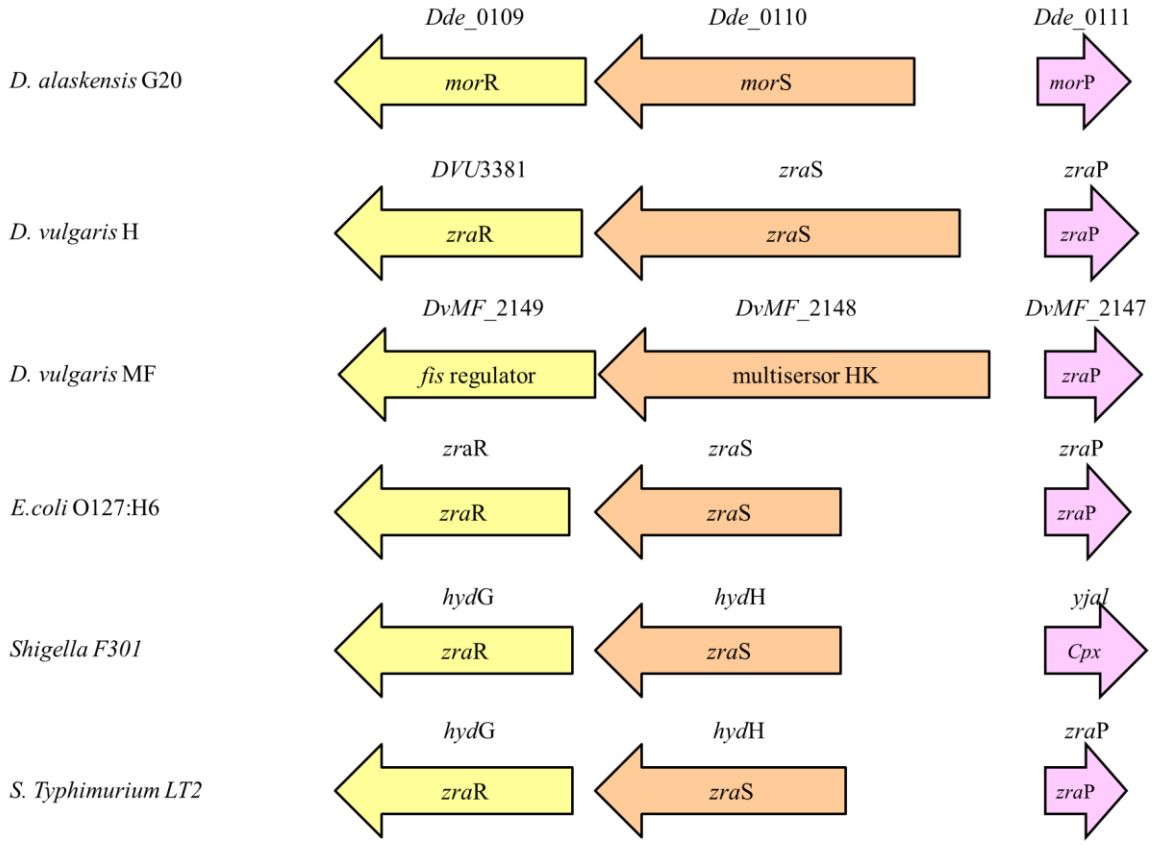

Figure II.6. Genomic comparison and organization between *mor*R and other similar response regulators in different types of gram negative bacteria. The genes are represented by arrows and the arrow direction shows the genomic orientation. The NCBI gene symbol is presented above and the description is inside the arrows. To facilitate the comprehension of this study, the *mor*R, *mor*S and *mor*P nomenclature isn't following the NCBI gene description. The scheme is organized according to megablast result taking into consideration the percentage of similarity (76% for *zra*R from *D. vulgaris* H, 72% for *fis* from *D.vulgaris* MF and 60% for *zra*R from *E.coli* O127:H6; *Shigella* F301 and *S. Typhymurium* LT2).

The *mor*P gene (*Dde*_0111), annotated in the genome as *zra*P, was found to be involved in Mo regulatory mechanisms in *D.alaskensis* G20;it is composed by 519 nucleotides[2]. According to NCBI datatabase, it codifies a putative zinc resistance-associated protein composed by 172 amino acids residues (GI:78355158). This protein contains a conserved CpxP domain identified in the amino acid sequence from residue 65 to 132. Proteins belonging to CpxP family have a periplasmic location, they are a part of TCS, and act as a global modulator of cell-envelope stress in gram-negative bacteria[8].

The *mor*S gene (*Dde*_0110) is formed by 1779 nucleotides, and codifies a putative histidine kinase (NtrB) containing 592 amino acids residues (GI: 78355157). According to Simple Modular Architecture Research Tool (SMART, http://smart.embl-heidelberg.de/), the translated sequence codifies a protein with five main conserved regions: two transmembrane domains, one signal sensor PAS domain (Per, Arnt, Sim superfamily), one HK A domain and one HK like ATPase domain. Proteins displaying this type of secondary structure architecture may be acting as biological sensors, and are involved in phosphorelay processes[9].

DNA analysis of the intergenic region between *mor*P and *mor*S displayed the presence of four putative promoters clustered in a double manner. Each cluster is composed by two promoters sequences oriented in an opposite direction.

The first cluster region, called σ_{54}-P, contains – 24 (GGCACG) and -12 (TTGC), (core consensus TGGCACG N4 TTGC)conserved promoters relative to the predictive *mor*P transcriptional +1 start[2]. These conserved sequences might be responsible for σ_{54} binding. Likewise, a ribosome binding site (rbs) is present 4 nucleotides upstream of *mor*P gene.

The second cluster, called σ_{70}-P, comprises -35 (TACACC) and -10 (GTATAAA) conserved boxes (core consensus TTGACA N17 TATAAT), that are located upstream of the predictive *mor*S transcriptional +1 start site. This second cluster was identified by the Prediction of Bacterial Promoters (BProm) software, and is a putative σ_{70} binding site. Additionally, other conserved features compose this cluster, such as: a conserved rbs situated five nucleotides upstream of *mor*S gene, and a conserved 16 bp spacer located between -35 and -10[10,11,12]. A schematic overview on the genomic context and intronic region between *mor*P and *mor*S is showed in figure II.7.

A

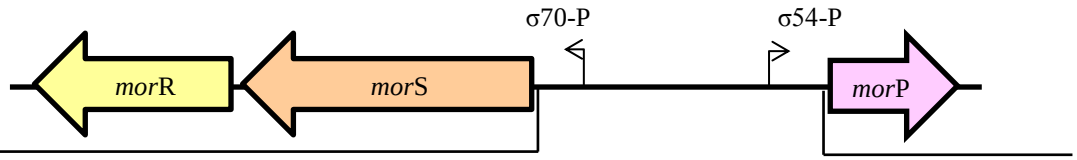

B

CATTGCCGTCACCTTGCGTGTTCAATATTTGTACAGCGTCTATTTTTTATACAGTGCTTT

5` ***morS*** **rbs** **-10**

3` GTAACGGCAGTGGAACGCACAAGTTATAAACATGTCGCAGATAAAAAATATGTCACGAAA

TTCTCAAAGGTGTATGTTTTTTATACACTGACTTTCACTGTACTGTCCCGCTTCTGTGCA

-35

AAGAGTTTCCACATACAAAAAATATGTGACTGAAAGTGACATGACAGGGCGAAGACACGT

-24 **-12**

TAACATGCCGGTTTGTTGTGCGATATTGCTTCATGTGCGTGTATGGCACGCCTGTTGCTC

ATTGTACGGCCAAACAACACGCTATAACGAAGTACACGCACATACCGTGCGGACAACGAG

rbs

TATCATGAGCAAATGCAAGCAACGCACCAGAAGGTGCACAAGGTAATCCGGAGGACATT

ATAGTACTCGTTTACGTTCGTTGCGTGGTCTTCCACGTGTTCCATTAGGCCTCCTGTAA

morP

ATG 3`

TAC 5`

Figure II.7. Genomic context of *mor*P, *mor*S and *mor*R. A) Genomic orientation. B) Intergenic region between morP and morS showing the conserved boxes, and ATG start codons. Arrows indicate the transcription direction.

The genomic profile presented for *mor*P, *mor*S and *mor*R indicates that those genes might be transcribed by divergent and non-overlapping promoters, and such a set of genes would be controlled by the cognitive response regulator: MorR.

II.2.2 Cloning

Classical genetic engineering tools were used as a strategy to obtain a recombinant plasmid carrying de *mor*R gene. The objective was to transform a competent cell with the recombinant plasmid, and control the *mor*R transcriptional level and expression.

The *mor*R gene from *D. alaskensis* G20 was amplified by PCR and visualized in 1% agarose gel (figure II.8 [1]). The result shows the presence of a single band in agarose gel between 1000 and 1500 bp corresponding to the *mor*R expected result (1401bp).

The PCR product and pET-21c (+) were digested with *Nhe*I and *EcoR*I, and no star activity was visualized. Both were purified and visualized in 1% agarose gel before ligation (figure II.8 [2]). After ligation, the recombinant plasmid was transformed in Nova Blues Giga Blues Competent Cells. Following bacterial growth, five colonies were selected, and identified by PCR. Four of the colonies were positive (figure II.9 [3]), and the resulting plasmid, carrying the *mor*R gene, was named as pETMorR. The plasmids were isolated from competent cells and purified (figure II.9 [4]). Then, they were submitted to DNA sequencing and the results showed no mutations and the gene was correctly oriented allowing induction of gene transcription and, subsequent, protein expression.

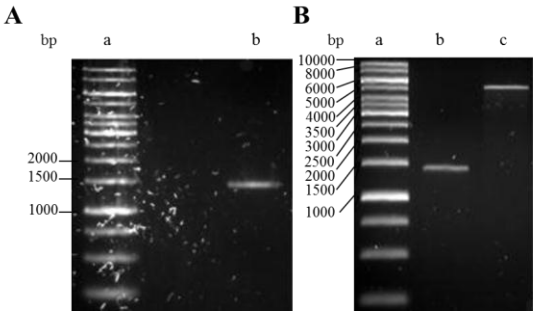

Figure II.8. Different steps of molecular cloning process: PCR and pure insert and plasmid after digestion. A): a) 1kb molecular ladder, b) PCR of *mor*R gene. B): a) 1kb molecular ladder, b) purified digested PCR product, c) purified digested pET-21c (+). Running was performed in 1% agarose gel, in buffer TAE 1X, during 25 minutes at 100 V.

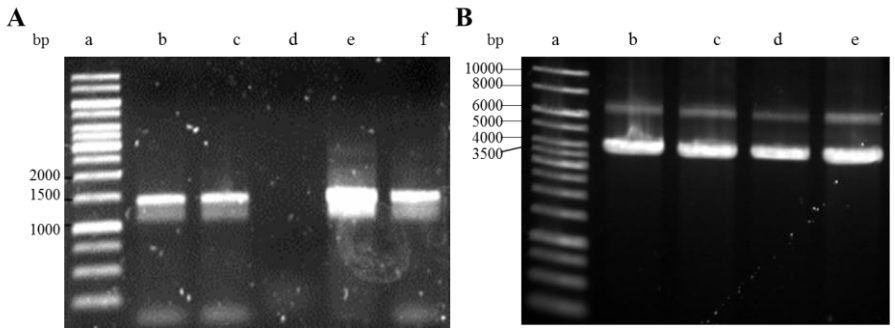

Figure II.9. Different steps of molecular cloning process: colony PCR and plasmid extraction. A): a) 1kb molecular ladder, b-f) Colony PCR: each band corresponds to a single recombinant colony. B): a) 1kb molecular ladder, b-e) Isolated recombinant plasmids, each band correspond to a single recombinant plasmid. Running was performed in 1% agarose gel, in buffer TAE 1X, during 25 minutes at 100 V.

The sequencing analysis of the recombinant plasmid revealed that *mor*R was preceded by the rbs binding site, and that no DNA mutation was created during the cloning procedure. The presence of the T7 promoter was not possible to verify through sequencing reaction.

II.2.3 Protein expression

II.2.3.1. Small scale expression

A small scale protein expression was performed in order to evaluate if *mor*R was under T7 promoter control, and to optimize the growth and induction conditions. The control parameters evaluated were the OD_{600} (0.5 and 1.0), the IPTG concentration (0, 0.5 and 1.0 mM), and the time of induction (4h and overnight).

The results show that the transcription of *mor*R is induced in all the conditions tested (figure II.10 and II.11). However, the majority of protein was obtained when bacteria was induced at OD_{600} of 1.0 with 1mM of IPTG and during an overnight period (figure II.11,[J]). Thus, this condition was chosen for the future experiments. The control experiment, with no IPTG induction, revealed a significant degree of *mor*R expression (figure II.10 [C, D] and figure II.11 [B, C]) indicating a misrule of the T7 RNA polymerase expression from lacUV5 promoter which represent a low degree of expression control. However, this same result suggests that MorR is a nontoxic product for *E.coli*, since the growth was not inhibited for this basal level of transcription.

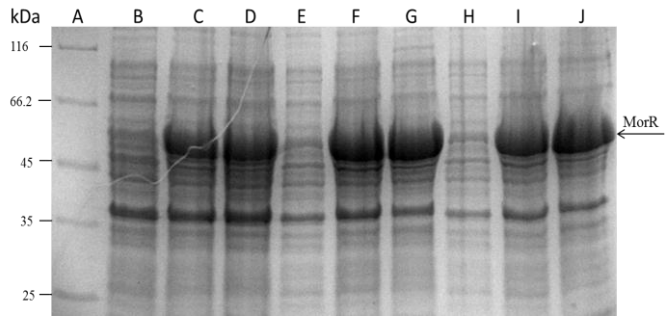

Figure II. 10. Small scale protein expression at OD_{600} 0.5. A 12.5% polyacrylamide SDS-PAGE showing the expression profile of transformed BL21 (DE3) competent cells induced at OD 0.5. A) Ladders. B) Cells with 0 mM IPTG at zero hour. C) Cells with 0 mM IPTG after 4 hour. D) Cells with 0 mM IPTG after an overnight period. E) Cells induced with 0.5 mM IPTG at zero hour. F) Cells induced with 0.5 mM IPTG after 4 hours. G) Cells induced with 0.5 mM IPTG after an overnight period. H) Cells induced with 1 mM IPTG at zero hour. I) Cells induced with 1 mM IPTG after 4 hours. J) Cells induced with 1mM IPTG after an overnight period.

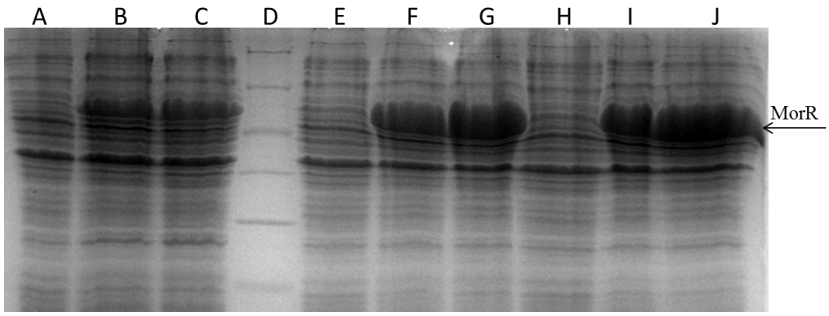

Figure II. 11. Small scale protein expression at OD_{600} 1.0. A 12.5% polyacrylamide SDS-PAGE showing the expression profile of transformed BL21 (DE3) competent cells induced at OD 1.0. A) Cells with 0 mM IPTG at zero hour. B) Cells with 0 mM IPTG after 4 hours. C) Cells with 0mm IPTG after an overnight period. D) Ladders (116, 66.2, 45, 35 and 25 kDa). E) Cells induced with 0.5 mM IPTG at zero hour. F) Cells induced with 0.5 mM IPTG after 4 hours. G) Cells induced with 0.5 mM IPTG after an overnight period. H) Cells induced with 1 mM IPTG at zero hour. I) Cells induced with 1 mM IPTG after 4 hours. J) Cells induced with 1mM IPTG after an overnight period.

The optimal condition chosen for protein expression was $O.D_{600}$ of 1.0 with 1mm of IPTG after an overnight period (figure II.11J) given that the results showed a high amount of MorR protein along this condition.

II.2.3.2. Large scale expression

The large scale protein expression was performed in order to evaluate where the expressed protein was localized in the cell and also as a preliminary step before protein purification. The experiment was performed in Bl21 (DE3) cells and following the

experimental conditions optimized in the small scale protein expression. This experiment is identify if the the protein is in the soluble fraction and not present as insoluble inclusion bodies or membrane protein. The heterologous protein was present in all cellular fractions with the highest amount existing as soluble form (figure II.12).

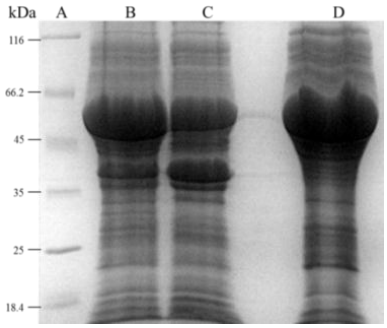

Figure II. 12. 12.5% SDS-PAGE showing the cellular localization of MorR. A) Ladder. B) Cell debris fraction. C) Membrane fraction. D) Soluble fraction.

The presence of a considerable amount of protein in the membrane fraction indicates an absence of an optimal condition during the cell lysis. Moreover, the presence of a high quantity of protein in the cell debris fraction may be related with an high percentage of protein expression which can block a correct protein folding and, therefore, part of the protein may be not available as soluble form.

II.3. References

1. Mierendorf, R. C., Morris, B. B., Hammer, B. & Novy, R. E. Expression and Purification of Recombinant Proteins Using the pET System. *Methods Mol. Med.* **13,** 257–92 (1998).

2. Rivas, M. G. *et al.* Molybdenum induces the expression of a protein containing a new heterometallic Mo-Fe cluster in Desulfovibrio alaskensis. *Biochemistry* **48,** 873–82 (2009).

3. Studholme, D. J. & Dixon, R. Domain Architectures of 54 -Dependent Transcriptional Activators. *J. Bacteriol.* **185,** 1757–1767 (2003).

4. Galperin, M. Y. Diversity of structure and function of response regulator output domains. *Curr. Opin. Microbiol.* **13,** 150–9 (2010).

5. Franke, S., Grass, G. & Nies, D. H. The product of the ybdE gene of the Escherichia coli chromosome is involved in detoxification of silver ions. *Microbiology* **147,** 965–72 (2001).

6. Ravikumar, S., Yoo, I., Lee, S. Y. & Hong, S. H. A study on the dynamics of the zraP gene expression profile and its application to the construction of zinc adsorption bacteria. *Bioprocess Biosyst. Eng.* **34,** 1119–26 (2011).

7. Appia-Ayme, C. *et al.* ZraP is a periplasmic molecular chaperone and a repressor of the zinc-responsive two-component regulator ZraSR. *Biochem. J.* **442,** 85–93 (2012).

8. Danese, P. N. & Silhavy, T. J. CpxP, a stress-combative member of the Cpx regulon. *J. Bacteriol.* **180,** 831–9 (1998).

9. Weiss, V., Kramer, G., Dünnebier, T. & Flotho, A. Mechanism of regulation of the bifunctional histidine kinase NtrB in Escherichia coli. *J. Mol. Microbiol. Biotechnol.* **4,** 229–33 (2002).

10. Alain Dolla, Rongdian Fu, M. J. B. and & Voordouw, G. Nucleotide Sequence of dcrA, a Desulfovibrio vulgaris Hildenborough Chemoreceptor Gene, and Its expression in Escherichia coli. *J. Bacteriol.* **174,** 1726–1733 (1992).

11. Ross, W. & Gourse, R. L. Analysis of RNA polymerase-promoter complex formation. *Methods* **47,** 13–24 (2009).

12. Typas, A. & Hengge, R. Role of the spacer between the -35 and -10 regions in sigmas promoter selectivity in Escherichia coli. *Mol. Microbiol.* **59,** 1037–51 (2006).

Chapter III

MorR biochemical characterization and DNA binding

MorR biochemical characterization and DNA binding

Context

The response regulatory proteins are mainly regulated by post-translational modifications, such as phosphorylation. The phosphorylation status and effect have been studied in some RR proteins that belong to TCS. Usually, those proteins are activated by phosphorylation which induces protein conformational changes that enhance specific transcriptional regulatory networks, usually through DNA binding. The biochemical characterization is the first step to perform protein studies. In order to study MorR, the recombinant plasmid carrying the *mor*R gene was induced to express the MorR protein. The protein was purified as soluble form and was characterized. MorR has an extinction coefficient of ε_{280}= 30823 M^{-1} cm^{-1} and the ICP-AES revealed the absence of Mg, Zn, Mo and Cu. The MorR was purified as a monomer and does not contain any phospho amino acid in its structure. In order to identify if MorR binds to DNA, the intergenic region between *mor*S and *mor*P was amplified and purified. The EMSA experiment revealed that MorR binds to the target intergenic region and the DNaseI footprinting experiment showed the site of binding. The interaction between phosphodonors and RR are reviewed given that RRs like MorR are susceptible to phosphorylation. In this way, the MorR was used in interaction studies with small phosphodonors in order to visualize possible conformational changes. The oligomeric status of MorR was not altered upon incubation with acetylphosphate and phosphoramidate.

III.1.Introduction

III.1.1. Phosphorylation and response regulators (RR)

Among RR proteins belonging to TCS, phosphorylation is the main post-translational signal capable to induce conformational changes and protein output response.Acetylation of RR has been reported, but only few examples are available[1,2]. The oligomeric states of RR have hardly been investigated, and post-translational modifications (e.g., phosphorylation) have been associated with the transformation of inactive monomers/dimers to active oligomers. Small phosphodonors, such as acetylphosphate, ammonium hydrogen phosphoramidate, carbamoyl phosphate and beryllofluoride have been identified as RR oligomer`s inducers[3,4,5,6].

As previously mentioned in chapter II, the MorR shares sequence similarities with ZraR and NtrC. To date, the ZraR (also known as HydG) has been characterized as a zinc/lead responsive protein which binds in the intergenic region between *zra*P and *hyd*H[7]. However, the ZraR mechanisms of DNA binding and post-translational modification are not well comprehended. On the other hand, research on the NtrC oligomerization coupled to phosphorylation progressed in recent years and can serve as an example for the present study.

A variety of analytical tools have been applied in order to elucidate RR oligomerization upon phosphorylation, such as: gel filtration and reverse-phase chromatography, fluorescence spectroscopy, scanning force microscopy and analytical ultracentrifugation. Changes in oligomeric state were investigated in proteins belonging to OmpR family (OmpR, DrrB, MtrA and NblR). OmpR is a TCS transcriptional activator protein involved in the regulation of *omp*C and *omp*F genes, which codifies two major outer membrane porin (OmpC and OmpF) in *E.coli*[8]. The OmpR family is characterized by the presence of two distinct domains: a N-terminal receiver domain with a conserved phosphoacceptor D55, and a C-terminal DNA binding wHTH domain[9]. *Thermotoga maritima* DrrB is a RR which can serve as a model for structural comprehension of OmpR family. The crystal structure of the protein has been solved. The oligomeric state of DrrB changed after incubation with ammonium hydrogen phosphoramidate. A small amount (30 µM) of DrrB was incubated with 100 mM of ammonium hydrogen phosphoramidate for 10 min at 60ºC. The sample was injected in a Superdex 75 10/30, and the unphosphorylated

DrrB presented a molecular mass of 22.2 kDa, and the phosphorylated DrrB had a molecular mass of 42.1 kDa. The results showed that DrrB forms a dimer when phosphorylated[10].

The role of phosphorylation was also investigated for *Corynebacterium glutamicum* MtrA, a RR involved in transcriptional repression and activation of genes required during hyperosmotic stress and cell wall peptidase secretion[11,12]. A HiLoad 26/60 Superdex 200 was used to monitor protein oligomerization, and ammonium hydrogen phosphoramidate (and not acetylphosphate) led to dimerization of MtrA (56.6 kDa). In both cases, the experimental concentration of phosphodonor was 50 mM. Moreover, the binding affinity between MtrA and DNA was also improved by ammonium hydrogen phosphoramidate[11].

The use of acetylphosphate as a protein conformational inducer was also investigated by analytical gel filtration for cyanobacteria *Synechococcus* sp NblR. NblR is a transcriptional activator of *nbl*A gene that is involved in nutrient starvation response exhibiting a phosphorylation-independent activity[13,14]. Gel filtration was carried out using a Superdex 200 HR 10/30, and no significant alteration in elution profile was visualized when NblR was incubated with 12.5 mM of acetylphosphate for 1h at room temperature. It is important to mention that NblR is a non-canonical RR, but contains a conserved phosphorylate site at D57. Moreover, phosphorylation of D57 is not required for NblR function[15].

The NtrC protein is a dimer in solution; it should interact with RNAPσ_{54} in order to activate the transcription[16,17]. Scanning force microscopy was used as a tool to visualize NtrC oligomerization after carbamoyl phosphate and NtrB (the physiological phosphodonor) incubation. The results clearly showed that NtrC dimers must built large oligomers to activate transcription. Interestingly, the NtrC behavior is completely different from eukaryotic enhancer-binding proteins: NtrC binds solely by protein-protein interaction in contrast to eukaryotic enhancers that bind directly to DNA[18]. In what concerns the NtrC binding profile, analytical ultracentrifugation showed that the unphosphorylated form binds as a dimer to a single site in DNA. Moreover, the NtrC-DNA interaction occurs essentially without cooperativity and the phosphorylated protein forms a complex (oligomers) at the enhanced sequence in the DNA duplex[19].The fluorescence anisotropy and fluorescence

correlation spectroscopy corroborate the previous assumption that NtrC binds with no cooperativity and that one dimer of NtrC forms two ion pairs (one per NtrC monomer) with the DNA backbone. In that way, one unphosphorylated NtrC dimer binds to one DNA binding site and two unphosphorylated dimers to two adjacent binding sites[20]. The phosphorylation is crucial to NtrC transcription initiation, which is coupled to the protein ATPase activity[21]. Thus, the phosphorylation status of the N-terminal REC domain regulates the activity of the central AAA^+ domain and this intermolecular interaction might be mediated by the contact of a flexible helix-α4 of the phosphorylated REC domain with the adjacent partner subunit[5,22]. X ray solution scattering and electron microscopy studies corroborates that a binding mechanism between the both subunits occurs and that the phosphorylation has a direct contribution to hexamer stability[23].

The variety of analytical tools used in order to comprehend the effect of phosphorylation into oligomerization of RR varies dramatically. Moreover, some RR shows a preference for a phosphodonor agent than other. This preference is not comprehended but might be correlated with the structural characteristic of the RR and/or the experimental conditions used.

III.2. Methodology

III.2.1. Protein purification

In order to obtain pure protein, the soluble fraction was dialyzed overnight against 10 mM Tris-HCl, pH 7.6 and loaded onto a DEAE Sepharose FF column (2.6 X 25 cm) previously equilibrated with the same buffer using a flow rate of 3 ml/min. The protein was eluted using a two-step discontinuous gradient. The first gradient, from 10 to 150 mM Tris-HCl, pH 7.6, was performed with one bed volume. The MorR was eluted using a second gradient, from 150 to 300 mM Tris-HCl, pH 7.6, over the course of two bed volumes. The protein was dialyzed against 10 mM Tris-HCl, pH 7.6, and loaded onto a Source 15Q (2.6 X 24 cm) equilibrated with the same buffer at a flow rate of 1 ml/min. Again, a two-step discontinuous gradient was applied. The first gradient, from 10 to 150 mM of Tris-HCl, pH 7.6, was performed over the course of one bed volume. The MorR

was then eluted using a gradient from 150 to 300 mM Tris-HCl, pH 7.6, over the course of four bed volumes.

All the dialysis procedures were performed using a membrane with a molecular mass cut-off of 10 kDa, activated by boiling for 10 min (distillated water) with 1 mM of EDTA. After each chromatographic step, the protein purity was checked by SDS-PAGE electrophoresis, in 12.5% acrylamide gels stained with Coomassie Blue.

An additional purification step using a Superdex 200 (2.6 X 66 cm) gel filtration column was performed. The column was equilibrated with 50 mM Tris-HCl, pH 7.6, and 150 mM NaCl using a flow rate of 2 ml/min. The central part of the peak obtained in the chromatogram corresponded to MorR. The corresponded fractions were collected, concentrated and dialyzed using a concentrator (Millipore) with a molecular weight cut-off of 30kDa, and stored in 10 mM Tris-HCl, pH 7.6, at -80ºC.The overall protein purification protocol is presented in figure III.1.

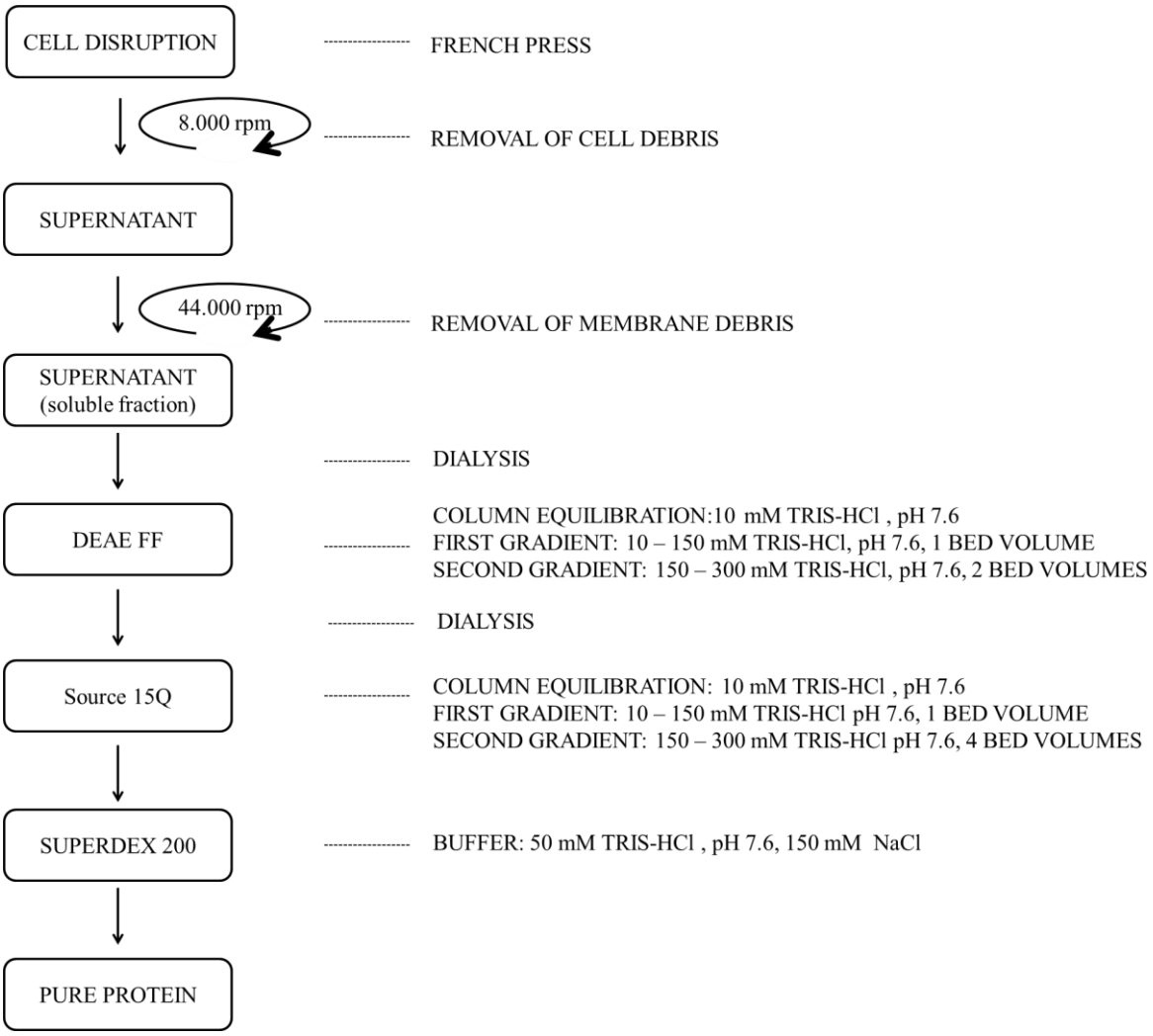

Figure III. 1. Diagram of MorR purification

III.2.2. UV-VIS spectroscopy

UV/VIS absorption data were recorded by Shimadzu UV-1800 spectrophotometer in 1cm quartz cuvettes.

III.2.3 Protein quantification

Protein was quantified according to Miller *et al.*, 1959[24]. This methodology applies some modification in the method described by Lowry (1951). A 200 µL of aliquots of alkaline copper reagent (composed of 10 parts of 10% sodium carbonate in 0.5% sodium hydroxide and 1 part of 0.5 % copper sulfate in 1% potassium tartrate) were added to 200 µL of protein sample in eppendorfs tubes. The mixture was incubated for 10 min at room temperature, and a 600 µL aliquot of a 1 to 11 dilution of Folin Ciocalteau reagent was added to the sample, mixed and incubated for 10 min at 50ºC. The mixtures were cooled to room temperature, and absorbance was measured at 660 nm in a Shimadzu UV-1800 spectrophotometer using a cuvette of 1 cm. The calibration curve was prepared with Bovine Serum Albumin (BSA) (stock 2 mg/ml) standards.

III.2.4. N- terminal sequencing

The N-terminal sequencing was performed by automated Edman degradation in an Applied Biosystem 120 analyser model 477, following the manufacture instructions. A total of 100 pmol of MorR was used.

III.2.5. Peptide Mass Fingerprint

The sample (100 pmol) was digested according to Santos *et al.*, 2007 with some modification[25]. The modification was the substitution of urea to 50% acetonitrile to denature the protein sample. The sample was analyzed by MALDI-TOF-MS (model Voyager-DE™ PRO Workstation) using a positive reflector as ionization mode and the peptides were identified using the MASCOT (http://www.matrixscience.com/cgi/search_form.pl) applying the following parameters:

Bank of data: NCBInr and SwissProt

Fixed modification: Carbamidomethyl (C)

Variable modification: Oxidation (M)

Enzyme: Trypsin

III.2.6. Protein metal analysis

Protein metal content (Zn, Mg, Mo and Cu) was quantitatively determinate by Inductively Coupled Plasma - Atomic Emission Spectroscopy (ICP-AES) (Horiba Jobin-Yvon, France), which uses a source of atomization temperature of 10000K to decompose sample components. A detection quantification limit of 1 ppb was attained for samples diluted in water, and 5 ppb for samples diluted in buffer. The Reagecom 23 ICP multielement was used for the calibration curve.

III.2.7. Molecular mass determination

The oligomeric state of the purified MorR was determined by two independent analytical gel filtration using the Superdex200 column (10/30 GL) equilibrated with 50 mM Tris-HCl (pH 7.6) and 150 mM NaCl using a flow rate of 0.4ml/min. The first calibration was performed at Faculdade de Ciência e Tecnologia at Universidade Nova de Lisboa using Ferritin (440 kDa), aldolase (158 kDa), conalbumin (75 kDa), ovalbumin (44 kDa) and ribonuclease A (13.7 kDa) (GE Healthcare Life Sciences) as protein standards. The second calibration was performed at Consejo Superior de Investigaciones Científicas (CSIC) using Thyroglobulin (670 kDa), Globulin (150 kDa), Ovalbumin (44 kDa) and Myoglobin (17 kDa) (BioRad) as protein standards. The distribution coefficient (Kav) was calculated as follows:

$$\boldsymbol{Kav = (Vr - V0)/(Vc - Vo)} \qquad \textbf{Eq.3. 1}$$

Where:
V0= void volume of the column
Vr= retention (elution) volume of the protein
Vc= the geometric bed volume in ml

The molecular mass of MorR was determined by matrix-assisted laser desorption ionization time of flight (MALD TOF) mass spectrometry. The spectrometer was equipped with a nitrogen laser radiating at 337 nm (Applied Biosystems, Foster City, USA, model voyager DE-PRO biospectrometry workstation). A total of 100 pmol of MorR was used.

III.2.7.1 Molecular mass determination upon phosphorylation

The oligomeric state of MorR was monitored after incubation with acetylphosphate (SIGMA A0262) or hydrogen phosphoramidate incubation. Both reactions were performed under the same experimental conditions:9 µM of MorR was diluted in 10 mM Tris-HCl, pH 7.6, with 2 mM MgCl2 and the sample was incubated with 50 mM of phosphodonor on ice for 30 min. Then, the sample was injected in Superdex 75 HR 10/30 equilibrated in 50 mM Tris-HCl and 150 mM NaCl. The chromatography was monitored at 280 nm.

III.2.8.Nano LC-MS mass spectrometry

III.2.8.1. In solution digest

For mass spectrometry analysis, approximately 1 pmol of the protein was dissolved in 4µL of 100mM ammonium bicarbonate (ABC) and submitted to disulfide bond reduction using 1µL of 1mM DTT in 100mM ABC for 45min at room temperature. Cysteine thiol groups were further blocked through alkylation using 1µL 5.5mM Iodacetamide in 100mM ABC for 1 hour at room temperature and dark environment. Sample volume was increased to 40µL with ABC, and 10µg of MS-grade modified trypsin (Promega) was added to the sample overnight at 37^{o}C. Enzymatic reaction was quenched by acidification using Trifluoroacetic acid (TFA). Before injection into the mass spectrometer, the salts were removed from the peptide mixture through C18 resin (Empore 3M) cleaning steps (STAGE-TIP method).

III.2.8.2. LC-MS/MS

Peptides were separated by reversed-phase liquid chromatography using a Dionex Ultimate 3000 nanoLC (Thermo) coupled directly to a QExactive mass spectrometer (Thermo) equipped with a nanoelectrospray source (Thermo). The organic gradient used for separation was performed during a 60 minute run, starting at 5% solvent B up to 35% solvent B (solvent A is 0.1% formic acid in water, while solvent B is 90% acetonitrile 0.1% formic acid in water). The stationary phase was an Acclaim PepMap 100 column (C18, 2 µm beads, 100 Å, 75 µm inner diameter). Flow used was 300nL/min.

The QExactive was operated in data-dependent mode to automatically switch between MS and MS/MS acquisition. Survey full scan MS spectra were collected at resolution 70,000 (at m/z 200), with scan range between 300 to 1750 m/z, Automatic Gain Control (AGC) target of 1E6 and maximum injection time of 20ms. The Top 10 most abundant ions in each scan were selected for isolation and fragmentation. MS/MS scans were collected at 17,500 resolution (at 200 m/z), AGC target of 2E5, maximum injection time of 60ms, isolation width of 3 m/z, and collision energy of 25%. Unassigned and single charged ions were excluded. Once selected for MS/MS, ions were dynamically excluded for re-sequence for 45s.

III.2.8.3. Protein identification

MS raw files were processed using the Proteome Discoverer software (Thermo). Sequence information was then submitted to an in-house Mascot server v2.2 (Matrix Science) using the following search parameters: Enzyme: Trypsin without proline restrictions; two miscleavages allowed; MS mass accuracy of 5ppm; MS/MS mass accuracy of 0.05 Da; cysteine carbamidomethylation as fixed modification; N-terminal glutamine pyroglutamate, N-terminal glutamic acid pyroglutamate, methionine oxidation, lysine acetylation, serine/threonine phosphorylation and aspartic acid phosphorylation as variable modification. Sequenced were compared to an updated NCBInr database for bacteria.

III.2.9.Electrophoretic mobility shift assay (EMSA)

EMSA is a technique used to detect DNA binding protein. The principle of this technique is that DNA bound to a protein migrates slowly through a polyacrylamide gel. Usually, the target DNA is labeled with radioactive isotopes like ^{32}P. An alternative to radioactive isotopes is the use SYBR® Green I (Promega) in order to visualize the DNA shift. The use of SYBR® Green I could be a good alternative to label DNA for EMSA experiment. It can serves as a screening method to detect DNA-protein interactions, but exhibit lower resolution when compared with isotopes methods. This feature limits the measurement of association constants using SYBR® Green I in EMSA experiments.

The intergenic region between *mor*P and *mor*S was amplified by PCR from *D.alaskensis* G20 cells using the primers forward (5'-TGCCGTCACCTTGCGT-3`) and reverse (5`-GTCCTCCGGATTACCTTGT-3`). The fragment was gel purified using the QI Aquick extraction kit (Qiagen), quantified at 260nm, and 0.078 μM of this fragment were mixed with 6 μM of purified MorR in a buffer containing 10 mM Tris-HCl, pH 7.6, 250 mM KCl, 0.2 mM EDTA, 0.2 mM DTT and glycerol 10%. The mixture (total volume of 19 μl) was incubated for 1 hour on ice. It was then applied in a native 7.5% polyacrylamide gel, running for 1h at 100 mV and stained with Syber green.

III.2.10.DNAse I Footprinting assay

The sequence-specific interaction of proteins to DNA can be studied using DNase I footprinting. In this technique an end-labeled DNA sequence is allowed to interact with a DNA-binding protein. Then the complex is digested with DNase I, where the bound protected region is intact from attack by the enzyme. The degraded DNA is submitted to electrophoresis, and the region of protection is detected as a gap in autoradiography. DNase I from Bovine pancreas has 29 kDa and approximately 40 Å in diameter. It binds in the minor groove of the DNA, and cleaves the phosphodiester bound of double and single strand DNA. The enzyme does not cleave the DNA indiscriminately, and the characteristics of DNase prevents it from cutting the DNA under and around a bound protein[26]. For footprinting experiment, the target DNA sequence should be labeled with a radioactive isotope. To construct the desired DNA molecule, a PCR reaction is performed using primers labeled with [γ-^{32}P]. For molecular biology purposes, the oligonucleotide probes (primers) are dephosphorylated by Calf Intestinal Alkaline Phosphatase (CIAP) in order remove the 5` phosphate from DNA, which allow the subsequent end-labeled with a radioactive phosphate by T4 Polynucleotide Kinase (T4 PNK) (5). For end-label short oligonucleotides, the enzyme T4 PNK catalyzes the transfer and exchange of the terminal [$\gamma$-$^{32}$P] of ATP to the 5`-hydroxyl terminus of DNA and RNA.

The primers used for amplification of the intergenic region (section III. 2.8) were labeled with [γ-^{32P}]ATP (4000 Ci mmol^{-1}) using T4 PNK (New England Biolabs). The labeled primer was separated from unincorporated [γ-^{32P}]ATP using the Nucleotide Removal Kit (Qiagen). The *morS-morP* intergenic region (233 bp) was PCR amplified

using *D. alaskensis* G20 chromosomal DNA as a template and with appropriate labeled and unlabeled primers. The footprint assays were performed as follows: the labeled DNA fragment was diluted to a concentration of ~1 nM in 50 µl of binding mix (10 mM Tris–HCl, pH 7.5, 50 mM NaCl, 2.5 mM $MgCl_2$, 0.5mM dithiothreitol, 4% glycerol, and 40 ng µl−1 poly(dI–dC)·poly(dI–dC)) to which different amounts of purified MorR (2-10 µM) were added. After 30 min of incubation at room temperature, DNase I was added (1.2 unit, Promega), and the reaction was conducted for 1 min, then stopped by the addition of 140 µl of DNase Stop Solution (192 mM sodium acetate, 32 mM EDTA, 0.14% SDS, and 64 µg ml−1 yeast RNA). Following DNA ethanol-precipitation in the presence of a DNA carrier (Pellet Paint co-precipitant, Novagen), the pellets were resuspended in a loading dye solution (95% formamide, 10 mM EDTA, 0.3% bromophenol blue, 0.3% xylene cyanol) and loaded onto a 8% polyacrylamide/6 M urea electrophoresis gel. The locations of the protected nucleotides were deduced by running a ladder with products of the Sanger reaction (Thermo Sequenase Cycle Sequencing Kit, Affymetrix).

III.2.11. Ammonium hydrogen phosphoramidate synthesis

The phospho-donor ammonium hydrogen phosphoramidate ($NH_4HPO_3NH_2$) was synthetized according to the method described by Sheridan *et al.*, 1972[27]. 18.3 ml of Phosphoryl chloride (Merck) were added to 300 ml of ice cold 10% aqueous ammonia solution, and stirred for 15 min. The mixture was diluted with 1L of acetone, resulting in the formation of two layers. The bottom layer was separated, neutralized with 8ml of glacial acetic acid, and cooled to 4ºC to induce the crystallization of the target compound. After crystallization, the compound was filtered, washed with Isopropanol, and air dried. In this work, for nomenclature simplification, ammonium hydrogen phosphoramidate is called as phosphoramidate.

III.2.11.1. Elemental Analysis of Carbon, Hydrogen, Nitrogen and Sulphur (CHNS)

After phosphoramidate synthesis, the resulting product was characterized based on the presence of carbon, hydrogen, nitrogen and sulfur in order to confirm the presence of the desired compound. In this way, an aliquot of 2 mg of the synthetized $NH_4HPO_3NH_2$ was submitted to CHNS analysis which was performed in aFlashEA 1112 analyzer

(Thermo Finnigan). The procedure of CHNS determination is based on the combustion of the sample by a special furnace heated at 900 – 1000ºC with a small proportion of oxygen which burns the organic and inorganic material, and, consequently, converts the sample into elemental gases that are separated in a column. Athermal conductivity detector (TCD) permits the elements concentrations identification.

III.2.11.2. Nuclear magnetic resonance (NMR)

The synthetized compound was also identified by NMR using a BlunkerAvance III of 400 MHz.A 20 mg of phosphoramidate was diluted in 600 μl of Deuterium Oxide (Sigma). The sample was analyzed by 1H and 31P. The data was collected using the Topspin 3.1 software.

III.3.Results and Discussion

III.3.1 Amino acid residues composition: MorR

Analysis of translated *mor*R nucleotide sequence indicated that this gene codifies a putative transcriptional regulatory protein belonging to *Fis* family, and shares 76% of similarity with *zra*R from *D. vulgaris* Hildenborough. According to Protein Data Bank (PDB), the putative protein shares sequence similarity and conserved domains with structural well solved proteins like ZraR (*S. typhimurium*) and NtrC (*S. typhimurium*). Additionally, it is possible to observe domain similarities with other proteins involved in transcriptional regulation, as such as DctD (*S.meliloti*) and Ntrc1 (*A.aeolicus)*. The amino acid sequences of the proteins cited above were aligned using the Jalview program (figure III.2).

The putative protein MorR (GI: 78355156) is composed by 466 amino acids residues which combine the three domains: a N-terminal, a central and a C-terminal domain. The N-terminal domain constitutes the receiver part of the protein, and includes the amino acids residues from 7 to 118. This domain is responsible for stimulus recognition from cognate histidine kinase (HK), it contains a phosphoacceptor site at a conserved aspartic acid (D55), and a dimerization interface. The central domain might be involved in ATP binding and interaction with σ54 subunit. It is comprised of the amino acids residues from 167 to 310, and contains conserved features which classify MorR as a member of the

AAA_+ superfamily due to the presence of a Walker A and Walker B motif, an arginine finger (R-finger) and a GAFTGA sequence. These conserved structures are involved in ATP binding/hydrolysis, and σ54 interaction. The C-terminal domain encompasses amino acids residues from 424 to 465 and forms a tri-helical helix-turn-helix (HTH) portion that controls the output response associated with DNA binding. This domain classifies MorR as a member of Fis family, and the HTH domain binds to the major groove of DNA being directly involved in transcriptional activation and/or repression.

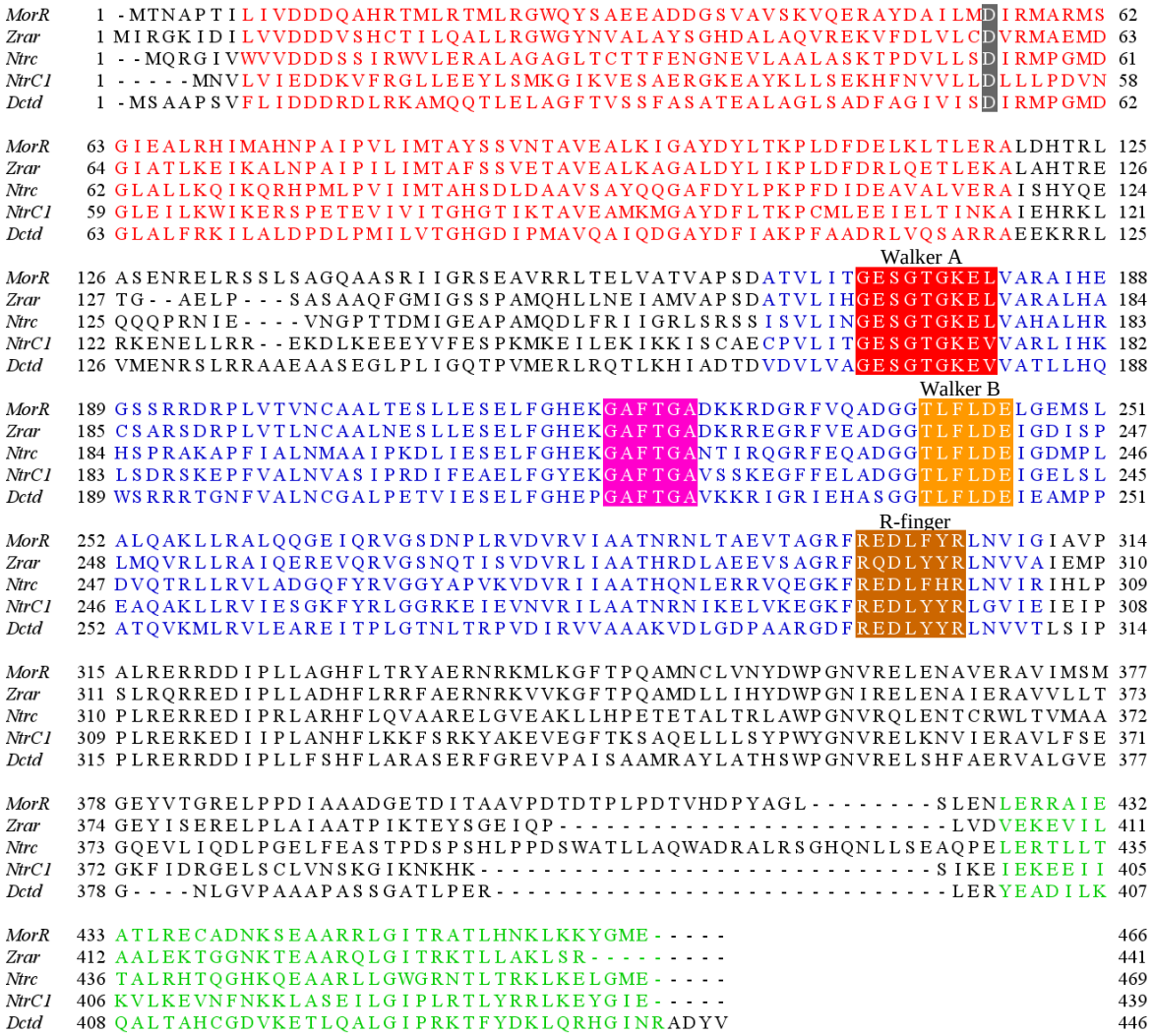

Figure III.2. Amino acids residues alignment of the *D. alaskensis* G20 MorR, *S. typhimurium*Zrar, *S. Typhimurium* NtrC, *A. aeolicus* NtrC1 and *S. meliloti*DctD. The three major conserved regions are represented as follows: receiver domain (red), ATPase domain (blue) and DNA binding domain (green). The

phosphoacceptor aspartic acid (D55), Walker A, Walker B, GAFTGA and arginine finger (R-finger) are detached.

To date, the MorR structure is not available. The related crystallographic structure available refer to response regulators containing single receiver domain (NtrC4, PDB ID: 3DZD), single central domain (NtrC1, PDB ID: 1NY6), single ATPase domain (Ntrc1, PDB ID: 3M0E), regulatory and central domain (NtrC1, PDB ID: 1NY5), and central and C-terminal domain (Zrar, PDB ID: 1OJL). According to PDB data bank, the last one exhibits the highest similarity (57%) with MorR, and its structure, as a monomer, is presented in figure III.3.

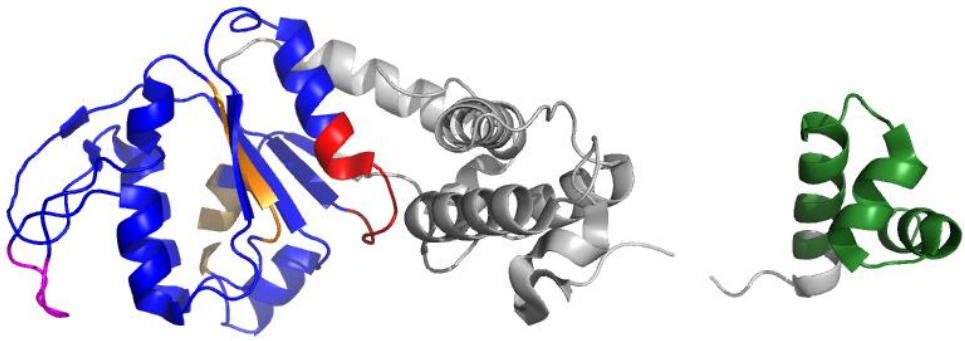

Figure III.3. Crystallographic structure of the central and C-terminal domains of ZraR from *S. typhimurium* (PDB ID:1OJL).The two major conserved regions with MorR are represented as follows: ATPase domain (blue) and DNA binding domain (green). In red (Walker A), in orange (Walker B), in magenta (GAFTGA) and the arginine finger (R-finger) are detached and shown in brown in the second plane.

III.3.2. Protein purification

The soluble fraction containing MorR was purified aerobically by three chromatographic steps: DEAE Sepharose FF, Source 15Q and Superdex 200 (figure III.4). The first chromatographic step (DEAE Sepharose FF) was very important given that removed the majority of the contaminants. The second chromatographic step used a strong anionic exchange matrix (Source 15Q that is based on a 15 μm monosized, rigid polystyrene/divinyl benzene polymer matrix). The combination of the Source 15Q properties with the application of a discontinuous gradient became a good methodological step for MorR purification. In this step, the remaining contaminants were highly removed and the MorR was recovered efficiently. However, even applying three optimized

chromatographic steps, the SDS-PAGE showed a low degree of a remaining contaminant with a molecular weight of approximately 90 kDa. After purification, 3 mg/ml of protein were obtained in a total volume of 10 ml.

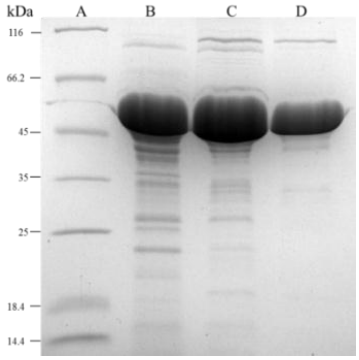

Figure III. 4. 12.5% SDS-PAGE of purified MorR after each purification step. A: ladders, B: after DEAE-FF column, C: after Source 15Q column, D: after Superdex 200 column.

III.3.3. UV-VIS spectroscopy

The electronic absorption spectrum of the pure MorR in 10 mM Tris-HCl, pH 7.6 is show in figure III.5. The molar extinction coefficient was calculated using the maximum absorbance peak at 280 nm: ε_{280} = 30823 M^{-1} cm^{-1}. For comparison, the theoretical molar extinction coefficient was calculated according to protparam (http://web.expasy.org/protparam/) as ε_{280} =27515M^{-1} cm^{-1}. Our results indicate a similarity between the practical and the theoretical molar extinction coefficient for MorR.

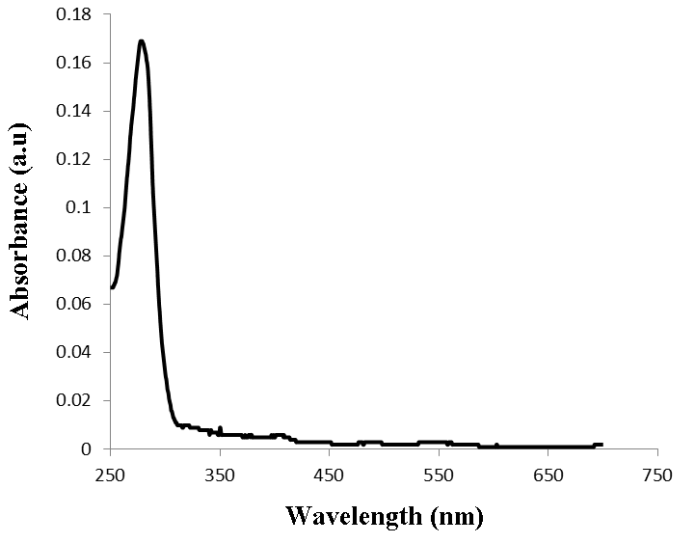

Figure III. 5. UV/VIS spectrum of purified MorR (20 μM) in 10 mM Tris-HCl, pH 7.6.

III.3.4. Sequencing

The N-terminal sequence is an important tool to confirm the presence of a recombinant protein. The N-terminal was determined for purified heterologous MorR from *D.alaskensis* G20, A S M T N A P T I L I V D D D Q A H R T, and is in agreement with the nucleotide sequence produced by genetic engineering. As previously mentioned in the methodology (cloning section) the *Nhe*I restriction site created six additional nucleotides at 5` end position. Analysis of the recombinant plasmid DNA sequence revealed the presence of an alternative ATG start codon, which is originated by the plasmid architecture. Consequently, three amino acids were added at N-terminal: methionine (M), Alanine (A) and Serine (S). However, the first methionine was absent in the N-terminal sequencing results, probably reflecting an alternative bacterial post-translational excision mechanism.

The purified MorR was also identified using the Peptide mass fingerprint (PMF) approach, it corresponded to the target protein (GI: 78355156), showing a sequence coverage of 63% with a score of 176. The complete recombinant plasmid DNA sequencing results, and the corresponding amino acids obtained by N-terminal and PMF are displayed in figure III.6.

```
      atggctagcatgacaaacgctcctaccatattgatagtggatgatgatcaggcgcacaga
1     ·M··A··S··M··T··N··A··P··T··I··L··I··V··D··D··D··Q··A··H··R·
      accatgctgcgcaccatgctgcgcggctggcagtactcggcggaagaagccgacgacggt
21    ·T··M··L··R··T··M··L··R··G··W··Q··Y··S··A··E··E··A··D··D··G·
      tccgtggccgtgagcaaggtgcaggagcgcgcatatgacgccatcctgatggatatccgc
41    ·S··V··A··V··S··K··V··Q··E··R··A··Y··D··A··I··L··M··D··I··R·
      atggcccgcatgagcggcatagaagccctgcggcatatcatggcccacaatccggccatt
61    ·M··A··R··M··S··G··I··E··A··L··R··H··I··M··A··H··N··P··A··I·
      cccgtgcttatcatgacggcatattcttcggtgaatacagcggtggaagccctgaaaata
81    ·P··V··L··I··M··T··A··Y··S··S··V··N··T··A··V··E··A··L··K··I·
      ggtgcttatgactacctgacaaagccgcttgatttcgacgagctgaaactgacgctggag
101   ·G··A··Y··D··Y··L··T··K··P··L··D··F··D··E··L··K··L··T··L··E·
      cgcgcgcttgatcacacgcggctggcctcggaaaacagagagctgcgcagctctctgtcc
121   ·R··A··L··D··H··T··R··L··A··S··E··N··R··E··L··R··S··S··L··S·
      gcggggcaggctgcctcgcgcattatcggccgcagcgaggccgtgcgccggcttaccgag
141   ·A··G··Q··A··A··S··R··I··I··G··R··S··E··A··V··R··R··L··T··E·
      ctggtggccacagtggcgcccagcgacgccacggtactcatcaccggagaatcgggcaca
161   ·L··V··A··T··V··A··P··S··D··A··T··V··L··I··T··G··E··S··G··T·
      ggcaaagaactggtggccagagccatacacgaaggaagcagcagacgtgacagaccgctg
181   ·G··K··E··L··V··A··R··A··I··H··E··G··S··S··R··R··D··R··P··L·
      gtaaccgtcaactgcgccgcccttacggaatcgctgctggaatcagaactgttcggccac
201   ·V··T··V··N··C··A··A··L··T··E··S··L··L··E··S··E··L··F··G··H·
      gaaaaaggtgcttttaccggtgcggacaaaaaacgcgacgggcggtttgttcaggcggac
221   ·E··K··G··A··F··T··G··A··D··K··K··R··D··G··R··F··V··Q··A··D·
      ggcggtacgttgtttctggatgaactgggcgaaatgtctctggcactgcaggcaaagctg
241   ·G··G··T··L··F··L··D··E··L··G··E··M··S··L··A··L··Q··A··K··L·
      ctgcgtgcgctgcagcagggtgaaatccagagggtgggcagcgacaacccgctgagagtc
261   ·L··R··A··L··Q··Q··G··E··I··Q··R··V··G··S··D··N··P··L··R··V·
      gatgtacgcgtcatcgccgcaaccaaccgcaatctgaccgcagaggtgaccgcaggcagg
281   ·D··V··R··V··I··A··A··T··N··R··N··L··T··A··E··V··T··A··G··R·
      ttccgcgaagacctgttttaccggctcaacgtcatcggcatagcggtaccggcactgcgg
301   ·F··R··E··D··L··F··Y··R··L··N··V··I··G··I··A··V··P··A··L··R·
      gaacggcgcgacgacatccccctgctggccggacactttctgacccgctatgccgaacgt
321   ·E··R··R··D··D··I··P··L··L··A··G··H··F··L··T··R··Y··A··E··R·
      aaccgcaagatgctcaaaggattcaccccgcaggccatgaactgtctggtcaactatgac
341   ·N··R··K··M··L··K··G··F··T··P··Q··A··M··N··C··L··V··N··Y··D·
      tggccgggcaatgtgcgtgaactggaaaacgccgtggagcgcgccgttatcatgagcatg
361   ·W··P··G··N··V··R··E··L··E··N··A··V··E··R··A··V··I··M··S··M·
      ggcgaatatgtcaccggacgcgaactgccgccggacattgcagcggctgacggcgaaacg
381   ·G··E··Y··V··T··G··R··E··L··P··P··D··I··A··A··A··D··G··E··T·
      gatatcaccgcagcagtgcccgatacggacacaccgctgcccgacaccgtccatgacccc
401   ·D··I··T··A··A··V··P··D··T··D··T··P··L··P··D··T··V··H··D··P·
      tatgcggggctctcgctggaaaatctggaacgccgcgccattgaggcaacgctgcgcgaa
421   ·Y··A··G··L··S··L··E··N··L··E··R··R··A··I··E··A··T··L··R··E·
      tgtgccgacaataaaagcgaagccgcccgccggctgggcatcacccgcgcaacactgcac
441   ·C··A··D··N··K··S··E··A··A··R··R··L··G··I··T··R··A··T··L··H·
      aacaagctgaaaaaatacggcatggaataa
461   ·N··K··L··K··K··Y··G··M··E··*·
```

Figure III.6. N-terminal and amino acid residues sequencing of MorR with the corresponding nucleotide sequencing of pETMorR. Bold in yellow: N-terminal sequencing result. Bold in red: matched peptides by peptide mass fingerprint.

III.3.5. Protein metal content

Metals are essential to maintain some functions that are associated with transcriptional regulatory proteins which shares conserved features with MorR. As an example, the conserved acid aspartic residue (D239) in the Walker B motif of NtrC is essential for ATP binding and this interaction requires the presence of Mg^{2+}. The absence of Mg^{2+} results in five folds decrease in the affinity between NtrC and ATP[28]. Another example of a transcriptional regulatory protein that shares conserved characteristics with MorR and requires metal is the ZraR. The interaction between ZraR and Zn^{2+} is not completely understood, but the evidence supports the idea that ZraR is a Zn-responsive TCS given that its expression increases in the presence of this metal[7]. However, to date, there is no information if ZraR has a Zn^{2+} binding site motif in its structure.

In spite of the evidences suggesting that transcriptional regulators, like MorR, can incorporate metals in its structure, the metal content analysis of purified MorR performed by ICP-AES revealed the absence of Mg, Zn, Mo and Cu.

III.3.6. Determination of the molecular mass

MorR has a theoretical isoelectric point of 5.6 and a theoretical molecular mass of 51kDa according to protparam. SDS-PAGE of the purified MorR showed a retention factor (Rf) of 0.33 with a mobility corresponding to a molecular mass of 42 kDa (figure III.7).

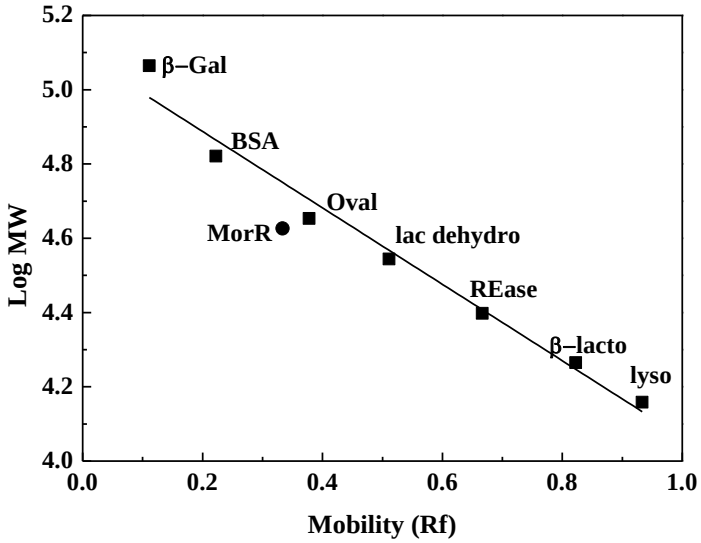

Figure III.7. Rf of standards proteins and MorR in 12,5% SDS-PAGE. β-galactosidase (β-gal), bovine serum albumin (BSA), ovalbumin (Oval), lactate dehydrogenase (lac dehydro), REase Bsp981 (REase), β-lactoglobulin (β-lacto), lysozyme (lyso) and MorR. Curve Equation: y=-1.0289x+5.0934. R^2=0.9779.

A molecular mass of 52 kDa ± 1.52 was estimated by MALD-TOF. This technique is more robust and shows a much smaller associated error when compared with the SDS-PAGE. An analytical Superdex 200 10/30 mm column was used in order to determine the oligomeric state of MorR. MorR presented a molecular mass of ~56 kDa ± 2.8, indicating that it is present as a monomer in solution (figure III.8).

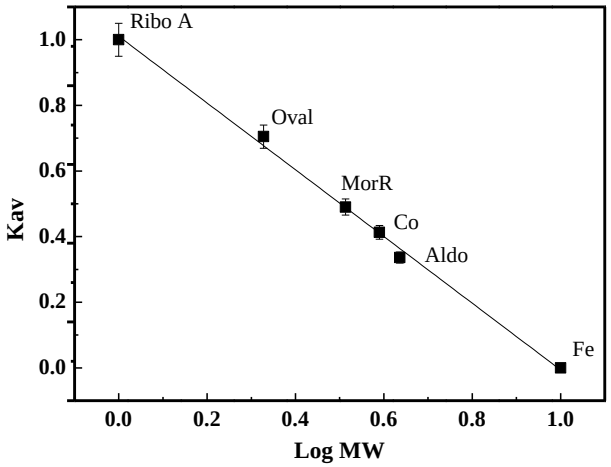

Figure III.8. Determination of the molecular mass by Superdex 200 10/30 mm gel filtration. The graphic shows the normalized values of distribution coefficient (Kav) and logarithm of molecular weight (Log MW). Standard proteins used for the calibration curve: Ribonuclease A (Ribo A), Ovalbumin (Oval), Conalbumin (Co), Aldolase (Aldo) and Ferritin (Fe). Curve Equation: y=-0.248x+1.5829. R^2=0.9971.

Another calibration at Consejo Superior de Investigaciones Científicas (CSIC) using the same type of column with different standards determined a molecular mass of ~60 kDa ± 3 for MorR, quite identical to the molecular mass determined previously.

The association between structure and the monomeric state of MorR differs from the oligomeric state of the closer related proteins where the structures were solved, such as ZraR, NtrC and NtrC1. It is important to note that MorR was purified entirely, *i.e*. containing all the three major domains: R (the regulator), C (the AAA^+ central) and D (C-terminal DNA binding). For that reason, we can also call the purified protein of this work as $MorR^{RCD}$. Crystal or NMR structural studies characterized several isolated domains or truncated construct, such as: $ZraR^{CD}$ (hexamer), active and non-active $NtrC^{R}$ (monomer), $NtrC^{D}$ (homodimer), $NtrC1^{RC}$ (inactive dimer) and $NtrC1^{C}$ (active ring-shaped heptamer)[29–34]. The full length variant of NtrC was determined by Small and Wide Angle X-ray Scaterring (SAXS/WAXS) and Electron Microscopy (EM). This $NtrC^{RCD}$ variant carried a S160F, R456A, N457A and R461A mutations that confers stability and prevents aggregation of the activated form. The studies support the idea that NtrC is an inactive homodimer where the unphosphorylated receiver subunit represses the formation of the assembly of the central AAA+ subunit. This inactive state is uncovered by phosphorylation which alleviates the repression status. The stability of the activated form of $NtrC^{RCD}$ occurs by the intersubunit contact between the activated receiver domain of one subunit with the ATPase domain of a second non-identical subunit, forming the activated hexameric ring. Moreover, the C-terminal DNA binding domain contain a dimerization determinant and that oligomerization seems to be a prerequisite for ATPase activity, but not for ATP binding[23]. In this context, $MorR^{RCD}$ shares a high similarity with ZraR and NtrC variants, but the monomeric state of $MorR^{RCD}$ shows that dimerization determinant might be structurally and/or functionally different from its counterparts.

III.3.7.Phosphorylation status of the pure MorR

Response regulatory proteins belonging to TCS are mainly characterized by an output response associated with post-translational modifications, such as phosphorylation. However, in heterologous protein expression, post-translational changes might occur, since host *E.coli* maintains this type of regulatory processes active. Taking into consideration, the

present study verified the existence of phosphoamino acid residues in heterologous MorR using nano liquid chromatography-tandem mass spectrometry. Two samples (in gel and lyophilized) were submitted for this analysis. The results identified, for both samples, the presence of a protein belonging to "two component Fis family transcriptional regulator" which matched with GI: 78355156 from *D. alaskensis* G20. The percentage of sequence coverage was 65% for gel sample, and 44% for lyophilized sample. No phosphoamino acid (serine, threonine and aspartic acid) were identified. The results showed that the purified monomeric form of MorR was not phosphorylated by the host bacteria.

III.3.8.Electrophoretic Mobility Shift Assay (EMSA)

In order to visualize if MorR binds to the intergenic region between *mor*S and *mor*P, a DNA-Protein interaction experiment was performed. A 233 bp comprising the entire intergenic region between *mor*P and *mor*S was amplified by PCR. A DNA mobility retardation was observed in the native PAGE when MorR was added in the reaction mixture (figure III.9). This results shows that MorR interacts with the intergenic region between *mor*P and *mor*S and might be involved in the gene regulation. As an alternative, the same experiment could be visualized through Coomassie Brilliant Blue staining, with BSA (bovine serum albumin) used as a control (figure III.10). These results show that the BSA do not interact with the intergenic region and shows that the interaction between the target DNA and MorR is specific.

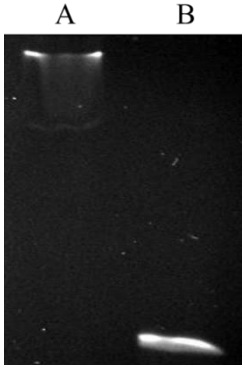

Figure III. 9. EMSA showing the DNA shift observed when MorR was mixed with the target DNA. The interaction was visualized in 7,5 % Native PAGE. A) DNA + MorR. B) free DNA.

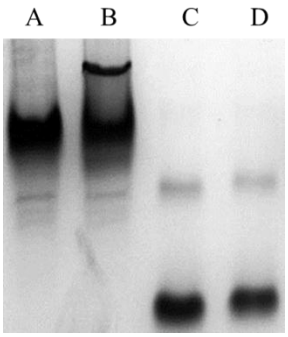

Figure III. 10. EMSA showing the protein shift observed when MorR was mixed with the 233 bp intergenic region between *mor*P and *mor*S in 7,5 % PAGE. A) Free MorR. B) MorR shift. C) Free BSA. D) BSA mixed with the intergenic region where no shift was observed.

III.3.9.DNaseI footprinting

In order to identify the specific DNA binding region, a DNaseI footprinting experiment was performed. The intergenic region between *mor*P and *mor*S was amplified using the same primers designed for EMSA studies. Radioactive labeling was used for DNA visualization, and different amounts of purified MorR were tested (0, 2, 6 and 10nM). The results showed that a region covered by 54 nucleotides was not subjected to DNaseI digestion. This indicates that the intergenic region between *mor*S and *mor*P is the specific binding region for MorR. The protected region encompassed positions -145 up to -200 relative to the *mor*P ATG transcription start site. It also encompasses the predicted -10 and -35 conserved boxes that might be responsible for MorR autoregulation. Five protected hot spots were identified, including a palindromic region (TTTTTTATA) (figure III.11).

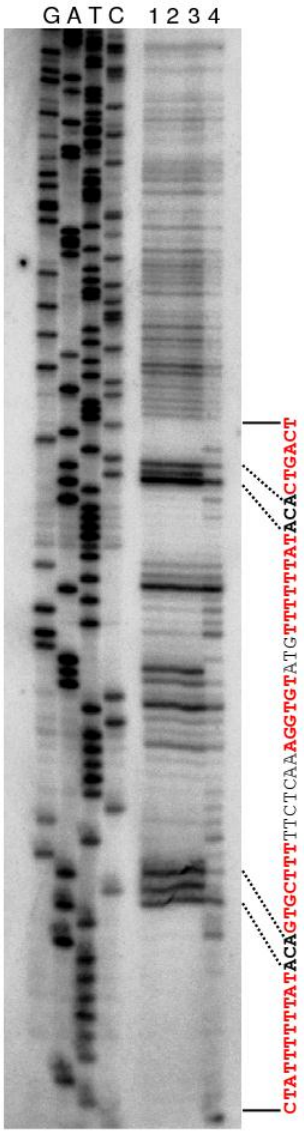

Figure III. 11. MorR DNaseI footprinting experiment using the intergenic region between *mor*P and *mor*S as DNA template. A 233bp labeled DNA fragment encompassing the intergenic region was digested with DNaseI. The MorR protected region are bolded in red. G, A, T and C are sequencing ladders. 1) 10 nM, 2) 6 nM, 3) 2 nM and 4) 0nM of heterologous MorR respectively.

The footprinting result is in agreement with the gene regulation mediated by σ_{54} transcriptional activators that binds ~80 to 150 nt upstream from the promoter they control. This result can elucidate how *mor*P gene transcription is enhanced when Mo is added to the medium. Probably, in the presence of Mo MorP incorporates this metal into its structure, and then derepress MorS (the HK sensor). The derepression hypothesis comes from the idea that MorP contains a Cpx domain, and might function as the CpxP (the envelope stress

chaperone) protein. Then, the MorS autophosphorylates and transfers the phosphoryl group to the cognate response regulator (MorR). The active form of MorR, can probably, interact with σ_{54} and activate the transcription of *mor*P gene. The activate form might be able to hydrolyze ATP and provide the mechanical force for RNAPσ_{54}.The results show that phosphorylation is not a prerequisite for MorR-DNA binding. Moreover, MorR binds to the putative -10 and -35 boxes that might be involved in the *mor*R autoregulation. The fact that MorR binds to the putative σ_{70} promoter can open a new insight onto the self-regulatory mechanism of *mor*S and *mor*R genes. So, the inactive (not phosphorylated) form of MorR binds to DNA and it is plausible to consider that MorR could control its own transcriptional level by interaction with RNPσ_{70}. Our hypothesis is that in the absence of Mo, MorR binds as a repressor to the intergenic region between *mor*S and *mor*P inhibiting the access of RNPσ_{70} but maintaining a basal level of transcription of those genes. In the presence of Mo, MorR acquires the active form;derepress its own promoter and acts as a transcriptional activator of *mor*P gene.

III.3.10. Ammonium hydrogen phosphoramidate synthesis

The synthesis of ammonium hydrogen phosphoramidate ($NH_4HPO_3NH_2$) produced 150mg of a crystal compound. The corresponding product was investigated by elemental analysis of carbon, hydrogen, nitrogen and sulphur which identified 22.65% of nitrogen, 0% of carbon and sulphur, and 5.93% of hydrogen. The results match the expected mass percentages of the compound: 24.56 % of nitrogen and 6.14% of hydrogen. Additionally, the resulting compound was identified by 1H and 32P NMR spectroscopy which confirmed its molecular structure.

III.3.11.Acetylphosphate and phosphoramidate as MorR oligomeric inductors

The oligomeric state of MorR was monitored after *in situ* phosphorylation using 50 mM of acetylphosphate or phosphoramidate. After reactions were performed, each mixture was applied in an analytical gel filtration column. A control experiment, where no phosphodonors were used, was also monitored. No changes in elution volume profile were observable with acetylphosphate or ammonium hydrogen phosphoramidate compared with the control. The resulting chromatograms are presented in figure III.12.

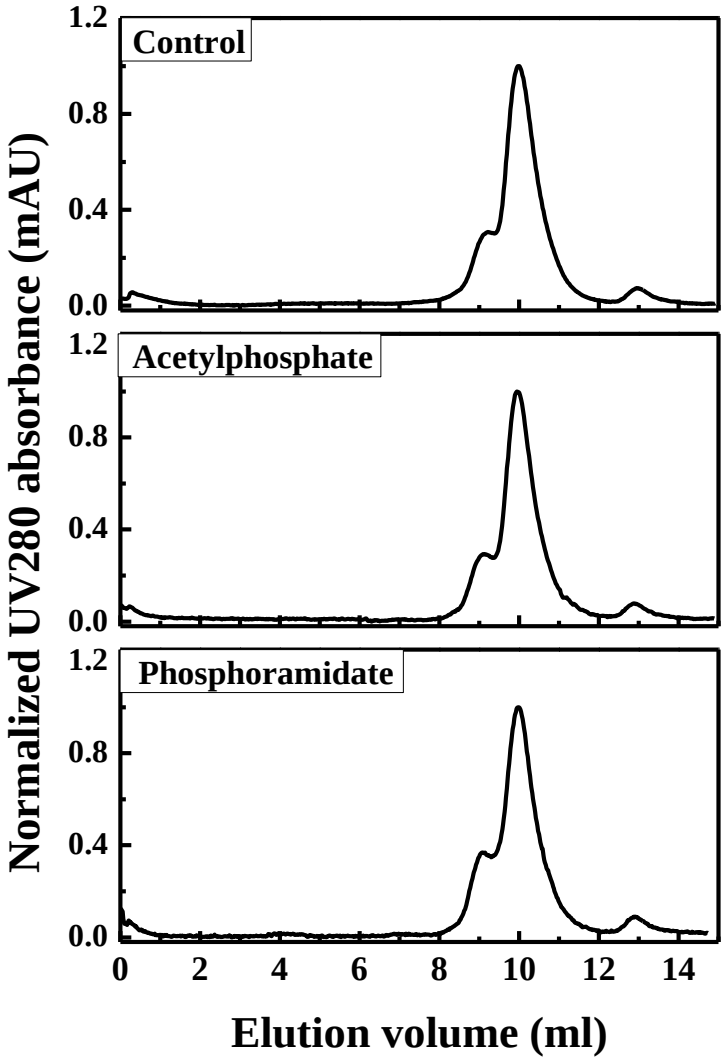

Figure III. 12. Analytical gel filtration chromatography showing the elution profile of MorR with and without incubation with acetylphosphate or ammonium phosphoramidate (phosphoramidate). The intensity of UV280 nm was normalized.

The results showed that the oligomeric status of MorR is not altered upon incubation with phosphodonors. We believe that the shoulder presented in the chromatograms is not associated with oligomerization after phosphorylation given that it is also present in the control experiment without phosphorylation. Although we could not exclude the possibility that native MorR can be present as different oligomeric form or that the shoulder might be due to a contaminant of approximately 100kDa that is always observed in small amounts after purification on the SDS-PAGE gels (figure III.4). Future

studies, like mass spectrometry identification of the protein corresponding to the shoulder or analytical ultracentrifugation, can help to solve it. However, MorR contains all the conserved features that support the idea that this protein has autophosphorylation capacity. We propose that MorR autophosphorylation activity could be very fast and, therefore, gel filtration is not properly accurate for MorR oligomer visualization. As a result, fluorescence spectroscopy and nano LC-MS were chosen in order to understand the real behavior of MorR upon phosphodonor incubation.

III.4. References

1. Yan, J., Barak, R., Liarzi, O., Shainskaya, A. & Eisenbach, M. In vivo acetylation of CheY, a response regulator in chemotaxis of Escherichia coli. *J. Mol. Biol.* **376,** 1260–71 (2008).

2. Liarzi, O. *et al.* Acetylation represses the binding of CheY to its target proteins. *Mol. Microbiol.* **76,** 932–43 (2010).

3. Wolfe, A. J. Physiologically relevant small phosphodonors link metabolism to signal transduction. *Curr. Opin. Microbiol.* **13,** 204–9 (2010).

4. Lukat, G. S., McCleary, W. R., Stock, a M. & Stock, J. B. Phosphorylation of bacterial response regulator proteins by low molecular weight phospho-donors. *Proc. Natl. Acad. Sci. U. S. A.* **89,** 718–22 (1992).

5. Lee, J., Owens, J. T., Hwang, I., Meares, C. & Kustu, S. Phosphorylation-induced signal propagation in the response regulator ntrC. *J. Bacteriol.* **182,** 5188–95 (2000).

6. Wemmer, D. E. & Kern, D. Beryllofluoride Binding Mimics Phosphorylation of Aspartate in Response Regulators. *J. Bacteriol.* **187,** 8229–8230 (2005).

7. Leonhartsberger, S., Huber, A., Lottspeich, F. & Bo, A. The hydH / G Genes from Escherichia coli Code for a Zinc and Lead Responsive Two-component Regulatory System. *J. Mol. Biol.* **4,** 93–105 (2001).

8. Head, C. G., Tardy, a & Kenney, L. J. Relative binding affinities of OmpR and OmpR-phosphate at the ompF and ompC regulatory sites. *J. Mol. Biol.* **281,** 857–70 (1998).

9. Itou, H. & Tanaka, I. The OmpR-family of proteins: insight into the tertiary structure and functions of two-component regulator proteins. *J. Biochem.* **129,** 343–50 (2001).

10. Robinson, V. L., Wu, T. & Stock, A. M. Structural Analysis of the Domain Interface in DrrB , a Response Regulator of the OmpR / PhoB Subfamily. *J. Bacteriol.* **185,** 4186–4194 (2003).

11. Brocker, M., Mack, C. & Bott, M. Target genes, consensus binding site, and role of phosphorylation for the response regulator MtrA of Corynebacterium glutamicum. *J. Bacteriol.* **193,** 1237–49 (2011).

12. Möker, N., Krämer, J., Unden, G., Krämer, R. & Morbach, S. In vitro analysis of the two-component system MtrB-MtrA from Corynebacterium glutamicum. *J. Bacteriol.* **189,** 3645–9 (2007).

13. KATO, H., CHIBAZAKURA, T. & YOSHIKAWA, H. NblR Is a Novel One-Component Response Regulator in the Cyanobacterium Synechococcus elongatus PCC 7942. *Biosci. Biotechnol. Biochem.* **72,** 1072–1079 (2008).

14. Luque, I., Zabulon, G., Contreras, A. & Houmard, J. Convergence of two global transcriptional regulators on nitrogen induction of the stress-acclimation gene nblA in the cyanobacterium Synechococcus sp. PCC 7942. *Mol. Microbiol.* **41,** 937–47 (2001).

15. Ruiz, D. *et al.* Phosphorylation-independent activation of the atypical response regulator NblR. *Microbiology* **154,** 3002–15 (2008).

16. Klose, K. E., North, A. K., Stedman, K. M. & Kustu, S. The major dimerization determinants of the nitrogen regulatory protein NTRC from enteric bacteria lie in its carboxy-terminal domain. *J. Mol. Biol.* **241,** 233–45 (1994).

17. Yan, D. & Kustu, S. "Switch I" mutant forms of the bacterial enhancer-binding protein NtrC that perturb the response to DNA. *Proc. Natl. Acad. Sci. U. S. A.* **96,** 13142–6 (1999).

18. Wyman, C. Unusual Oligomerization Required for Activity of NtrC, a Bacterial Enhancer-Binding Protein. *Science (80-.).* **275,** 1658–1661 (1997).

19. Rippe, K., Mücke, N. & Schulz, a. Association states of the transcription activator protein NtrC from E. coli determined by analytical ultracentrifugation. *J. Mol. Biol.* **278,** 915–33 (1998).

20. Sevenich, F. W., Langowski, J., Weiss, V. & Rippe, K. DNA binding and oligomerization of NtrC studied by fluorescence anisotropy and fluorescence correlation spectroscopy. *Nucleic Acids Res.* **26,** 1373–81 (1998).

21. Weiss, D. S., Batut, J., Klose, K. E., Keener, J. & Kustu, S. The phosphorylated form of the enhancer-binding protein NTRC has an ATPase activity that is essential for activation of transcription. *Cell* **67,** 155–67 (1991).

22. Tripathi, S. & Portman, J. J. Allostery and Folding of the N-terminal Receiver Domain of Protein NtrC. *J. Phys. Chem. B* **117,** 13182–93 (2013).

23. De Carlo, S. *et al.* The structural basis for regulated assembly and function of the transcriptional activator NtrC. *Genes Dev.* **20,** 1485–95 (2006).

24. Miller, G. Protein Determination of Large Numbers of Samples. *Anal. Chem.* **31,** 964–964 (1959).

25. Santos, H. M. *et al.* Improving sample treatment for in-solution protein identification by peptide mass fingerprint using matrix-assisted laser desorption/ionization time-of-flight mass spectrometry. *J. Proteome Res.* **6,** 3393–9 (2007).

26. Moss, T. *DNA-Protein Interactions: Principles and Protocols (Methods in Molecular Biology), 2nd Edition*. (Humana Press, 2001).

27. F.A, C. *Inorganic Syntheses Vol XIII*. (Mc-Graw Hill Book Company, 1972).

28. Rombel, I. *et al.* MgATP binding and hydrolysis determinants of NtrC, a bacterial enhancer-binding protein. *J. Bacteriol.* **181,** 4628–38 (1999).

29. Sallai, Â. & Tucker, P. A. X-ray crystallographic characterization and phasing of an NtrC homologue crystallization papers. *Acta Crystallogr.* **D59,** 1656–1658 (2003).

30. Sallai, L. & Tucker, P. a. Crystal structure of the central and C-terminal domain of the σ54-activator ZraR. *J. Struct. Biol.* **151,** 160–170 (2005).

31. Kern, D. *et al.* Structure of a transiently phosphorylated switch in bacterial signal transduction. *Nature* **402,** 894–8 (1999).

32. Volkman, B. F., Nohaile, M. J., Amy, N. K., Kustu, S. & Wemmer, D. E. Three-dimensional solution structure of the N-terminal receiver domain of NTRC. *Biochemistry* **34,** 1413–24 (1995).

33. Pelton, J. G., Kustu, S. & Wemmer, D. E. Solution structure of the DNA-binding domain of NtrC with three alanine substitutions. *J. Mol. Biol.* **292,** 1095–110 (1999).

34. Lee, S.-Y. *et al.* Regulation of the transcriptional activator NtrC1: structural studies of the regulatory and AAA+ ATPase domains. *Genes Dev.* **17,** 2552–63 (2003).

Chapter IV

MorR-DNA association and phosphorylation

MorR-DNA association and phosphorylation

Context

MorR interacts with the intergenic region between *mor*S and *mor*P. The knowledge about the association constant involved in this interaction could be useful to understand the real behavior between those two macromolecules given that it describes the strength of binding. Fluorescence anisotropy was applied in order to determine the association constant between MorR and the target DNA. To understand the parameters that need to be controlled in the interaction process and in order to obtain as accurate result for the association constant, the acid-base equilibria influence in the fluorescence of 6-carboxyfluorescein (6-FAM) covalently attached to the DNA duplex was characterized and the binding conditions were optimized. This optimization was of paramount importance to guarantee that anisotropic variation of 6-FAM was a consequence of MorR-DNA binding and no other stimulus.

The MorR oligomeric experiments using gel filtration chromatography have showed no apparent oligomerization of this protein upon its interaction with phosphodonors. However, the amino acid composition of MorR and its homology with other response regulators reinforce the idea that MorR could autophosphorylate and oligomerize in the presence of phosphodonors. Because of that, fluorescence emission of MorR-tryptophan was monitored in the presence of phosphodonors in order to identify if those compounds caused a protein conformational change mediated by phosphorylation. Finally, nano-LC-MS was applied to identify which (if any) amino acid residue was phosphorylated and mathematical biochemistry calculations were applied in order to clarify the experimental results.

IV.1. Introduction

Fluorescence spectroscopy has been widely used in biological sciences. It has a broad range of applications in DNA technology, *e.g.* in DNA sequencing, nucleic acid hybridization assay and DNA arrays for genetic analyses, and in biochemistry in what respects protein-ligand interaction, conformational changes and activity assays[1]. The present introduction shows the principal topics in fluorescence spectroscopy with a special focus in fluorescence emission and anisotropy.

IV.1.1 Basic concepts of fluorescence

When molecules are excited by the absorption of a photon, the passage from the singlet ground state S_0 to an excited state S_n ($n > 1$) is induced. The excited molecules will return to S_0 following successive steps. The Jablonski diagram (figure IV.1) is convenient for visualizing in a simple way the possible processes: internal conversion, fluorescence, intersystem crossing, phosphorescence, delayed fluorescence and triplet-triplet transition. In that way the singlet electronic states are denoted as S_0, S_1 and S_2, and the triplet states. T_1 and T_2 [2]. The process represented in the diagram is described below:

1. $S_n \rightarrow S_1$ (internal conversion). The molecule S_n returns to the lowest excited state S_1 by dissipating a part of its energy. This process is followed by a vibrational relaxation toward the lowest vibrational level of the final electronic state.

2. $S_1 \rightarrow S_0$ (fluorescence). Emission of photon. It's the transition from the excited singlet state S_1 to lower vibrational level S_0. The fluorescence intensity decreases exponentially with a characteristic time, reflecting the average lifetime of the molecule in the S_1 excited state.

3. $S_1 \rightarrow T_1$ (intersystem crossing). Non-radiative transition between two isoenergetic vibrational levels belonging to electronic states of different multiplicities.

4. $T_1 \rightarrow S_0$ (phosphorescence). In solution at room temperature, non-radiative de-excitation from the triplet state T_1, is predominant over radiative de-excitation. The radiative rate constant is very low, and this transition is forbidden.

5. $T_1 \rightarrow S_1$ (delayed fluorescence). A reverse intersystem crossing can occur when the energy difference between S_1 and T_1 is small and when the lifetime of T_1 is long enough.

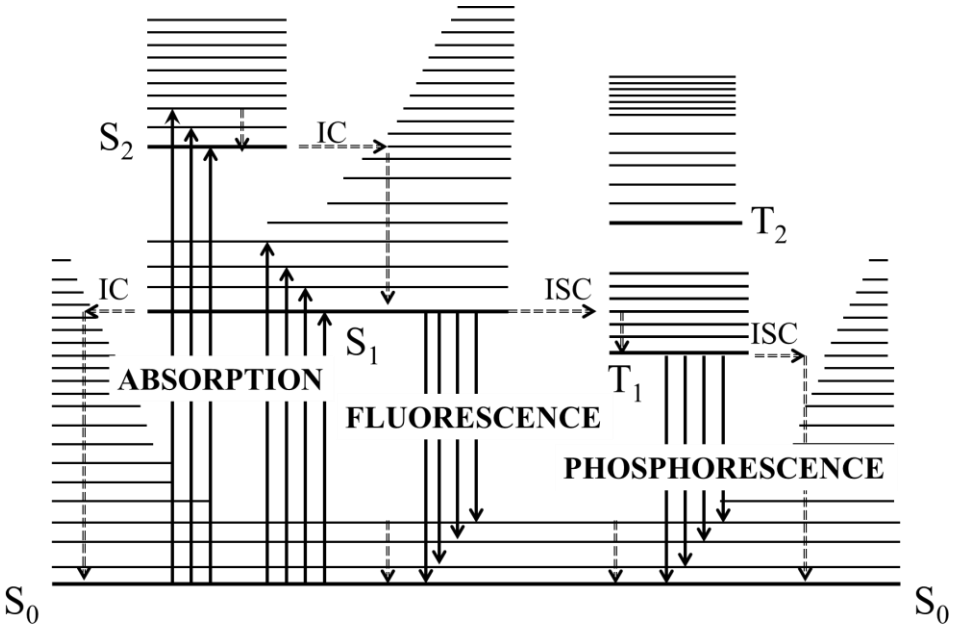

Figure IV.1. Jablonski diagram and illustration of the relative positions of absorption, fluorescence and phosphorescence spectra. IC: internal conversion (i.e. direct return to the ground state without emission of fluorescence). Dashed arrows: vibrational relaxation. ISC: intersystem crossing (possibly followed by emission of phosphorescence). Adapted from Bernard Valeur in *Molecular Fluorescence: Principles and Application, 2001*.

Absorption of photons allows a chromophore to reach an excited state. The absorption energy is higher than the emission energy. As observed by the Jablonski diagram, the energy absorbed by the molecule is released in the medium via different ways. Thus, the energy of the emitted photons is lower than the energy of the absorbed photons. A fluorophore is a chromophore that emits a photon, and this emission occurs from a population of *n* excited fluorophores with intensity I. The intensity, position of the emission wavelength, and lifetime are some of the recognizable parameters that will distinguish a fluorophore. The resulting fluorescence spectrum is the plot of the fluorescence intensity as a function of wavelength [3].

The fluorescence quantum yield (Φ) is the fraction of excited molecules that return to S_0 with emission of fluorescence photons. Upon external perturbation, the Φ is proportional to the lifetime (τ) of the excited state, as observed in dynamic quenching or during variation of temperature. The τ of the excited state is defined by the average time the

molecule spends in the excited state prior to its return to the ground state. The τ determines the time available for the fluorophore to interact with or diffuse in its environment, and hence collect the information available from its emission [4].

IV.1.2. Types of fluorophore

There are two types of fluorophore: intrinsic and extrinsic. An intrinsic fluorophore occurs naturally and is a small part of a molecule, while an extrinsic is when it is added to the molecule. Proteins display intrinsic fluorophores due to the presence of aromatic amino acids residues (phenylalanine, tyrosine and tryptophan). Extrinsic fluorophores, such as fluorescein and rhodamines, can be linked to different macromolecules. Those fluorophores are mainly used to bind covalently to lysines and cysteines of protein, and to 5` or 3` ends of DNA. Their fluorescence properties are dependent on their structure and on the surrounding environment [3].

The fluorescence of phenylalanine (F) is not considerable in the presence of other aromatic groups. When excited at 280 nm wavelength, tyrosine (Y) contributes to protein fluorescence; however its fluorescence is detected in low yield in the presence of tryptophan (W). Moreover, proteins containing W display a fluorescence spectrum that can be attributed to this amino acid residue alone, even when Y predominate. Typically, W fluorescence is essentially selected when using an excitation of 295nm. At this wavelength, Y and F emission fluorescence are superimposed by W. The position of the maximum of the fluorescence spectrum of W in proteins varies from 307 to 352 nm, giving five possibilities to spectral forms (figure IV.2).

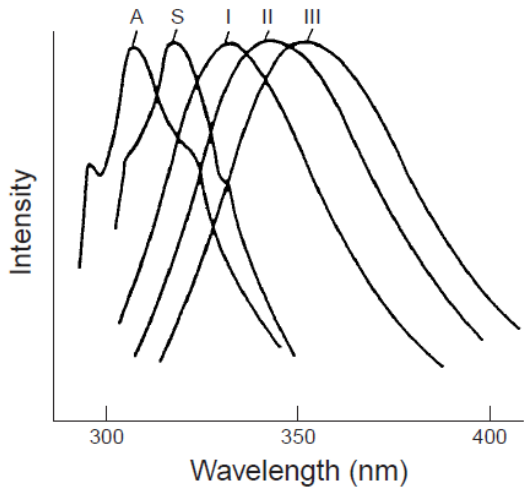

Figure IV.2. Normalized fluorescence spectra of W emission residues belonging to five spectral classes A, S, I, II and III. The variability of the emission of the indole fluorophore makes W fluorescence a sensitive toll in protein analysis. Taken from Alexey S. Lakoklin in *Encyclopedia of Analytical Chemistry - Fluorescence spectroscopy in peptide and protein analysis,* 2000.

The form A is due to fluorescence emission of the indole chromophores in non-polar environment. It can be exemplified by the azurin protein that display the shortest $\lambda_{máx}$ emission indicating that the W residue is located in a very strong hydrophobic region. The spectral form S ($\lambda_{máx}$ 307 to 317 nm) correspond to the emission of the indole located in the relatively nonpolar environment inside the protein globule forming 1:1 exciplex with neighboring polar groups. The spectral form I ($\lambda_{máx}$ 330 nm) correspond to the emission of indole located in polar but rigid environment inside the protein globule forming 2:1 exciplex with neighboring polar groups. The form I can be exemplified by the emission spectra of actin, chrymotrypsin and tetrameric melitin under high salt conditions. The spectral form II ($\lambda_{máx}$ 340 nm) corresponds to the emission of the indole chromophores at the protein surface in contact with bound water. The spectral form III ($\lambda_{máx}$ 350 nm) corresponds to the emission of indole located at the protein surface in contact with free water molecules. For those reason, the spectral form and maximum intensity of W can be a good indicator of the local surroundings[5].

Fluorescein and rhodamine are extrinsic fluorophores examples that are widely used in biosciences because of their spectroscopic properties. These compounds have a

broad range of applications like labeling of antibodies for immunoassays, or oligonucleotides for hybridization assay or even in DNA-protein interaction studies. The reasons for selecting these probes include the high quantum yields and the long wavelengths of absorption and emission, which minimize the problems of background fluorescence of biological samples and eliminate the need for quartz optics. The lifetimes of these compounds are about 4 ns and their emission spectra are not significantly sensitive to solvent polarity [4].

IV.1.2.1. Fluorescein

The high fluorescence intensity of fluorescein allowed a wide application of this fluorophore in physics and biology. The protolytic forms of free fluorescein can vary according to acid-base equilibria, and its spectroscopic properties have been well studied. The fluorescence of fluorescein is stronger in alkaline solution than in acidic medium. According to acid-base equilibria there are seven prototropic species: cation, monoanion, dianion, and neutral that are present as quinonoid, lactone and zwitterion (figure IV.3), each of them having an associated fluorescence intensity, but the dianion form shows the strongest absorptivity. Particular species predominate along the pH range. The spectra at pH 0, 3.3, 5.5 and 12 are due to cation, the neutral, monoanion and the dianion, respectively [6,7,8,9].

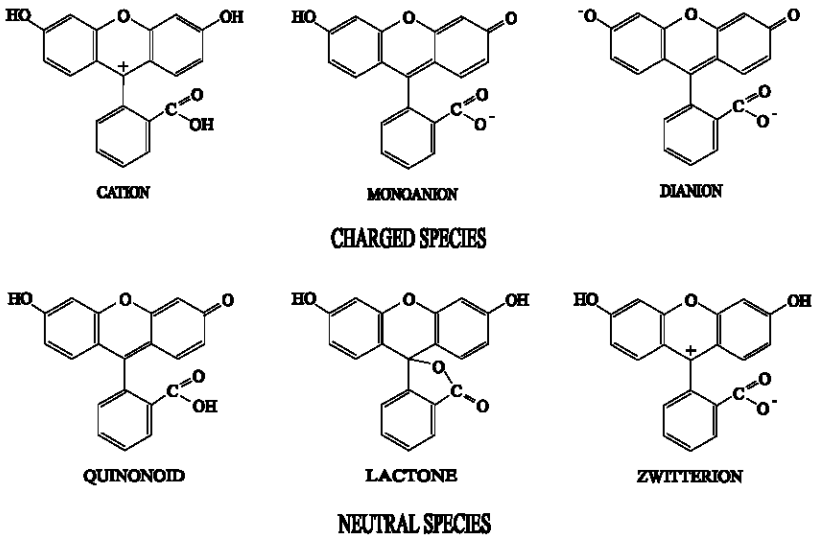

Figure IV.3. Six ionic forms of fluorescein after Zanker and Peter (1958). Taken from Smith and Pretorius (2002) Water SA, 28, 395-402.

In biochemistry, fluorescein has been used to label macromolecules and its acid-base properties can be modified upon conjugation [10,11,12,13]. Oligonucleotides attached to fluorescein derivatives, like fluorescein isothiocyanate (FITC) and 6-carboxyfluorescein (6-FAM), have been used in biology to monitor oligonucleotide hybrid formation, DNA-protein interactions, and as an alternative to the use of radiolabeled oligonucleotides [14,15,16,17].

IV.1.3. Fluorescence quenching

Fluorescence quenching is any process that depopulates an excited state of a molecule in a non-radiative away. A fluorescence quencher is a compound that participates in this process and leads to a decrease of the fluorescence quantum yield and lifetime. In protein biochemistry, the fluorescence quenching of W can be used to determine the fraction of protein fluorescence accessible to quenchers, the protein conformational changes and folding. It is important to consider that quenchers can also induce protein denaturation, and, consequently, take W from a buried to an exposed state. Acrylamide, disulfides, hydrogen peroxide and imidazole are some examples of W quenchers [4].

Fluorescence quenching can be classified as static or dynamic (also called collisional). Both require molecular contact between the fluorophore and quencher. However, quenching mechanism can also occur by excited-state reactions, molecular rearrangements, energy transfer or ground-state complex formation [4].

Quenching data is presented as plots of I_0/I versus [Q], where I_0 and I are the fluorescence intensities in the absence and presence, respectively, of a concentration of quencher [Q].

In biochemistry, the fluorescence quenching data of proteins that contains two W (W_A and W_B) can be calculated using the following equation:

$$I=I_A f_A+I_B(1-f_A) \qquad \text{Eq.4.1}$$

Where: I is the total intensity, I_A is the intensity of W_A, f_A is the fraction of W_A and I_B is the intensity of W_B.

The equation 4.1 could be applied if a dynamic quenching results from a diffusive encounter between the fluorophore (W) and quencher during the lifetime of the excited state.

Static quenching is characterized by the formation of a nonfluorescent ground state complex between the fluorophore and quencher. An important characteristic of static quenching is its decrease with increasing temperature, since the stability of the complex in the ground state is generally lower at higher temperatures. The principal difference between dynamic and static quenching refers to a decrease in the lifetime of fluorophore. Both mechanisms lead to a reduction in the fluorescence intensity, but a decrease in fluorescence lifetime is only observed if dynamic quenching occurs within the time-scale of the time-resolved experiment [4].

The fluorescence static quenching can be expressed in terms of quantum yields (ϕ). The ϕ gives the efficiency of the fluorescence process since it is a ratio of photons emitted to photons absorbed. This parameter is useful to understand the quenching of W, by the following equation:

$$\boldsymbol{\phi = \phi^{N} * \chi_{N} + \phi^{Q}(1 - \chi_{N})} \qquad \text{Eq.4.2}$$

Where ϕ^{N} is the quantum frequency of the native protein, χ_{N} is the fraction of native protein and ϕ^{Q} is the quantum frequency of the quenched protein.

IV.1.4. Fluorescence Anisotropy

The natural light is unpolarized; which means that it has no preferential direction. Excite the fluorophores with a polarized light (definite orientation) and record the emitted light in a polarized system enables to study the molecules dynamics during the excited-state lifetime. When excitation is performed with polarized light, absorption of the fluorophore will depend on the orientation of its dipole in the ground state compared to the polarized excitation light [3]

Fluorescence anisotropy can be very useful in molecular biophysics. The anisotropy is defined as the ratio of the difference between the emission intensity parallel to

the polarization of the electric vector of the exciting light ($I_{||}$) and that perpendicular to that vector ($I_{\perp}$) divided by the total intensity (I_T) [18].

$$\boldsymbol{A = (I_{||} + I_{\perp})/(I_{||} + 2I_{\perp})} \qquad \text{Eq.4.3}$$

Because the anisotropy of emission (A) is related to the correlation time of the fluorophore (τ_c) through the Perrin equation:

$$\boldsymbol{A_0/A - 1 = \tau/\tau_c} \qquad \text{Eq.4.4}$$

where A_o is the limiting anisotropy of the probe, which depends on the angle between the absorption and emission transition dipoles and τ is the fluorescence lifetime. These measurements can be used to obtain hydrodynamic information concerning macromolecules and macromolecular complexes [18].

The anisotropy is based on the observation that when a small fluorescent molecule is excited with plane-polarized light, the emitted light is largely depolarized because molecules tumble in solution during its τ_0. Nevertheless, if the small molecule is bound to a bigger molecule its effective molecular volume is increased. In that case, the molecular rotation of the fluorophore is slowed down so that the emitted light is in the same plane as the excitation energy. The bound and free states of the fluorophore each have an intrinsic polarization values: a high value for the bound state and a low value for the free state [4] (figure IV.4).

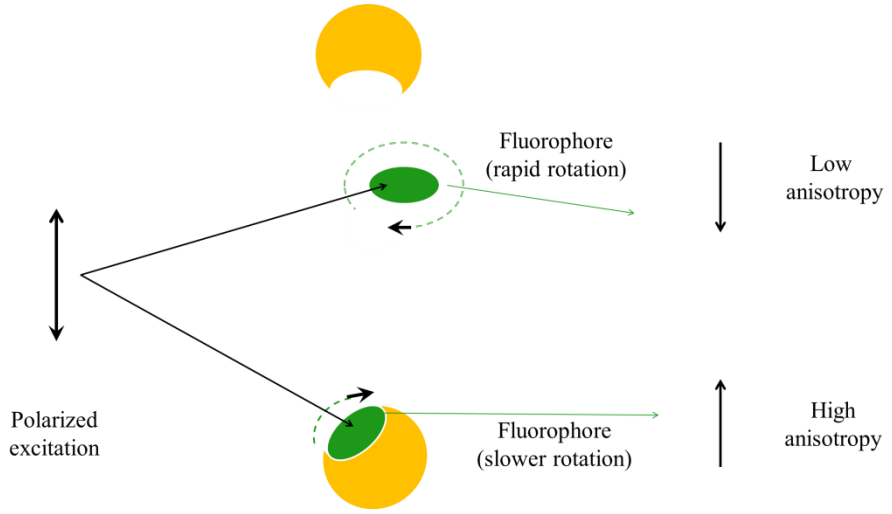

Figure IV.4. Scheme of fluorescence anisotropy of a fluorophore according to molecular motion upon interaction with a molecule (ligand). Adapted from Rossi A.M & Taylor C.W (2011) Nature Protocols, 6, 365-387.

In spite of all the physic processes involved in molecular motion, the complexation between two macromolecules always leads to an increase in the steady-state fluorescence anisotropy. If no alteration in quantum yield occur upon complexation, the data can be fitted in terms of the equilibrium constant. The sensitivity of this approach has recently been significantly improved such that it is now applicable to the study of high-affinity protein-nucleic acid interactions [18].

IV.2. Methodology

IV.2.1 dsDNA labelling with fluorescein

The DNA sequences used in this section were selected based on the MorR binding sites identified by the DNaseI footprinting experiment. Purified complementary DNA oligonucleotides containing a 67 bp and 58 bp of the intergenic region between *mor*P and *mor*S were purchased from SIGMA. The 5′ end of each duplex was labeled with 6-carboxyfluorescein (6-FAM). The labeled oligonucleotide sequences are presented in table IV.1.

Table IV. 1. Oligonucleotide sequences which were labeled with 6-FAM at 5` end.

Oligonucleotide name	Oligonucleotide sequence
6-FAM-67-mer	6-FAM-5′GTACAGCGTCTATTTTTTATACAGTGCTTTTTCTCAAA GGTGTATGTTTTTTATACACTGACTTTCA-3′
6-FAM-58-mer	6-FAM-5′CTATTTTTTATACAGTGCTTTTTCTCAAAGGTGTATGT TTTTTATACACTGACTTTCA-3′

For duplex DNA (dsDNA) formation, 10 μM of each complementary strand was mixed in a buffer consisting of 10 mM Tris-HCl, pH 7.6, 250 mM NaCl, 0.5mM EDTA. This mixture was annealed by heating at 95ºC for 5 min, cooled until 60ºC (1.5ºC/seg), and left cooling for 1 hour until reaching room temperature. The annealing was performed using MyCycler thermal cycling instrument (BioRad).

The DNA absorbance measurements were performed on a Shimadzu UV-1800 spectrophotometer using a transparent disposable cuvette (Sarstedt). The dsDNA quantity was determined according to equation 4.5:

$$\boldsymbol{M} = ([\boldsymbol{OD}_{260} - ((\varepsilon_{260}\boldsymbol{F})/(\varepsilon_{495}\boldsymbol{F}))\boldsymbol{OD}_{495}])/(\varepsilon_{260}) \qquad \text{Eq.4.5}$$

where: M is the molar concentration of the fluorescein-labeled strand, OD_{260} and OD_{495} are the absorbance values at 260 and 495 nm, ε_{260} is the molar extinction coefficient of dsDNA at 260 nm and was obtained from IDT biophysics (http://biophysics.idtdna.com/), ε_{260F} and ε_{495F} are the molar extinction coefficients of 6-FAM at 260 and 495 nm (26000 and 75000 cm^{-1} M^{-1}; pH 8.0) [19].

IV.2.2. Tunning the pK_a of dsDNA labeled with 6-FAM

The 6-FAM dsDNA pK_a determination assays were performed at 22ºC using a dsDNA concentration of 0.3 μM. The titration experiment was performed in 10 mM MES/Tris-HCl (pH 9.2) buffer containing 250 mM KCl, 0.2 mM EDTA, 0.2 mM DTT and 10% glycerol. HCl 0.1 M was used to obtain a pH range from 9.2 to 4.6. The pH measurements were performed using a 713 pH Meter (Metrohm). Fluorescence emission and anisotropy data were recorded for each pH value using a SPEX Fluorolog-3 (Horiba) spectrofluorometer equipped with a 450 W continuous Xenon lamp as excitation source.

Suprasil® quartz fluorescence cuvette, pathlength 10x10 mm with a chamber volume of 500 μL was used during the experiment.

The emission data were collected using an excitation wavelength of 475 nm and monitoring the emission from 490 to 650 nm. The band-pass was 5 nm for excitation and emission, and the integration time was 0.5 sec. All the emissions values were corrected for the respective dilution factors.

The anisotropy data were recorded using an excitation wavelength of 475 nm and monitoring the emission from 505 to 535 nm. The band pass was 5 nm for excitation and emission, and the integration time was 2 sec. All the fluorescence measurements were made under magic angle conditions.

The present study used a three pK_a fluorescein model in order to evaluate the distribution of different species according to the ionic strength of the medium. The concentration of each species was determined according to the equilibrium equation (Eq. 4.6) where "F" represents the deprotonated state of fluorescein molecule:

$$F^{2-} + H^+ \leftrightarrows FH^- + H^+ \leftrightarrows FH + H^+ \leftrightarrows FH^+ \qquad \text{Eq.4.6}$$

$$\boldsymbol{K_1} = [\mathbf{FH^-}]/([\mathbf{F^{2-}}]\,[\mathbf{H^+}]) \qquad \text{Eq.4.7}$$

$$\boldsymbol{K_2} = [\mathbf{FH}]/([\mathbf{FH^-}]\,[\mathbf{H^+}]) \qquad \text{Eq.4.8}$$

$$\boldsymbol{K_3} = [\mathbf{FH^+}]/([\mathbf{FH}]\,[\mathbf{H^+}]) \qquad \text{Eq.4.9}$$

Rearrangement of equations 4.7, gives:

$$[\boldsymbol{FH^-}] = \boldsymbol{K_1}[\boldsymbol{F^{2-}}][\boldsymbol{H^+}] \qquad \text{Eq.4.10}$$

Replacing 4.10 on 4.8 and rearranging it gives,

$$[\boldsymbol{FH}] = \boldsymbol{K_1 K_2}[\boldsymbol{F^{2-}}][\boldsymbol{H^+}]^2 \qquad \text{Eq.4.11}$$

And replacing 4.11 on 4.9 gives,

$$[\boldsymbol{FH^+}] = \boldsymbol{K_1K_2K_3}[\boldsymbol{F^{2-}}][\boldsymbol{H^+}]\boldsymbol{3} \qquad \text{Eq.4.12}$$

The corresponding concentration fraction (α) of F^{2-} is given by:

$$\alpha[F^{2-}] = \frac{[F^{2-}]}{[F^{2-}]+[FH^-]+[FH]+[FH^+]} \qquad \text{Eq. 4.13}$$

Substituting 4.10, 4.11 and 4.12 into 4.13, we obtain:

$$\boldsymbol{\alpha}[\boldsymbol{F^{2-}}] = \frac{\mathbf{1}}{\mathbf{1}+\boldsymbol{K_1}[\boldsymbol{H^+}]+\boldsymbol{K_1K_2}[\boldsymbol{H^+}]^2+\boldsymbol{K_1K_2K_3}[\boldsymbol{H^+}]^3} \qquad \text{Eq.4.14}$$

The same procedure was done for α[FH^-] and α[FH]

$$\alpha[FH^-] = \frac{[FH^-]}{[F^{2-}]+[FH^-]+[FH]+[FH^+]}$$

$$\boldsymbol{\alpha}[\boldsymbol{FH^-}] = \frac{\boldsymbol{K_1}[\boldsymbol{H^+}]}{\mathbf{1}+\boldsymbol{K_1}[\boldsymbol{H^+}]+\boldsymbol{K_1K_2}[\boldsymbol{H^+}]^2+\boldsymbol{K_1K_2K_3}[\boldsymbol{H^+}]^3} \qquad \text{Eq.4.15}$$

$$\alpha[FH] = \frac{[FH]}{[F^{2-}]+[FH^-]+[FH]+[FH^+]}$$

$$\alpha[FH] = \frac{K_1K_2[H^+]^2}{1+K_1[H^+]+K_1K_2[H^+]^2+K_1K_2K_3[H^+]^3} \qquad \text{Eq.4.16}$$

$$\alpha[FH^+] = \frac{[FH^+]}{[F^{2-}]+[FH^-]+[FH]+[FH^+]}$$

$$\alpha[FH^+] = \frac{K_1K_2K_3[H^+]^3}{1+K_1[H^+]+K_1K_2[H^+]^2+K_1K_2K_3[H^+]^3} \qquad \text{Eq.4.17}$$

IV.2.3 Protein-DNA binding

Fluorescence anisotropy of the 6-FAM attached to the 5′end of dsDNA was used to monitor the interaction between MorR and the intergenic region located between *mor*P and *mor*S. Two different DNA strand were used: one containing 67 and other 58

oligonucleotides. The 6-FAM was attached to 5′ end of both molecules; however, it was covalently attached to guanine (purine) in 67-mer dsDNA, and to cytosine (pyrimidine) in 58-mer dsDNA.

The MorR-DNA binding reaction was performed identically for both 6-FAM labeled dsDNA. The reaction occurred in 10 mM Tris-HCl, pH 7.6, with 250 mM NaCl, 0.2 mM of EDTA and DTT, and 10% glycerol. The MorR protein was also diluted in the same buffer. A fixed concentration of 6-FAM dsDNA, 8.3 nmol, was used, with MorR being titrated from 0 to 60 μM until a final volume of 3 ml in a Suprasil® quartz fluorescence cuvette, pathlength 10x10 mm, with chamber volume of 3.5 ml. Fluorescence emission and anisotropy were recorded using a SPEX Fluorolog-3 (Horiba) spectrofluorimeter equipped with a 450 W continuous Xenon lamp as excitation source.

The emission and anisotropy parameters were the same used for determination of pKa (unit IV.2.2) except for the integration time that was 0.5 sec.

For MorR-DNA binding, a model consisting of two nucleotide binding sites was evaluated in order to determine the association constants (K_1 and K_2). This model contemplates the consecutive binding of two protein monomers to the DNA, according to equation 4.18.

$$\boldsymbol{DNAfree + P \leftrightharpoons DNAP + P \leftrightharpoons DNAP_2} \quad \text{Eq.4.18}$$

$$\boldsymbol{K_1} = [\boldsymbol{DNAP}]/([\boldsymbol{DNAfree}][\boldsymbol{P}]) \quad \text{Eq.4.19}$$

$$[\boldsymbol{DNAP}] = \boldsymbol{K_1}[\boldsymbol{DNAfree}][\boldsymbol{P}] \quad \text{Eq.4.20}$$

$$\boldsymbol{K_2} = ([\boldsymbol{DNAP_2}])/([\boldsymbol{DNAP}][\boldsymbol{P}]) \quad \text{Eq.4.21}$$

$$[\boldsymbol{DNAP_2}] = \boldsymbol{K_2}[\boldsymbol{DNAP}][\boldsymbol{P}] \quad \text{Eq.4.22}$$

And substituting the equation 4.20 into equation 4.22, we obtain:

$$[\boldsymbol{DNAP2}] = \boldsymbol{K1\ K2}\ [\boldsymbol{DNAfree}][\boldsymbol{P}]^{\boldsymbol{2}} \quad \text{Eq.4.23}$$

The total concentration of DNA (DNA_T) is equal to:

$$[\boldsymbol{DNA_T}] = [\boldsymbol{DNAfree}] + [\boldsymbol{DNAP}] + [\boldsymbol{DNAP_2}] \quad \text{Eq.4.24}$$

And the fraction of DNAfree is equal to:

$$\alpha[DNAfree] = \frac{[DNA_{free}]}{([DNAfree]+[DNAP]+[DNAP_2])} \quad \text{Eq.4.25}$$

Substituting the equation 4.20 and 4.23 into 4.25 gives,

$$\alpha[DNAfree] = \frac{1}{(1+K_1[P]+K_1K_2[P]^2)} \quad \text{Eq.4.26}$$

The same procedure was done for α[DNAP] and α[$DNAP_2$]

$$\boldsymbol{\alpha[DNAP]} = \frac{[\boldsymbol{DNAP}]}{([\boldsymbol{DNAfree}]+[\boldsymbol{DNAP}]+[\boldsymbol{DNAP_2}])} \quad \text{Eq.4.27}$$

$$\boldsymbol{\alpha[DNAP]} = \frac{\boldsymbol{K_1[P]}}{(\boldsymbol{1+K_1[P]+K_1K_2[P]^2})} \quad \text{Eq.4.28}$$

$$\boldsymbol{\alpha[DNAP2]} = \frac{[\boldsymbol{DNAP2}]}{([\boldsymbol{DNAfree}]+[\boldsymbol{DNAP}]+[\boldsymbol{DNAP_2}])} \quad \text{Eq.4.29}$$

$$\boldsymbol{\alpha[DNAP2]} = \frac{\boldsymbol{K_1K_2[P]^2}}{(\boldsymbol{1+K_1[P]+K_1K_2[P]^2})} \quad \text{Eq.4.30}$$

The data were evaluated according to equations 4.26, 4.28 and 4.30 and fitted according to the nonlinear last square calculation.

IV.2.4. MorR oligomerization

The fluorescence emission of MorR was measured in the presence of the phosphodonors acetylphosphate and phosphoramidate. The reaction was performed with 2 μM of MorR diluted in a buffer consisting of 10 mM Tris-HCl, pH 7.6, with 2 mM of

$MgCl_2$ in a final volume of 3 ml. A Suprasil® quartz fluorescence cuvette was used, pathlength 10x10 mm, with chamber volume of 3.5 ml.

The fluorescence emission was recorded using a SPEX Fluorolog-3 spectrofluorometer equipped with a 450 W continuous Xenon lamp as excitation source. The W was excited at 290 nm and emission was monitored from 300 to 550 nm. The band pass was 2 nm for excitation, and emission, and the integration time was 0.5 sec. All the emissions values were corrected for their respective dilution factors.

The data were evaluated as Static Quenching according to equation 4.31:

$$\phi = \phi^{\boldsymbol{N}}\chi_{\boldsymbol{N}} + \phi^{\boldsymbol{Q}}(\mathbf{1} - \chi_{\boldsymbol{N}}) \qquad \text{Eq.4.31}$$

Where ϕ^N is the quantum frequency of the Native protein (without quencher), χ_N is the fraction of the native protein and ϕ^Q is the quantum frequency of the quencher.

Rearrangement of equation 4.31, gives:

$$\phi/\phi^{\boldsymbol{N}} = \chi_{\boldsymbol{N}} + \phi^{\boldsymbol{Q}}/\phi^{\boldsymbol{N}}(\mathbf{1} - \chi_{\boldsymbol{N}}) \qquad \text{Eq.4.32}$$

$$\phi/\phi^{\boldsymbol{N}} = \chi_{\boldsymbol{N}} + \phi^{\boldsymbol{Q}}/\phi^{\boldsymbol{N}}(\mathbf{1} - \chi_{\boldsymbol{N}}) \qquad \text{Eq.4.33}$$

$$\chi_{\boldsymbol{N}} = \mathbf{1}/(\mathbf{1} + \boldsymbol{K}[\boldsymbol{Q}]) \qquad \text{Eq.4.34}$$

$$\phi/\phi^{\boldsymbol{N}} = \chi_{\boldsymbol{N}}\,(\mathbf{1} - \phi^{\boldsymbol{Q}}/\phi^{\boldsymbol{N}}) + \phi^{\boldsymbol{Q}}/\phi^{\boldsymbol{N}} \qquad \text{Eq.4.35}$$

$$\frac{\phi}{\phi^{\boldsymbol{N}}} \Leftrightarrow \frac{\boldsymbol{I}}{\boldsymbol{I_0}} = \frac{\mathbf{1}}{\mathbf{1}+\boldsymbol{K}[\boldsymbol{Q}]}\left(\mathbf{1} - \frac{\phi^{\boldsymbol{Q}}}{\phi^{\boldsymbol{N}}}\right) + \frac{\phi^{\boldsymbol{Q}}}{\phi^{\boldsymbol{N}}} \qquad \text{Eq.4.36}$$

Where $\phi^Q/\phi^N = \alpha$ = quenching efficiency

Rearrangement of equation 4.36, gives:

$$I/I_0 = 1/(1 + K[Q]) + \alpha\,(1 - 1/(1 + K[Q])) \qquad \text{Eq.4.37}$$

$$I/I_0 = \alpha + 1/(1 + K[Q])\ (1 - \alpha) \qquad \text{Eq.4.38}$$

where: I is the total intensity, I_o is the intensity of tryptophan in the absence of quencher (Q) and *K* is the quenching constant. The data was fitted using nonlinear least square calculation.

IV.2.5. Computational biochemistry

All geometry optimizations were performed with Gaussian 09, applying density functional theory methods[20]. Becke's three-parameter exchange functional was used together with the functional of Lee et al. (B3LYP) [21,22,23]as implemented in Gaussian and the 6-31G(d) basis set. In all geometry optimizations, we first searched for the transition state starting from a structure similar to the reactants model. This was generally obtained with mono-dimensional scans where the reaction coordinate that we were interested in, was shortened or stretched. Once the transition state was located, the reactants and the products, associated with it, were determined through internal reaction coordinate (IRC) calculations. In all cases, the geometry optimizations and the stationary points were obtained with standard Gaussian convergence criteria. The transition state structures were all verified by vibrational frequency calculations, having exactly one imaginary frequency with the correct transition vector, even using frozen atoms, which shows that the frozen atoms are almost free from steric strain.

IV.3. Results and Discussion

IV.3.1. Fluorescein labeled oligonucleotide pK_a determination

In order to understand the fluorescence behavior of the fluorophore that was chosen for the DNA labeling, the fluorescence emission and anisotropy of 6-FAM-67-mer dsDNA were measured at different pHs. The raw and area normalized spectra obtained are present in figure IV.5.

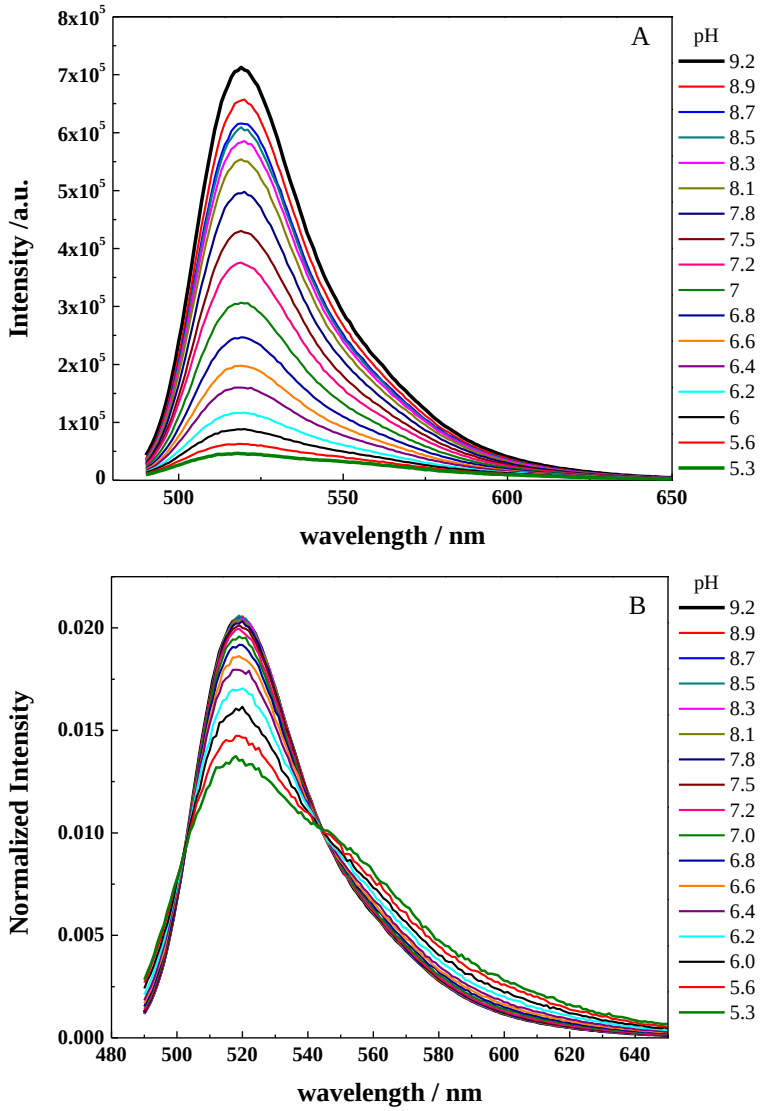

Figure IV.5. Fluorescence emission and anisotropy of 6-FAM-67-mer dsDNA at different pH, ranging from 5 to 9.2. A) Fluorescence emission raw spectra. B) Area normalized fluorescence emission spectra.

The results showed that as the pH becomes more acidic, the total fluorescence emission decreases. However, the fluorescence shifted at 545 nm where the fluorescence intensity of 6-FAM increased in acidic conditions. Moreover, the decrease in fluorescence emission intensity is accompanied by an increase in anisotropy (figure IV.6). This result is important for protein-DNA interaction studies where oligonucleotides are labeled with 6-FAM and when anisotropy is used to monitor the binding reaction. In those cases, the fluorescence emission should not vary during the experiment, and the anisotropy values

should be the only parameter allowed to change upon binding. Because of that, it is important to control the reaction in order to avoid variations of pH.

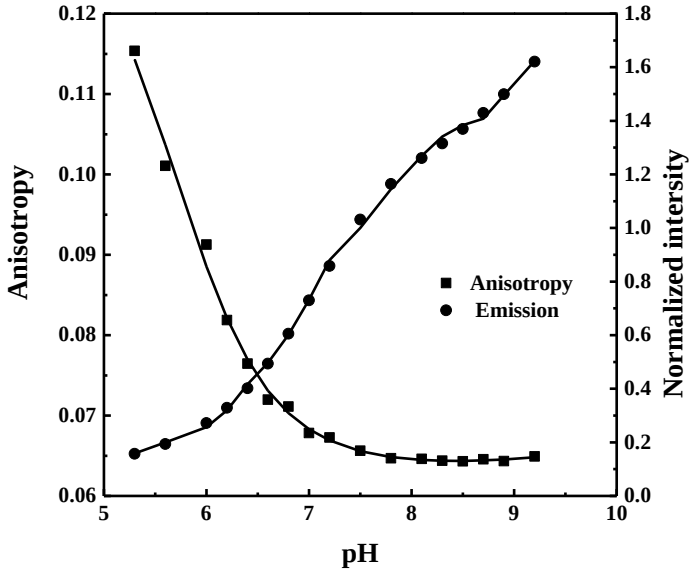

Figure IV.6. pH dependence of fluorescence intensity (circles) and steady-state anisotropy (squares) of 6-FAM-67-mer dsDNA. Experimental fluorescence emission values were normalized. Lines represent the fitting of the data assuming acid-base equilibrium which allowed the determination of pK_a's.

The 6-FAM-67-mer dsDNA diagram species was based on the three pKa fluorescein model (methodology section IV.2.2) that considers four types of fluorescein species: the cationic (FH^+), neutral (FH), monoanionic (FH^-), and dianionic (F^{2-}). In acidic conditions, at pH 5.3, 71% of the fluorescein is FH^+, and 29% is FH. Once the pH became more alkaline, the percentage of cationic species decreases and, at pH 7, only 3% is FH^+, 53% is FH, 45% is FH^- and no F^{2-} form is present. Under the experimental conditions used for the present study (pH 7.5), 72% is FH^- and 27% is FH. The FH^- is the predominant species from pH 7.5 to 9.2 (figure IV.7). It is known that the dianionic fluorescein has the highest fluorescence intensity over the other fluorescein species[9]. However, our results shows that this species starts to emerge above a pH 8 and its fluorescence intensity is modest even at pH 9 and therefore the use of reactional conditions to obtain a considerable amount of dianionic fluorescein are not suitable for protein stabilization. The presence of the monoanionic species under the pH used in this study does not invalid assays of MorR-DNA interaction. The monoanionic species pursues a considerable degree of fluorescence that is capable to sense the interaction between two macromolecules. Moreover, the

anisotropy of 6-FAM does not changed significantly from pH 7 to 8. So any significant anisotropic change observed for MorR-DNA interaction in a future experiment using a buffer around this pH range would be a result of a reliable macromolecules association.

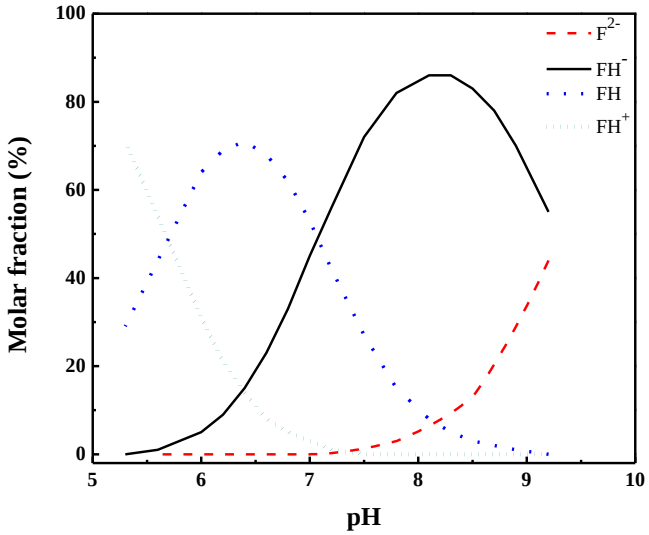

Figure IV.7. Diagram species of 6-FAM-67-mer dsDNA. At pH 7.5 the monoanioc specie is prevalent (72%), followed by neutral (26%), dianionic (1%), and cationic (0.4%).

The fitting of both set of data (fluorescence emission and anisotropy) allowed the calculation of apparent pK_a's for the 6-FAM-67-mer dsDNA which were compared with those of fluorescein free in solution, and FITC-9-mer dsDNA as presented on the table IV.2.

Table IV. 2. pK_a values of free fluorescein, FITC-9-mer dsDNA and 6-FAM-67.mer dsDNA.

	pKa1	pKa2	pKa3
"free fluorescein"[a]	2.3	4.2	6.3
FITC-9-mer dsDNA [b]	-	-	7.02
6-FAM-67-mer dsDNA	5.7	7.1	9.3

a – taken from H. Diehl (1989) Talanta, 36, 413-415
b – taken from R. Sjöback (1998) Biopolymers, 46, 445-453

The studies about the fluorescein attached to DNA are under constant evolution, and there is a debate concerning the influence of oligonucleotide length on any spectroscopic alterations, pK_a and anisotropy values. However, the prevalence of the fluorescein monoanionic species under the experimental conditions of this study (pH 7.5) is

not in agreement with some previously published data. Sjöback *et al*., (1998) reported that at pH 7.46, 72% of fluorescein conjugated with DNA oligonucleotides was in the dianion form and 28% as monoanion [24]. This study proved that the oligonucleotide length (ranging from 9 to 18 bp) did not significantly alter the fluorescein pK_a values when compared with solution of free fluorescein (pK_a of 6.43). However, other studies regarding the characteristics of fluorescein-labeled oligonucleotides have shown that differences in the oligonucleotide length and base pair composition beside the fluorophore caused spectroscopic variations. Anderson *et al*., (2008) verified that smaller (17 pb) oligonucleotides had higher anisotropy upon protein binding than longer (22 bp) oligonucleotides [25]. Moreover, changes in anisotropy and quantum yields have been identified after a single strand fluorescein-labeled oligonucleotide hybridizes to its complementary strand [26,27]. The evaluation of the GC content of the oligonucleotides reported by Sjöback and Anderson showed no significant difference: 43.15% and 54.4%, respectively. However, the 6-FAM position differed between them. The oligonucleotides studied by Sjöback were linked at the 5′ end of the duplex; on the contrary Anderson labeled the probes at 3′ end. Moreover, based on the Sjöback work, some studies which used fluorescein labeled oligomers were carried out under the fundamental assumption that the dianionic form predominates or that a single fluorescein species was present under pH 7 to 8 [28,29]. Our results show the absence of single fluorescein specie and a low degree of the dianionic species around pH 7 to 8. Around this pH at least 2 species predominated (FH- and FH).

The present study evaluated the prototropic forms of 6-FAM attached to the 5′ end of a 67-mer oligonucleotide with 31% of GC content. The results indicate that fluorescein acid - base equilibrium changed upon conjugation to the nucleic acids. However, it is not possible to predict if this equilibrium is affected by DNA length, conformations or composition.

The present study showed that the anisotropy values were affected by the protonation status of the fluorophore (figure IV.6). In this context, the acid base equilibrium of fluorescein-labeled oligonucleotide is an important tool to optimize binding assays. The variation in 6-FAM fluorescence emission was related with the emerging fluorescein species along the pH range (figure IV.7). Because of that, a constant 6-FAM

emission should be a prerequisite during studies that monitor DNA-protein binding using anisotropy as a tool to access the interaction.

IV.3.2. MorR-DNA interaction

Fluorescence anisotropy of MorR-DNA interaction was measured in order to determine the association constant between the target intergenic region and MorR. For this reason and considering the results obtained from the calculation of the apparent pK_a, a constant fluorescence emission was made a prerequisite, and solely the anisotropy values varied. Moreover, two 6-FAM labeled dsDNA were constructed (figure IV.8). Both molecules contained the entire MorR binding sites identified by DNaseI footprinting. The first molecule is the 6-FAM-67-mer dsDNA where fluorescein is covalently attached to guanine (purine), and the second molecule is the 6-FAM-58-mer dsDNA where fluorescein is covalently attached to cytosine (pyrimidine).

Figure IV.8. 6-FAM labeled dsDNA used for fluorescence anisotropy experiments. The MorR nucleotide binding sites identified by DNaseI footprinting are represented in red, and the position of 6-FAM is evidenced. A) 6-FAM-67-mer dsDNA. B) 6-FAM-58-mer dsDNA.

In both experiments, a fixed concentration of 6-FAM dsDNA was used, and the MorR concentration varied from 0 to 60 µM. The results show that fluorescence emission was constant along the titration so that a single fluorescein species was present during the experiment (figure IV.9) and therefore the anisotropy values were a result of MorR-DNA interaction and are not due to protonation status of the fluorophore.

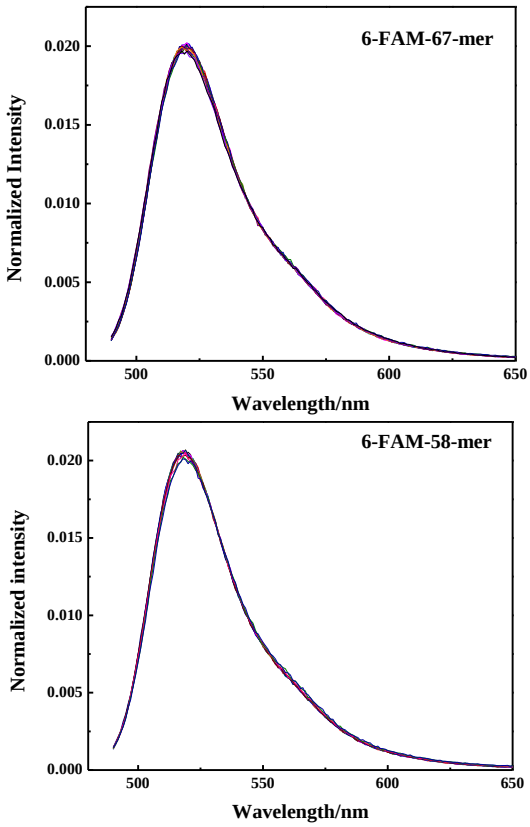

Figure IV.9. Area normalized fluorescence emission of 6-FAM-67-mer dsDNA and 6-FAM-58-mer dsDNA along the titrations experiments.

The anisotropy values were enhanced with increasing concentrations of MorR, and the resulting binding curve was fitted to the proposed two steps model (see equation 4.18) (figure IV.10). Furthermore, the anisotropy of 6-FAM-67-mer dsDNA was shown to vary from 0.071 to 0.107, and that of 6-FAM-58-mer dsDNA from 0.073 to 0.127.

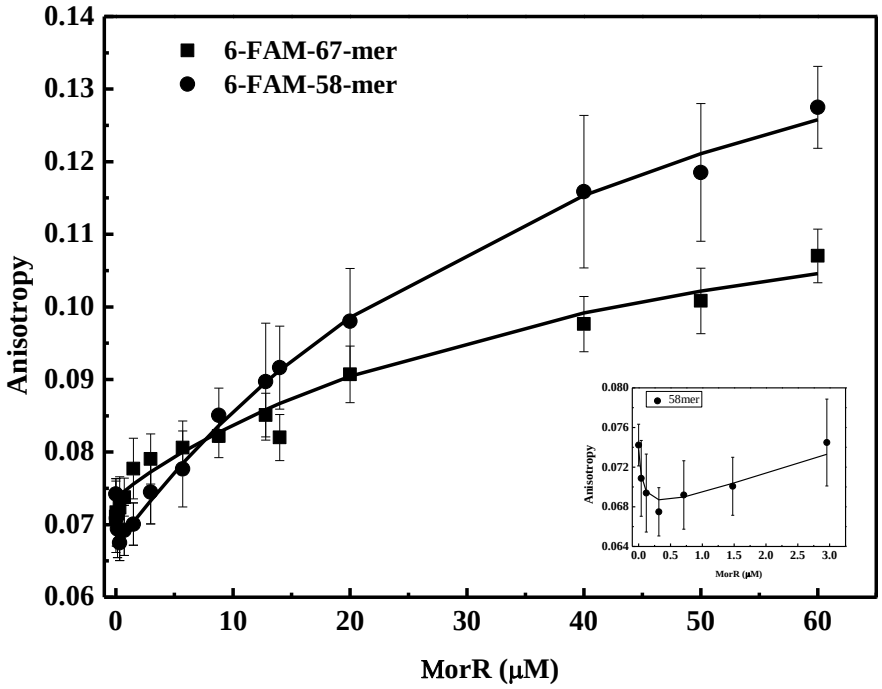

Figure IV.10. Fluorescence anisotropy of 6-FAM-67-mer dsDNA and 6-FAM-58-mer dsDNA during the titrations experiments. The graphic shows the variation of anisotropy, where errors bars represent the standard deviation, and the squares and circles show the medium value obtained from seven anisotropy readings for each DNA strand. The equilibrium binding was analyzed according to equations 4.18, and the nonlinear least square mathematical model was applied and is presented as a straight line. The insert shows the anisotropy variation for 6-FAM-58-mer dsDNA from 0 to 3μM.

The similarity of both experiment allowed the fitting of both data using nonlinear least square in order to determine the association constant between MorR and DNA and also the anisotropy values (r) of the fluorophore according to the binding state (table IV.3).

Table IV.3. Association constants determined for MorR binding to the intergenic region between *mor*S and *mor*P following the two step binding model. K_1 is the association constant for the first binding site and K_2 for the second binding site. The anisotropy value (r) of the fluorophore is also shown.

	Association constants	
dsDNA	K_1 ($x10^5$ M^{-1})	K_2($x10^5$ M^{-1})
	15.5	0.02
Anisotropy	r1	r2
	0.074	0.127

The observed data for 6-FAM-67-mer and 6-FAM-58-mer is presented in table IV.4 and figure IV.11. The interaction of MorR with 6-FAM-67-mer dsDNA reveals that

the protein binds highly to a first binding site and with lower affinity to a second binding site. Analysis of the data showed that when MorR reached a concentration of 8.78 µM, 13% of the 6-FAM-67-mer DNA was free, 85% of the first binding site was bound, and 1% of the second binding site was occupied. As soon as MorR concentration increases, a greater fraction of first and second binding sites is bound. However, the first binding site reaches a plateau at 20 µM of MorR, with 90% of the site was occupied by the protein. This is followed by a slight decrease in the percentage of occupancy of this site. In an opposite way, there was no observable plateau for the second binding site. When MorR reached a final concentration of 60 µM, 2% of the DNA remained free, 88% of the first binding site was occupied, and 10% the second binding site was bound.

The affinity of MorR to 6-FAM-58-mer dsDNA is similar to the one observed for 6-FAM-67-mer dsDNA, except for the fact that fluorescein position facilitated the visualization of the MorR binding to the second site. This result is in agreement with the DNaseI footprinting experiment given that, in this case, the fluorescein was positioned nearest of the binding site. When MorR reached a concentration of 8.78 µM, 0% of the 6-FAM-58-mer dsDNA was free, while 84% was bound to the first binding site, and 16% of the second binding position. Increasing the concentration of MorR leads to increase in the number of occupied sites. At 20µM of MorR, 0% of the DNA was free, 70% of the first binding site was bound, and 30% of the second binding site was occupied. When MorR reached a final concentration of 60 µM, there was no (0%) free DNA, 44% of the first binding site was bound, and 56% of the second binding site was occupied.

Table IV.4. MorR binding sites proposed occupancy according to the two binding sites model.

Site of occupancy	MorR (µM)	% of occupancy	
		67mer	58mer
free	8.78	13	0
	20	6	0
	60	2	0
1st	8.78	85	84
	20	90	70
	60	88	44
2nd	8.78	1	16
	20	3	30
	60	10	56

A

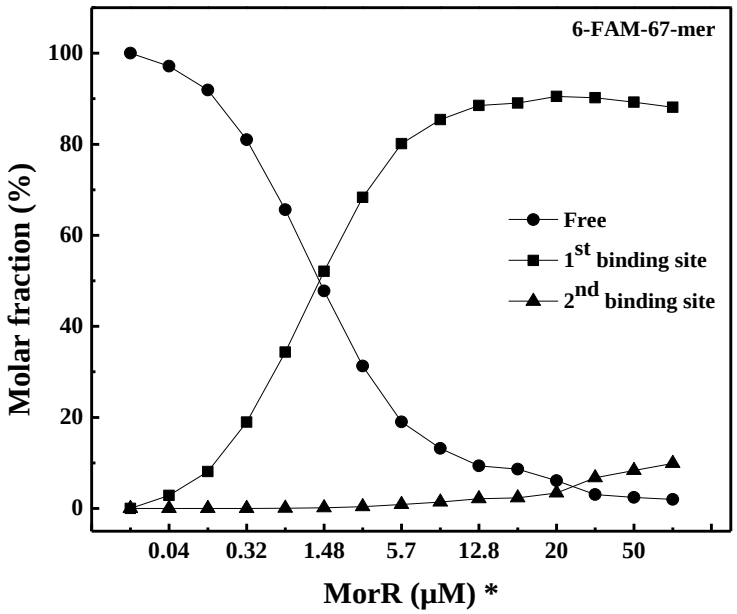

B

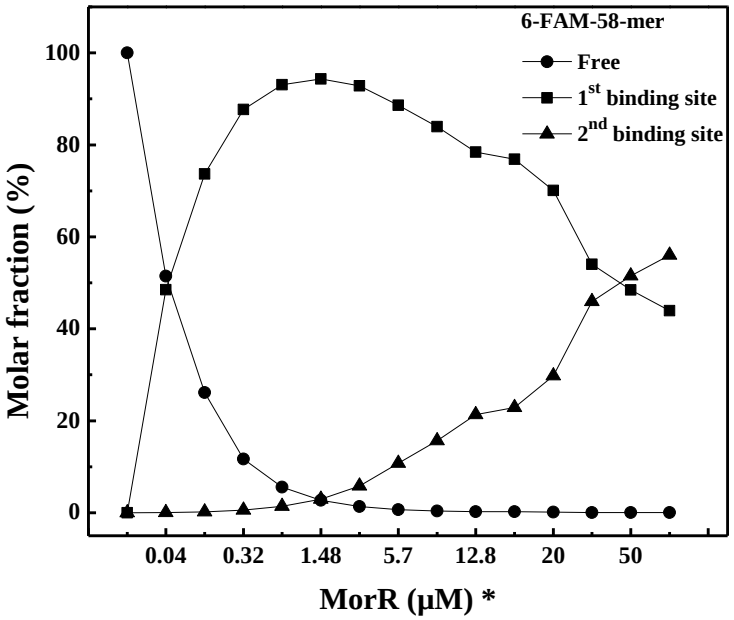

(*) Multiple concentration scale in different orders of magnitude in order to better visualize the distribution of the MorR occupation sites.

Figure IV.11. Occupation of the nucleotide binding sites of 6-FAM-67-mer and 6-FAM-58-mer dsDNA in response to MorR interaction. The free DNA where that is no interaction with MorR is presented as line and circles. The first binding site occupancy is represented by a line and square. The second binding site occupancy is represented as line and triangle.

The fluorescence anisotropy of both molecules followed the same profile, since increase in the concentration of MorR leads to enhanced anisotropy values. Moreover, a considerable increase in anisotropy was visualized above a MorR concentration of 8.78 μM. At this point, the second binding site starts to be occupied (figure IV.12). The results showed that the anisotropy increases as soon as the second binding site was bound, even though with lower affinity, and this interaction could be visualized because of the proximity of the fluorophore to this site (figure IV.8, B). The data comparison between 6-FAM-67-mer and 6-FAM-58-mer showed that changes in 6-FAM position influenced in the sensitivity of the assay for MorR interaction with the second binding site (figure IV.12, B). This assumption is based on the analysis of MorR binding profile to 6-FAM-58-mer. In that way, it is plausible to consider that MorR binds firstly to a site located far from 6-FAM (with high affinity giving rise to low anisotropy values), and subsequently the protein interacts to a second binding site positioned near to the fluorophore (figure IV.13). Those binding sites cover the predicted -35 (first site) and -10 (second site) promoters sequences (figure II.7). We cannot predict if this protein behavior occurs *in vivo*, but it indicates that MorR could acts as a repressor given that it occupies a binding site that might be used by RNA polymerase for transcription initiation.

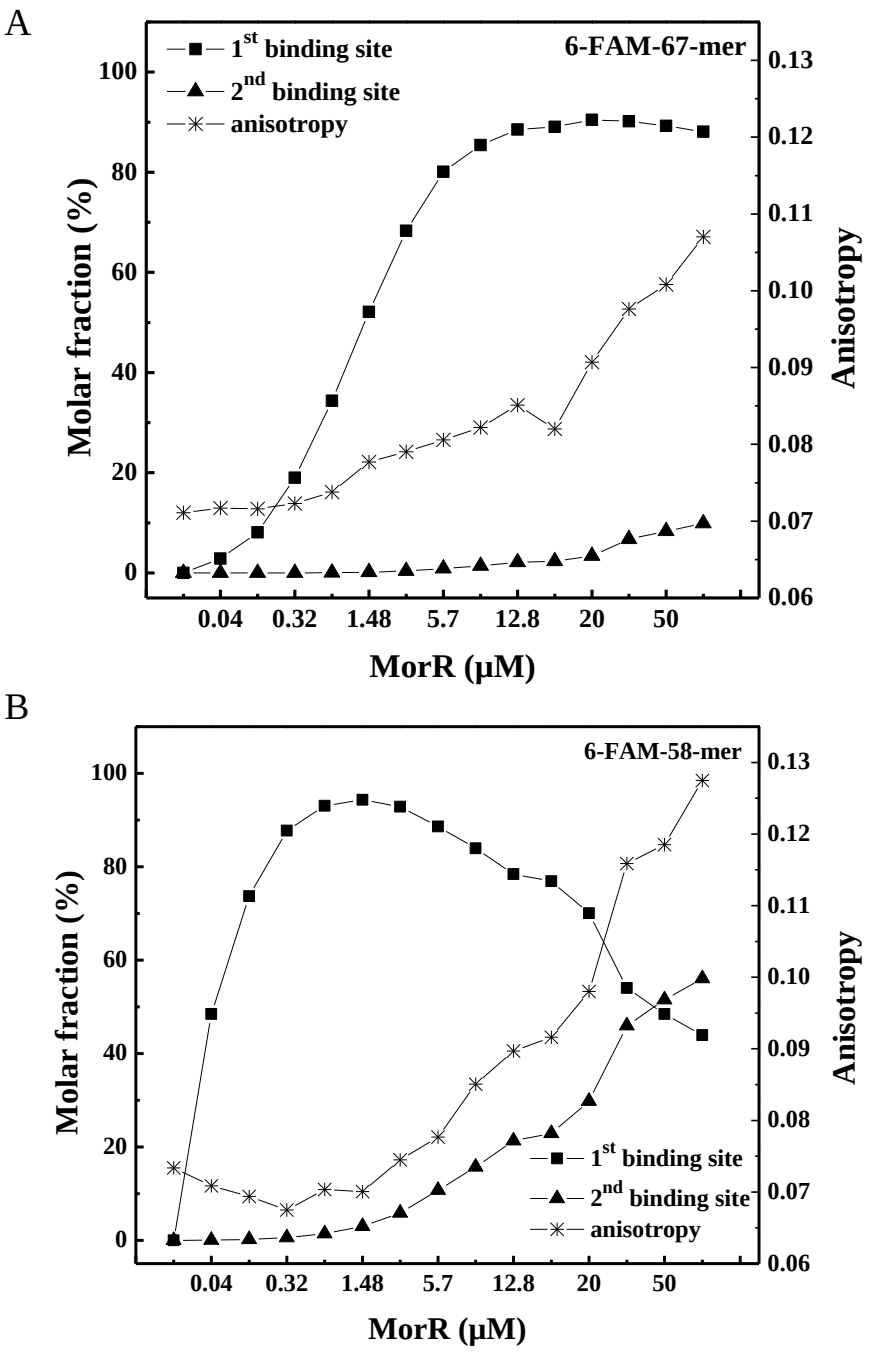

Figure IV.12. Binding sites occupancy of 6-FAM-67-mer and 6-FAM-58-mer molecules with the fluorescence anisotropy enhancement. The first binding site occupancy is presented as line and square. The second binding site occupancy is presented as line and triangle, and the anisotropy is presented as line and asterisk.

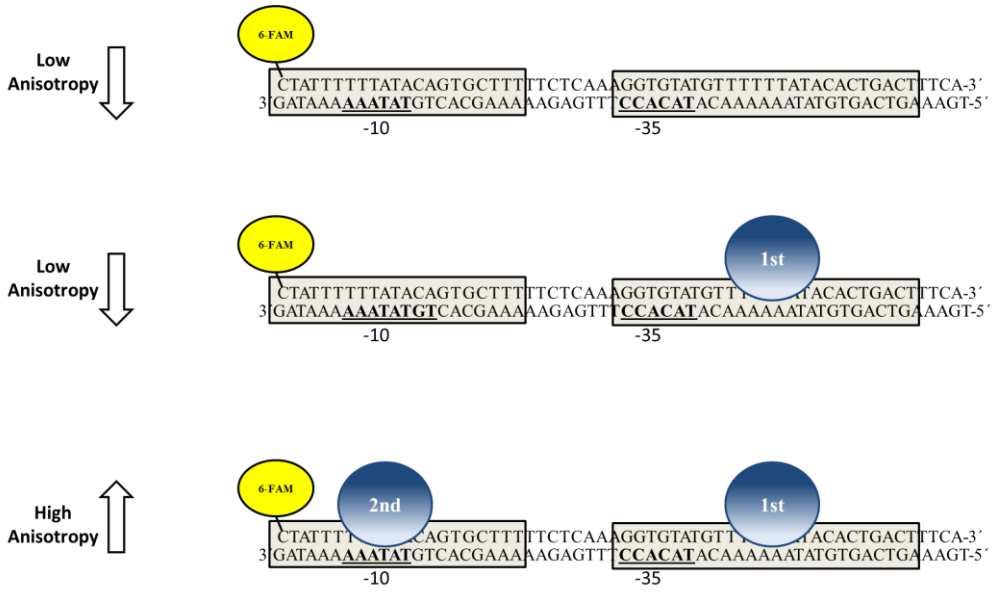

Figure IV.13. Predict model for MorR-DNA interaction. The 6-FAM position is evidenced and the two DNA binding sites are delimitated by rectangles. The blue circles represents the MorR protein.

Regarding the 6-FAM-58-mer interaction with MorR, the anisotropy shape of the fluorophore during the initial stage of the binding curve showed a decrease in the values ranging from 0.074 (no protein) to 0.069 (0.7μM of protein) (figure IV.10, internal graphic). This result is not in line with the conjecture that the interaction between the protein and DNA increase the anisotropy values of the fluorophore. Additionally, this behavior was not observed for MorR interaction with 6-FAM-67-mer. So, any factor (pH or fluorescence lifetime) enhanced the fluorophore rotational capacity of 6-FAM-58-mer. There are two possible explanations for this result:

1. or the addition of MorR changed the local acid condition around the fluorophore leading to emergence of other fluorescein species.

2. or the interaction of MorR with 6-FAM-58-mer led to a DNA conformational change that facilitated the rotational capacity of the fluorophore.

In other to solve this question, the fluorescence lifetime of the 6-FAM-58-mer dsDNA was evaluated under the same experimental conditions, and the results are presented in table IV.5

Table IV.5. Fluorescein-dsDNA single-photon counting analysis as a function of the MorR protein concentration.

[MorR] /μM	τ /ps	χ^2
0.0	3432	1.081
0.9	3416	1.104
4.4	3461	1.163
4.1	3472	1.246
8.0	3537	1.183

The result shows a quite constant fluorescence lifetime of the fluorophore upon MorR interaction and a mono-exponential decay profile. Those evidences reinforce the assumption that a single fluorescein species was present during the experiment (excluding the pH variation hypothesis) and indicate that fluorescein became more available to rotate after MorR addition. Finally, we conclude that a conformational change of the 6-FAM-58-mer DNA occurred upon MorR binding, which increased the fluorophore rotation. We propose that 6-FAM-58-mer dsDNA was coiled (with 6-FAM less available to rotate) and MorR binding straightened the molecule during the first interaction process enhancing the fluorophore rotational capacity.

IV.3.3. Study of MorR phosphorylation by fluorescence spectroscopy

The comprehension about the protein photochemical characteristics associated with phosphorylation by small phosphodonors is an important aspect to understand the real influence of its compounds in the oligomerization status of transcriptional regulatory protein belonging to two component systems.

Analysis of the amino acid sequence of MorR revealed the presence of 2 W, 9 F and 11 Y. The first W is at position 29 and the second at 360, and they are part of the receiver and central domain, respectively. In order to study the MorR conformational change induced by small phosphodonors, the MorR fluorescence emission was excited during independent titration reactions using two different phosphodonors: acetylphosphate and phosphoramidate. The results showed that both phosphor-donors induced a decrease in W fluorescence intensity (figure IV.14). However, phosphoramidate caused a higher decrease in W emission but without any observed shift (figure IV.15).

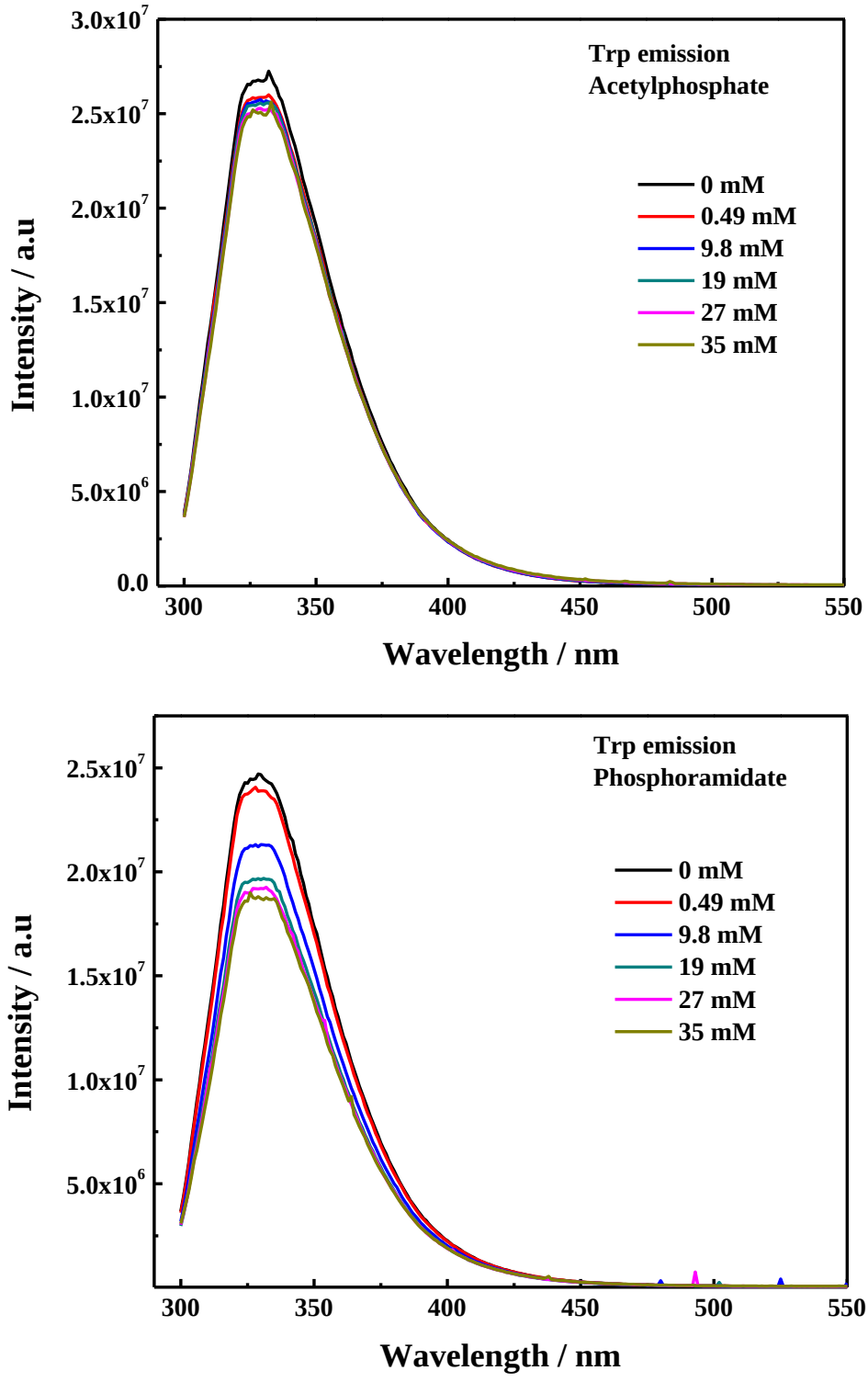

Figure IV.14. Raw spectra of MorR tryptophan emission during a titration with phosphodonors. A) Acetylphosphate. B) Phosphoramidate.

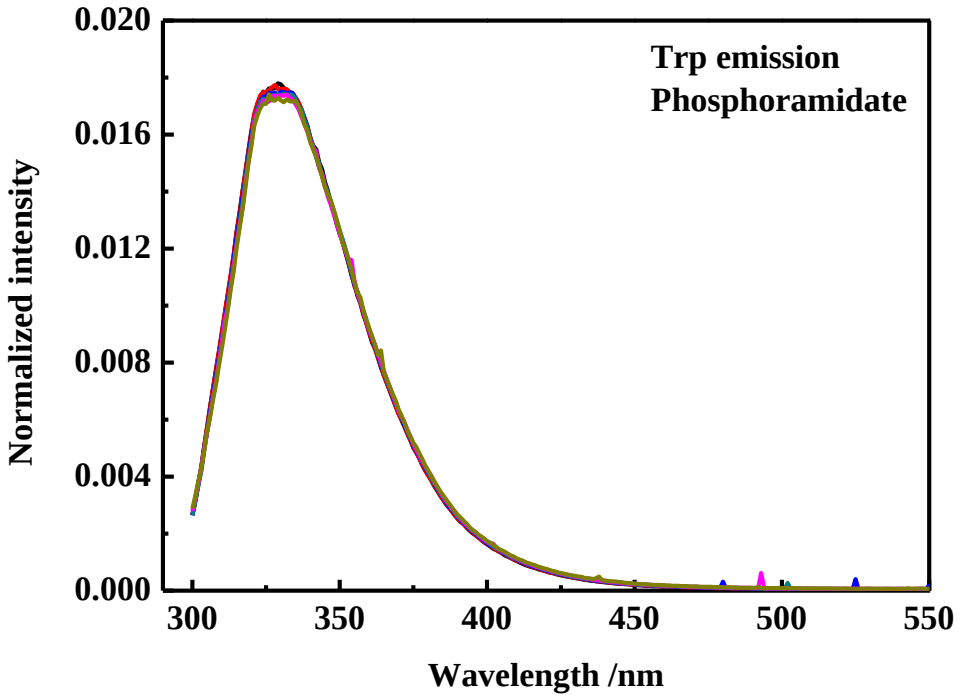

Figure IV.15. Area normalized spectra of W emission during a titration with phosphoramidate.

The data obtained using phosphoramidate were evaluated according to the dynamic quenching based on the equation 4.1 and fitted according to the nonlinear least square calculation. However, the result gives a k_q (the bimolecular quenching constant) of $5x10^{10}$ M^{-1} s^{-1} which is incompatible with a diffusion controlled quenching. The best result was obtained when the data was analyzed as static quenching, according to the equation 4.31.

The result for static quenching of W by phosphoramidate is present in figure IV.16. It gives a quenching constant of 0.079 mM^{-1} and indicates that 30% of the W emission was suppressed.

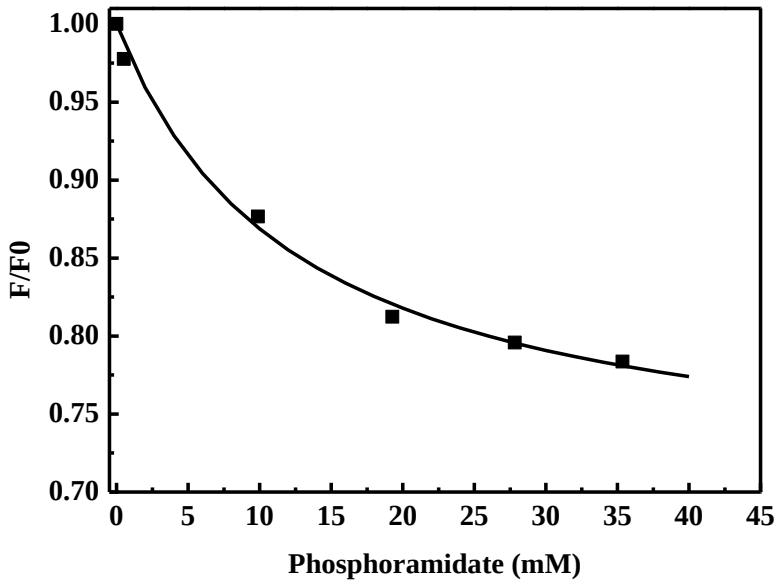

Figure IV.16. Static quenching for MorR titration with phosphoramidate. The line represents the fitting of the data using nonlinear least square and the squares represents the experimental data.

The results show that MorR interaction with phosphoramidate, and not with acetylphosphate, caused a considerable decrease in fluorescence emission of W. This quenching probably is not followed by any conformational alteration in the protein structure since no wavelength shift was observed. This result is in agreement with the gel filtration chromatography where no MorR oligomerization was visualized in the presence of phosphodonors. The fluorescence quenching of W caused by the phosphodonor is not a direct prove that the protein was phosphorylated. In order to visualize phospho-amino acid (if existent), the samples that were submitted to titration with both phosphodonors were analyzed by nano-LC-MS.

IV.3.4. Identification of MorR phospho-peptides

In order to identify the presence of phospho-amino acid in the MorR that was submitted to phospho-donors titrations, the samples were analyzed by nano LC-MS tandem mass spectrometry. Phospho-peptides were identified in both samples, with coverage of 89% and 95% for MorR with acetylphosphate, and phosphoramidate, respectively. The results showed the presence of common phospho peptides for the two phosphodonors, but

addition phosphorylated peptides were found for the sample treated with phosphoramidate (table IV.6).

Table IV. 6. Post-translational modifications (phosphorylation) identified by nano LC-MS mass spectrometry. The modifications are highlighted; the phospho-amino acids are underlined.

Sample	Post-translational modification
Common (acetylphosphate/phosphoramidate)	VG<u>S</u>DNPLR
	NLTAEV<u>T</u>AGR
	SSL<u>S</u>AGQAASR
	AY<u>D</u>AILMDIR
	AVIM<u>S</u>MGEYVTGR
	D<u>D</u>IPLLAGHFLTR
	GWQY<u>S</u>AEEADDG<u>S</u>VAVSK
Exclusive for phosphoramidate	LTELVTAVAPSDATVLITGE<u>S</u>GTGK
	DRPLVTVNCAALTE<u>S</u>LLESELFGNEK

The analysis of the primary structure of MorR revealed that the majority of phospho-amino acids residues are present in the central domain (figure IV.17). Both phosphodonors were capable to phosphorylate the conserved aspartic acid (D) located in the receiver domain. In addition to phosphorylation of D in the receiver domain, the phosphoramidate phosphorylated two serine residues (S) at positions 32 and 40. It is important to mention that both S are located nearby to the W 29. This physical proximity probably was one of the reasons that leaded to fluorescence quenching with phosphoramidate. Furthermore, no phosphoamino-acid was identified in the DNA binding domain. The mechanism involved in this process is not comprehended. However, the presence of a buried domain is excluded to answer this question, since the DNA binding domain is accessible (as proved by MorR-DNA binding experiments), and the receiver domain is characterized as a mobile and exposed domain.

Figure IV. 17. The MorR amino acid composition with conserved regions detached, and the phospho-amino acids identified by nano LC-MS. The amino acids are colored according to its domain localization: red for receiver domain, blue for ATPase domain and green for DNA binding domain. W are bolded in yellow. The phospho-amino acids identified in both samples are bolded in grey and highlighted with an asterisk (*). The phospho-amino acids identified solely in sample submitted to phosphoramidate are bolded in red and highlighted with an hashtag (#).

Analysis of the alignment (figure III.2) shows that both tryptophan residues are conserved between MorR and ZraR. However, the ZraR crystal structure available (PDB code: 1OJL) lacks the receiver domain containing the W 29 residue. Moreover, the receiver domain of MorR shares similarities with the RR CheY (31.4%). However, the amino acid residue alignment between MorR and CheY revealed the absence of the conserved W (figure IV.18). As the inactive state of NtrC shows an intrinsic flexibility of the receiver domain [30]. So, this characteristic is attributed to solvent exposed domains [31] we may expect that this can also occur for the MorR receiver domain. Hence, it is reasonable to predict that the MorR receiver domain has a similar characteristic and might be solvent exposed.

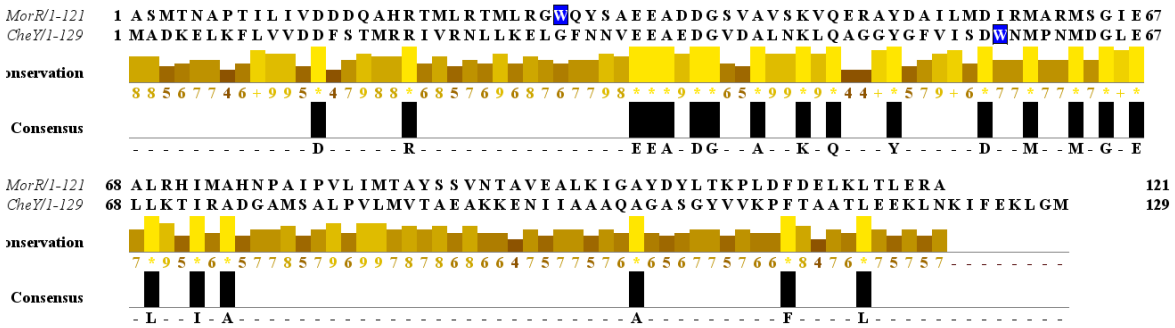

Figure IV. 18. Alignment between N-terminal receiver domain of MorR and *E. coli* CheY. The W are bolded in blue. Conservation is based on the physic-chemical properties of amino acids and the consensus is the percentage of the modal residue per column.

In order to have a better idea about the phospho-aminoacids localization in the central domain and its proximity to W 360, figure IV.19 shows the phospho-amino acids sites in ZraR crystal structure. The analysis revealed that W 360 is far from the phospho-amino acids identified in both samples (figure IV.19, A). On the other hand, W 360 is surrounded by the phospho-amino acids identified solely in the MorR sample submitted to phosphorylation by phosphoramidate: phospho-aspartate 324, phospho-serine 177 and phospho-serine 378 (figure IV.19, B). This comparative analysis also shows that W 360 might be not buried into ZraR structure. It is an indicative that the quenching observed during titration with phosphoramidate might be a consequence of phosphorylation of amino-acids residues located nearby W 360. Moreover, the present study indicates that exposure of the two W (29 and 360) might occur, and the phosphorylation of amino-acids residues located nearby might be the cause of the observed fluorescence quenching with phosphoramidate.

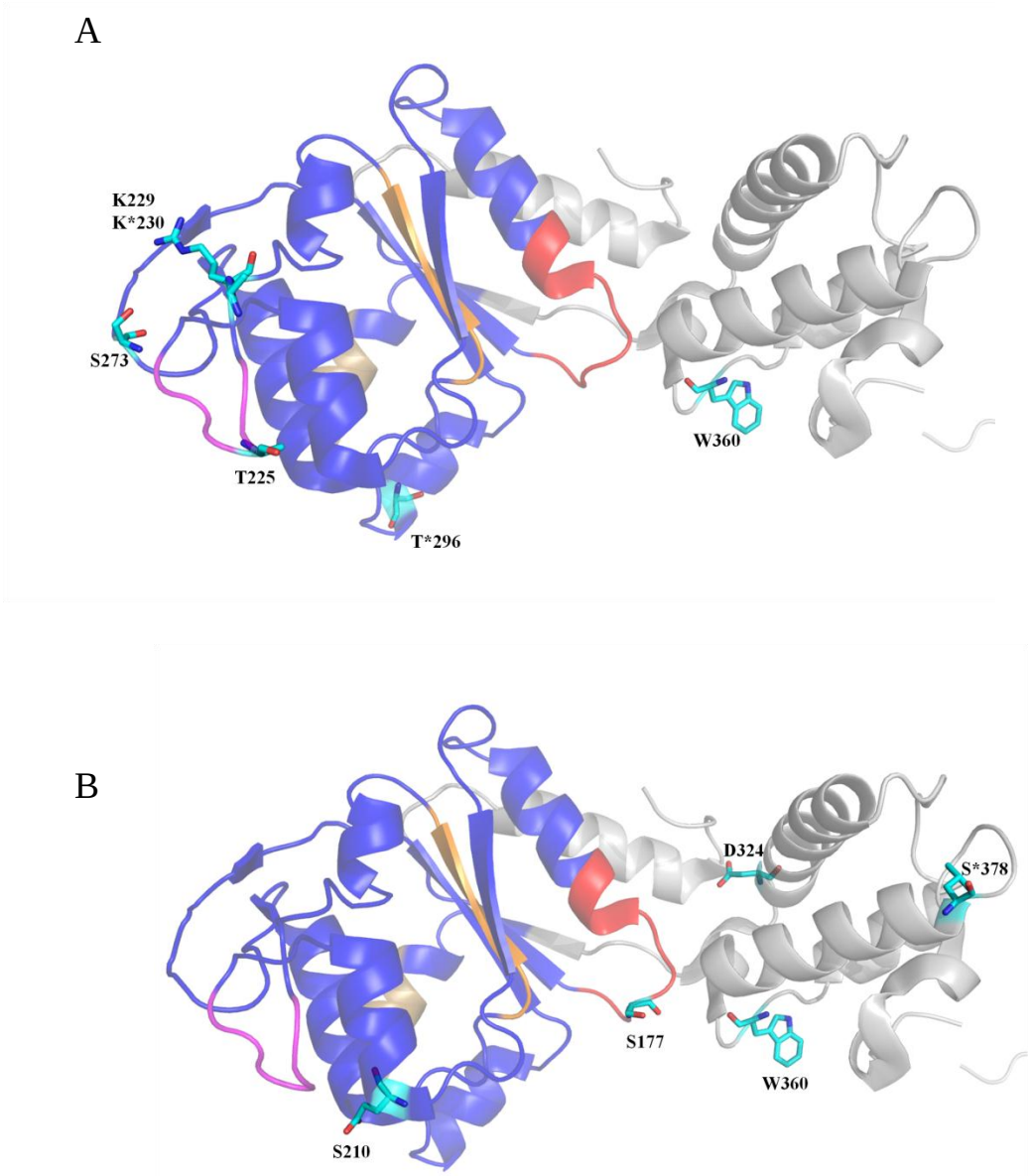

Figure IV.19. Comparison of MorR phospho-amino acids localization in the ZraR central domain crystal structure. A) Phospho-amino acids residues identified in sample submitted to phosphorylation with acetylphosphate and phosphoramidate. B) Phospho-amino acids residues identified solely in sample submitted to phosphorylation with phosphoramidate.

The results obtained by nano LC-MS corroborate the data observed during the fluorescence spectroscopy experiments. The data indicate that W emission is quenched when amino acids positioned around the fluorophore are phosphorylated. The first phospho-S (G<u>W</u>QY**<u>S</u>**AEEADDGSVAVSK) identified solely in the sample submitted to titration with phosphoramidate is positioned two amino acids away from W 29 (located at the receiver domain). Furthermore, the ZraR crystal structure comparison shows that the W 360 residue might not be buried inside the protein structure, indicating that its fluorescence was affected by phosphorylation of amino-acids residues located near its position. So, these results show that the fluorescence quenching was not attributed to any oligomerization process. Moreover, no fluorescence shift was observed during the experiments (figure IV.15). Our results indicate that W fluorescence emission quenching reflected the phosphorylation process that occurred in amino acids located surrounding it.

There are some works reporting the use of fluorescence W emission to monitor phosphorylation process in RR proteins[32,33,34]. A study evaluating the fluorescence spectrum of six different copies of CheY upon interaction with acetylphosphate showed that a conserved W^{106} emission was quenched in the presence of this phosphodonor. In spite of the highest similarity between the target proteins, the fluorescence profile was not the same among them. One of the proteins, the variant CheY1, does not present any W quenching upon interaction with acetylphosphate. In order to answer this unexpected result, the authors postulated that the conformational alteration of CheY1 mediated by acetylphosphate did not change the environment around the W [35]. The fluorescence studies of W quenching in RR have the same principal focus: monitor the phosphorylation status of the adjacent phospho-accepting D residue upon phosphorylation. Our results show that other aminoacids, rather than D, are phosphorylated in the presence of phosphodonors.

However, an open question remains. Why does phosphoramidate have an enhanced capacity to phosphorylate MorR when compared to acetylphosphate? To answer this question we have performed some theoretical calculations regarding the catalytic mechanism of the phosphorylation process using density functional theory and the 6-31G(d) basis set.

Regarding the total number of phospho-amino acids identified by nano-LC MS, most of them are serines, we have studied the catalytic mechanism of phosphorylation only

with serine. We believe that such mechanism can serve as a general example for the phosphorylation mechanism of any amino acid.

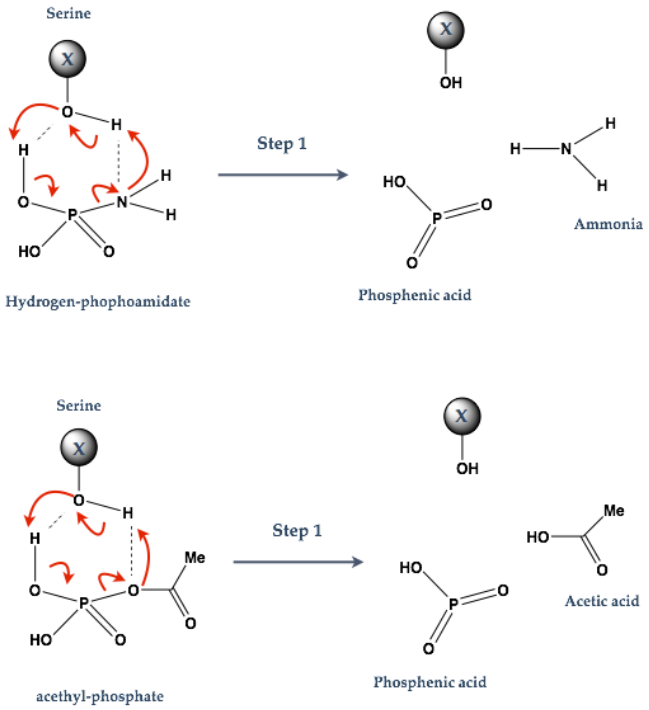

Figure IV.20. First step of the phosphorylation process with hydrogen-phosphoamid and acethyl-phosphate.

The theoretical calculations have shown that the phosphorylation process requires two sequential steps. The first step (figure IV.20) involves two concerted proton transfers involving serine as catalyst. In both cases, the proton of one of the hydroxyl groups of the phosphate groups is abstracted by the hydroxyl group of serine, at the same time that the proton some hydroxyl group of serine is transferred to the amino group or the acetate group of the phosphate compound depending on the phosphorylating agent. In the end of both reactions, two products are obtained: phosphenic acid and ammonia when the phosphorylating agent is phosphoramidate and phosphenic acid and acetic acid if the phosphorylating agent is acetylphosphate.

Although the mechanism of the first step of both reactions is apparently similar, the energetic profile is very different. When the phosphorylating agent is phosphoramidate this reaction requires 10.1 kcal/mol and is endothermic in 3.6 kcal/mol. While when the

phosphorylating agent is acetylphosphate the reaction is less favorable requiring 19.6 kcal/mol for the activation energy and 19.1 kcal/mol for the reaction energy. The differences observed in the calculated energies are dependent on how easy the hydrogen atom transfer occurs between serine and the phosphorylating agent. The higher energies observed with acetylphosphate result from the bulkier nature of the groups attached to the oxygen atom that receives the proton and therefore difficulties the reaction.

It must be mentioned that we have also tried to study the same reaction without the presence of serine as catalyst. In all the studied cases there was no reaction, a results that indicates that the phosphorylation process requires the presence of a catalyst.

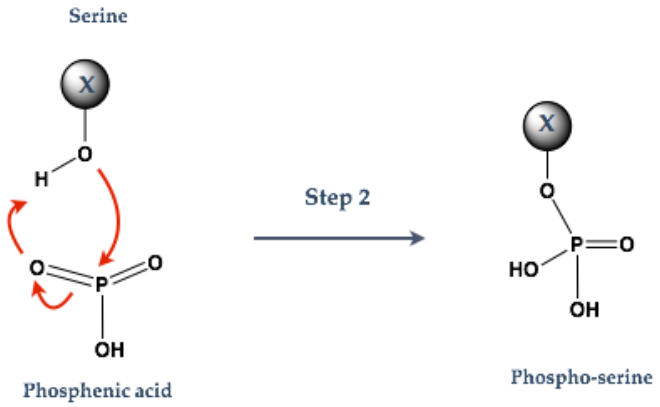

Figure IV.21. Second step of the phosphorylation process.

The second step of both reactions (figure IV.21) is identical in both cases and involves the nucleophilic attack of serine to the phosphenic acid that resulted from the first step of both reactions. The theoretical calculations revealed that in the course of this process the proton from the hydroxyl group of serine is transferred to one of the keto groups of the phosphenic acid. This allowed the formation of phospho-serine in a single step without requiring additional steps. This reaction requires 11.0 kcal/mol and it is exothermic in -8.9 kcal/mol.

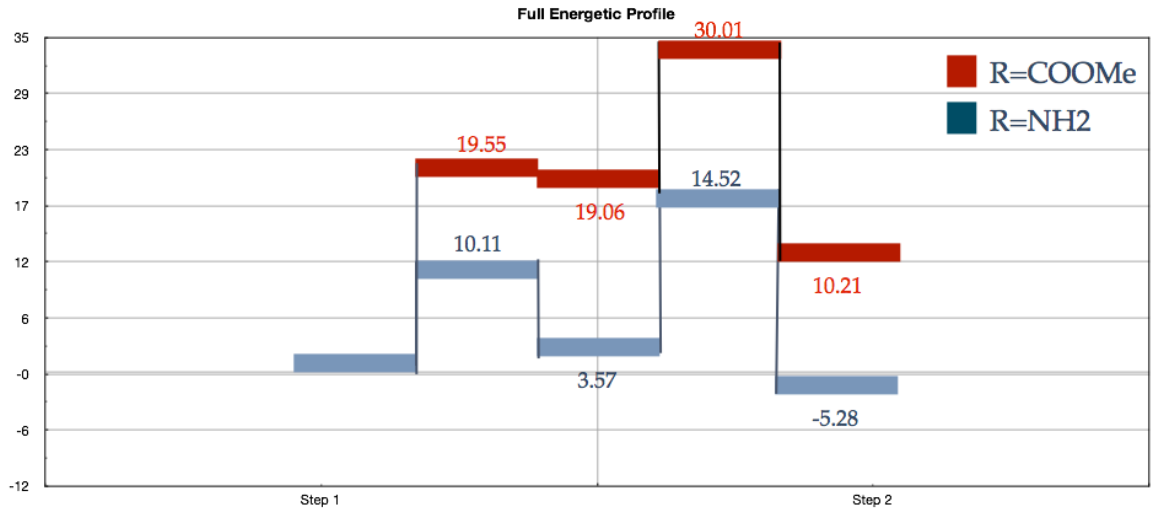

Figure IV. 22. Full energetic profile of the phosphorylation process.

The full energetic profile of both reactions is displayed at figure IV.22. This figure shows that when the phosphorylating agent is phosphoramidate, the full energetic profile of the reaction is exothermic in -5.3 kal/mol, while when the phosphorylating agent is acetylphosphate it is endothermic in 10.2 kcal/mol. In addition the energies involved in the phosphorylation of serine by phosphoramidate are much lower when compared to the ones obtained with the acetylphosphate. These two facts reveal that the phosphorylation of serine is from the kinetic and thermodynamic point of view much more favorable when the phosphorylation takes place with phosphoramidate than with acetylphosphate. The reasons behind such behavior is dependent on the first step of the mechanism and how easy the concomitant hydrogen atom transfer occurs between serine and the phosphorylation agent that is required for the formation of the phosphenic acid. These data goes in line with the fluorescence and nano LC-MS results and explain why phosphoramidate phosphorylate more amino acids than acetylphosphate

When looking into family of proteins, similar to MorR, the conserved D56 present at the receiver domain is the amino acid residue that usually undergoes phosphorylation. This process leads to an effective output response associated with enhanced of DNA binding. In the present study the anisotropy of 6-FAM dsDNA was investigated in the presence of phospho-MorR. However, no changes in anisotropy values were observed relatively to control experiments (data not shown). However, we believe that

some experimental optimatimization should be performed to conclude any influence of MorR phosphorylation in DNA binding.

IV.4. References

1. JOSEPH R. LAKOWICZ. *Topics in Fluorescence Spectroscopy, Vol. 7: DNA Technology*. (KLUWER ACADEMIC PUBLISHERS, 2003).

2. Bernard Valeur. *Molecular Fluorescence: Principles and Applications*. (Wiley-VCH Verlag GmbH, 2001).

3. Albani, J. R. *Principles and Applications of Fluorescence Spectroscopy*. (Blackwell, 2007).

4. JOSEPH R. LAKOWICZ. *Principles and Applications of Fluorescence Spectroscopy, 2nd Edition*. (KLUWER ACADEMIC PUBLISHERS, 1999).

5. Ladoklin, A. S. *Fluorescence Spectroscopy in Peptide and Protein Analysis*. 5762–5779 (in Encyclopedia of Analytical Chemistry, 2000).

6. Sjback, R., Nygren, J. & Kubista, M. Absorption and fluorescence properties of fluorescein. *Spectrochim. acta part A* **51,** L7–L21 (1995).

7. Gholivand, M. B., Ghasemi, J. B., Saaidpour, S. & Mohajeri, A. Spectrophotometric study of the effects of surfactants and ethanol on the acidity constants of fluorescein. *Spectrochim. Acta. A. Mol. Biomol. Spectrosc.* **71,** 1158–65 (2008).

8. Smith, S. A. & Pretorius, W. A. Spectrophotometric determination of pKa values for fluorescein using activity coefficient corrections. *Water SA* **28,** 395–402 (2002).

9. Martin, M. M. & Lindqvist, L. The pH dependence of fluorescein fluorescence. *J. Lumin.* **10,** 381–390 (1975).

10. Klonis, N. & Sawyer, W. H. Spectral properties of the prototropic forms of fluorescein in aqueous solution. *J. Fluoresc.* **6,** 147–157 (1996).

11. Lavis, L. D., Rutkoski, T. J. & Raines, R. T. Tuning the pKa of Fluorescein to Optimize Binding Assays. *Anal. Chem.* **79,** 6775–6782 (2007).

12. Stanton, S. G., Kantor, A. B., Petrossian, A. & Owicki, J. C. Location and dynamics of a membrane-bound fluorescent hapten a spectroscopic study. *Biochim. Biophys. Acta* **776,** 228–236 (1984).

13. Friedrich, K., Woolley, P. & Steinhäuser, K. G. Electrostatic potential of macromolecules measured by pKa shift of a fluorophore. 2. Transfer RNA. *Eur. J. Biochem.* **173,** 233–9 (1988).

14. Murakami, A. *et al.* Fluorescent-labeled oligonucleotide probles: detection of hybrid formation in solution by fluorescence polarization spectroscopy. *Nucleic Acids Res.* **19,** 4097–4102 (1991).

15. Qin, J. *et al.* Convergent evolution of a new arsenic binding site in the ArsR/SmtB family of metalloregulators. *J. Biol. Chem.* **282,** 34346–55 (2007).

16. Reedstrom, R. J., Brown, M. P., Grillo, a, Roen, D. & Royer, C. a. Affinity and specificity of trp repressor-DNA interactions studied with fluorescent oligonucleotides. *J. Mol. Biol.* **273,** 572–85 (1997).

17. Ballal, R., Cheema, A., Ahmad, W., Rosen, E. M. & Saha, T. Fluorescent oligonucleotides can serve as suitable alternatives to radiolabeled oligonucleotides. *J. Biomol. Tech.* **20,** 190–4 (2009).

18. Royer, C. a. Approaches to teaching fluorescence spectroscopy. *Biophys. J.* **68,** 1191–5 (1995).

19. Heyduk, T., Ma, Y., Tang, H. & Ebright, R. H. Fluorescence anisotropy: rapid, quantitative assay for protein-DNA and protein-protein interaction. *Methods Enzymol.* **274,** 492–503 (1996).

20. M. J., D. J. F. *et al.* Gaussian09. *Gaussian, Inc., Wallingford CT* (2009).

21. Becke, A. D. Density-functional thermochemistry. III. The role of exact exchange. *J. Chem. Phys.* **98,** 5648 (1993).

22. Lee, C., Yang, W. & Parr, R. Development of the Colle-Salvetti correlation-energy formula into a functional of the electron density. *Phys. Rev. B. Condens. Matter* **37,** 785–789 (1988).

23. Stephens, P. J., Devlin, F. J., Chabalowski, C. F. & Frisch, M. J. Ab Initio Calculation of Vibrational Absorption and Circular Dichroism Spectra Using Density Functional Force Fields. *J. Phys. Chem.* **98,** 11623–11627 (1994).

24. Robert Sjoback, Jan Nygren, M. K. Characterization of Fluorescein – Oligonucleotide Conjugates and Measurement of Local Electrostatic Potential. *Biopo* **46,** 445–453 (1998).

25. Anderson, B. J., Larkin, C., Guja, K. & Schildbach, J. F. Using fluorophore-labeled oligonucleotides to measure affinities of protein-DNA interactions. *Methods Enzymol.* **450,** 253–72 (2008).

26. Nazarenko, I., Pires, R., Lowe, B., Obaidy, M. & Rashtchian, A. Effect of primary and secondary structure of oligodeoxyribonucleotides on the fluorescent properties of conjugated dyes. *Nucleic Acids Res.* **30,** 2089–195 (2002).

27. Wang, L., Gaigalas, a K., Blasic, J. & Holden, M. J. Spectroscopic characterization of fluorescein- and tetramethylrhodamine-labeled oligonucleotides and their complexes with a DNA template. *Spectrochim. Acta. A. Mol. Biomol. Spectrosc.* **60,** 2741–50 (2004).

28. Kumke, M. U., Li, G., McGown, L. B., Walker, G. T. & Linn, C. P. Hybridization of fluorescein-labeled DNA oligomers detected by fluorescence anisotropy with protein binding enhancement. *Anal. Chem.* **67,** 3945–51 (1995).

29. Delgadillo, R. F. & Parkhurst, L. J. Spectroscopic properties of fluorescein and rhodamine dyes attached to DNA. *Photochem. Photobiol.* **86,** 261–72 (2010).

30. Liu, M. S. *et al.* Coarse-grained dynamics of the receiver domain of NtrC: fluctuations, correlations and implications for allosteric cooperativity. *Proteins* **73,** 218–27 (2008).

31. Roche, P., Mouawad, L., Perahia, D., Samama, J.-P. & Kahn, D. Molecular dynamics of the FixJ receiver domain: movement of the beta4-alpha4 loop correlates with the in and out flip of Phe101. *Protein Sci.* **11,** 2622–30 (2002).

32. Lukat, G. S., McCleary, W. R., Stock, a M. & Stock, J. B. Phosphorylation of bacterial response regulator proteins by low molecular weight phospho-donors. *Proc. Natl. Acad. Sci. U. S. A.* **89,** 718–22 (1992).

33. Schuster, M., Silversmith, R. E. & Bourret, R. B. Conformational coupling in the chemotaxis response regulator CheY. *Proc. Natl. Acad. Sci. U. S. A.* **98,** 6003–8 (2001).

34. McCleary, W. R. The activation of PhoB by acetylphosphate. *Mol. Microbiol.* **20,** 1155–63 (1996).

35. Ferré, A., De La Mora, J., Ballado, T., Camarena, L. & Dreyfus, G. Biochemical study of multiple CheY response regulators of the chemotactic pathway of Rhodobacter sphaeroides. *J. Bacteriol.* **186,** 5172–7 (2004).

Chapter V
Conclusion

Chapter V

V. Conclusion

Analysis of the intergenic region between *mor*S and *mor*P reveals the presence of two divergently transcribed promoters (σ_{54} and σ_{70}). The σ_{54} promoter might be involved in gene transcription regulation of *mor*P gene. The σ_{70} might be involved in regulation of *mor*S and *mor*P genes.

The *mor*R gene was cloned on a pET expression vector and the expression conditions to obtain MorR protein were optimized. The expression profile reveals that *mor*R is transcribed even in the absence of transcription inducer (IPTG). This evidence indicates a misrule of T7 RNA polymerase expression from *lac*UV5 promoter revealing the leaky nature of the pET expression systems, but also that MorR is a nontoxic product for *E.coli*.

The MorR protein was expressed as soluble protein and purified. It is a monomer in solution, with a molecular mass of ~52kDa and a molar extinction coefficient at 280 nm of $30823 M^{-1}cm^{-1}$.

EMSA determine that MorR protein binds the intergenic region between *mor*P and *mor*S and therefore might be involved in gene transcription regulation of those genes. This regulation might be mediated from the divergently σ_{54} and σ_{70} promoters. DNA footprinting assays have shown that MorR binds to a target 54 bp intergenic region. This protected region covers positions -145 to -200 relative to *mor*P transcription start site +1. This result is in agreement with a transcription mediated via RNAPσ_{54}, where transcriptional activators bind far from the promoter they control. The MorR protein also binds to the putative -10 and -35 promoters located upstream of *mor*S gene. This result indicates that MorR could control *mor*S transcriptional level and its own transcriptional by interaction with RNAPσ_{70} since both genes *mor*R and *mor*S might be are encoded by the same operon.

MorR binds to a palindromic region (TTTTTTATA) located in the intergenic region between *mor*S and *mor*P. This evidence suggests that MorR has two distinct binding regions.

The prototropic form of 6-FAM-67mer carrying the target intergenic region was determinate in order to define which fluorescein specie is present under experimental procedures. The fluorescence spectroscopy characterization of the 6-FAM revealed that

anisotropy varies according to the acid-base equilibrium of the medium. This is an important parameter to consider for biochemistry studies that wish to determine protein-DNA interaction using fluorescein as a probe. For such studies, a constant fluorescein emission is a prerequisite to determine association constants between macromolecules.

The fluorescence spectroscopy results confirmed that MorR binds to the target DNA at two different regions. The result identified two association constants: 15.5 μM^{-1} for the first binding site and 0.02μM^{-1} for the second binding site. The results also demonstrated that MorR has different affinities for those two binding sites. In this way, MorR binds firstly and highly to the conserved DNA region that covers the putative -35 box. Then, the protein binds with low affinity to the second binding site that covers the -10 conserved box.

The monoanionic specie of fluorescein covalently attached to 67-mer oligonucleotide was predominant under pH 7.5.

The 6-FAM position near the protein binding site, rather than the oligonucleotide length, is the factor that influences in the anisotropy values. So, this proximity of the fluorophore to the protein binding site increased the sensitivity of the assay. The pka of fluorescein labeled with DNA is different from the pka of free fluorescein. This evaluation is important for optimization of techniques that use fluorescein conjugated with oligonucleotides.

The nano-LC-MS revealed that MorR was purified without any phospho amino acid. The MorR conformational change induced by phosphorylation was investigated using acetylphosphate and phosphoramidate as small phosphodonors. The phosphorylation status of MorR was determined by gel filtration and the experiments revealed that MorR do not oligomerize in the presence of those small phosphodonors.

Phosphoramidate, rather than acetylphosphate, caused a static quenching in the MorR-tryptophan emission. The tryptophan emission is 30% suppressed in the presence of phosphoramidate. This quenching is not followed by a shift in the tryptophan emission. Therefore, the MorR oligomerization may not occur in the presence of phosphoramidate which corroborate with the gel filtration experiments. Additionally, the conserved acid aspartic residue (D55) was phosphorylated by both small phosphodonors.

Conclusion

The phosphorylation reaction of serine, mediated by phosphoramidate and acetylphosphate, requires two sequential steps. The first step is crucial to determine the reactivity of the reaction. In this way, the reaction is more favorable when the phosphorylating agent is phosphoramidate. Therefore, phosphorylation of serine residues is kinetic and thermodynamically more favorable with phosphoramidate than acetylphosphate. This result explains why phosphoramidate phosphorylated more amino acids than acetylphosphate.

The quenching of MorR indicates that amino acids located near to the tryptophan were phosphorylated. As a perspective, it will important to determine if the phosphorylation alter the MorR binding affinity to the intergenic region between *mor*S and *mor*P.

The present study proposes a new mechanism for *mor*P, *mor*S and *mor*R transcription regulation (figure V.1). We postulate that the inactive form of MorR represses its own promoter by binding to the -35 conserved box, blocking the $RNAP_{\sigma 70}$ polymerase activity. This model considers that a basal level of transcription of *mor*P, *mor*S and *mor*R exists. The inactive MorR (not phosphorylated) although bound to the target intergenic region is powerless to enhance the *mor*P transcription through σ_{54} promoter. We believe that the inactive form does not have all the potential to give the mechanical force that is necessary to $RNAP_{\sigma 54}$ activity.

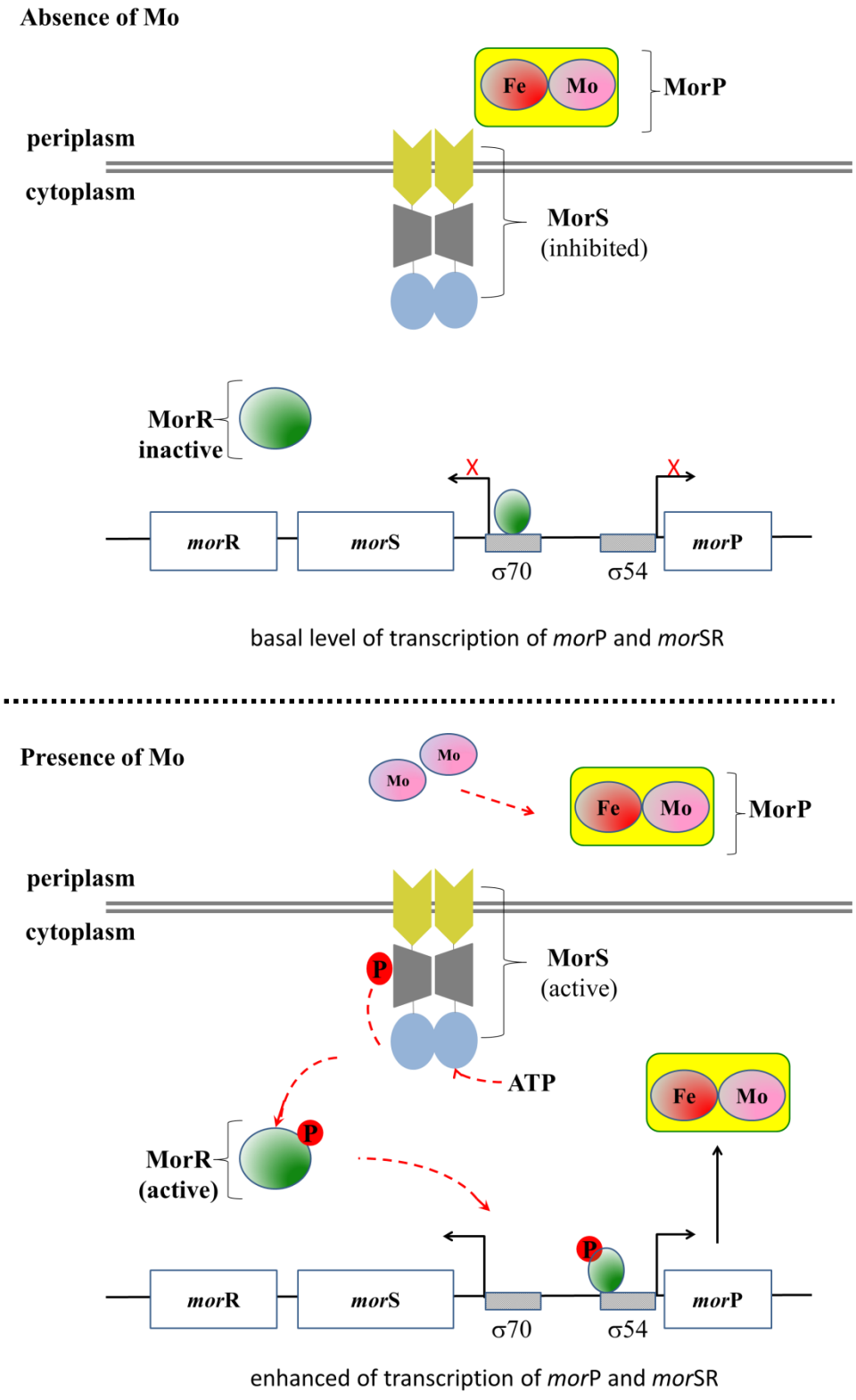

Figure V. 1. Model for *mor*SR and *mor*P transcriptional regulation proposed by the present work.

In the presence of Mo in the medium (figure V.1, B), MorP incorporates this metal in its structure which leads to a protein conformation change. Then, the uninhibited MorS is capable to autophosphorylates and transfer the phosphoryl group to MorR. However, we believe that this route for MorR activation isn't unique and the MorR autophosphorylation enhanced capacity should be considered. The active form of MorR might has an enhanced ATPase activity that allows the interaction with $RNAP_{\sigma 54}$ which leads to *mor*P transcription activation. In this way, the activated form is not able anymore to binds to the putative -35 conserved sequence which allows the transcription of *mor*SR genes by $RNAP_{\sigma 70}$. We believe that the MorR binding to the putative -10 conserved box (less preferable for MorR binding) could be an additional way for transcriptional regulation of *mor*SR. This mechanism might be involved with an enhanced capacity for deactivation of the transcriptional apparatus that are necessary for Mo homeostasis.

V.1. Future Perspectives

- Perform crystallographic studies of MorR
- Identify if the DNA binding constants are altered when MorR is phosphorylated
- Perform transcriptional assay studies to address if the activated form of MorR enhance the transcription of the *mor*P gene
- Perform transcriptional assay studies to address if MorR acts as a negative self-regulator of *mor*R gene and *mor*S and identify if the activated form derepress the mor*RS*.
- Identify if other post translational modifications, such as glycosylation, alters the conformational structure of MorR and if it has any influence on the function of the protein.
- Perform ATPase activity experiments